UNIVERSITÀ
DEGLI STUDI
DI TRIESTE

UNIVERSITÀ DEGLI STUDI DI TRIESTE

XXXIV CICLO DEL DOTTORATO DI RICERCA IN

NANOTECNOLOGIE

Nanoparticles anti-GPC1 for glioblastoma multiforme treatment

Settore scientifico-disciplinare: **BIO/14**

DOTTORANDA
FEDERICA DI CINTIO

COORDINATORE
PROF. ALBERTO MORGANTE

SUPERVISORE DI TESI
DR. GIUSEPPE TOFFOLI

ANNO ACCADEMICO 2020/2021

Index of the contents

Abstract

Glioblastoma multiforme (GBM) the most aggressive (WHO grade IV) diffuse glioma, is also by far the most frequent one. After standard treatment, the 2-year overall survival of GBM patients is approximately only 25%. Although numerous experimental drugs have been tested in clinical trials, GBM patients have not yet profited from curative treatments. To overcome the big limitations regarding GBM treatment, we address the challenge of developing a drug delivery system based on highly biocompatible chitosan nanobubbles (NBs) conjugated with an anti-glypican1 (GPC1) antibody loaded with docetaxel as a chemotherapeutic agent. This drug delivery approach has been proposed to counter major challenges as overcoming the BBB, allowing the therapeutic release exclusively to tumor cells, and minimizing the possible side effects in cancer patients. The GPC1 proteoglycan has been chosen as a useful target for drug delivering with NBs, therefore GPC1 expression was characterized *in-vitro*, being found expressed in GBM cell lines (e.g., T98G, U87-MG) but not found expressed in non-GBM cell lines. Consistently, we assessed the localization of GPC1 protein expression on the cell surface and in the cytoplasm of GBM cell lines whereas it was lacking in the negative control cells. Of note, in primary tumor sections of these 10 GBM cases, GPC1 was found overexpressed whereas in normal tissues was found not expressed. To obtain a specific anti-GPC1 antibody recognizing the last 70 amino acids of GPC1 protein and therefore the cell-surface form of GPC1, mouse immunization has been performed. Hybridomas have produced three different anti-GPC1 specific clones (A, B, C). By using the B and C clones, GPC1 expression was detected in GBM cells at levels comparable to the levels obtained by using the commercially available antibody (a-GPC1c) by the B and C clones. On the contrary, the A clone was not capable to recognize GPC1. Therefore, we purified the B and C clones to obtain specific anti-GPC1 monoclonal antibodies. Moreover, C and B appeared to be more efficient than the a-GPC1c for the detection of GPC1 expression levels. According to the results of antibody testing in GBM cell lines and negative control cell lines, the B clone was chosen to be conjugated to the NBs to develop the active drug delivery strategy. To select the drug to be loaded in the NBs, the killing capability of temozolomide (TMZ), paclitaxel (PTX), and docetaxel (DTX) was evaluated in GBM cells. DTX has the highest killing capability compared to PTX and TMZ. Therefore, we used DTX for the NBs loading encapsulation. The *in-vitro* characterization of NBs showed an average diameter of about 350 nm and a positive charge and spherical morphology. *In-vitro* analysis of the treatment of NBs in GBM cells, showed the localization of NBs conjugated with B antibody in cell cytoplasm around the nucleus. In contrast, lower mean fluorescence intensity was observed for the cells treated with unconjugated NBs. For the *in-vitro* cytotoxic effect of NBs, NB loaded with DTX, NBs loaded with DTX and conjugated with

B antibody, showed a killing capability correlated with the concentration in each evaluated point, with cell viable levels comparable to those of free DTX for some concentrations. Blank NBs, NB conjugated with Cy 5.5, and NB conjugated with B antibody were not toxic at all tested concentrations. *In-vivo* and *ex-vivo* tests of the biodistribution of anti-GPC1 NBs in xenograft GBM mouse model showed that the presence of the conjugation with the B antibody seems to allow a major accumulation of the injected NBs in the tumor as well as a higher retention time at least until the last time point of 96 h of treatment. In conclusion, the proposed active drug delivery approach using anti-GPC1 conjugated NBs loaded with DTX could be useful for the treatment of GBM.

1. Introduction

1.1 Glioblastoma

1.1.1 Glioblastoma classification

Glioblastoma (GBM) is the most common and aggressive primary central nervous system (CNS) tumor and is classified as a grade IV tumor. GBM has been included in the group of diffuse astrocytic and oligodendroglia tumors by the 2016 CNS WHO [1–9].

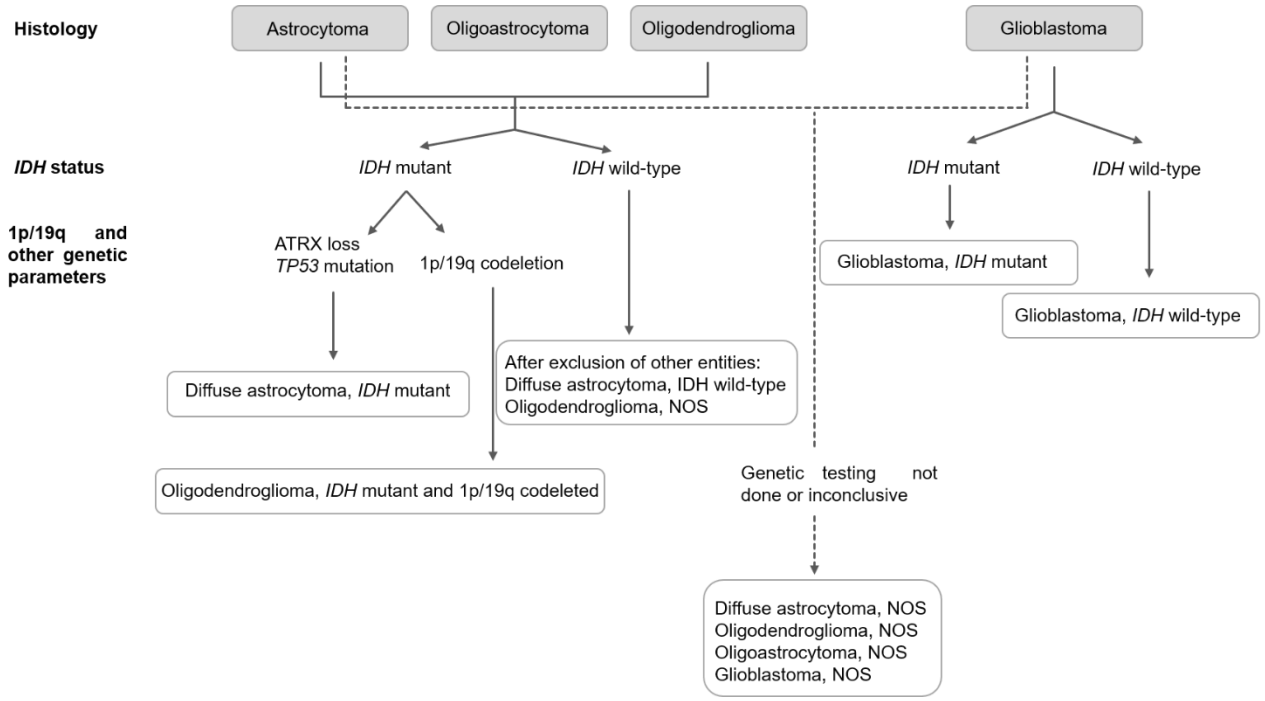

Figure 1. Classification of the diffuse gliomas based on histological and genetic features (2016 CNS WHO). (Adapted from Louis et al., *Acta Neuropathol* 2016)

It is thought that genetic alterations affecting neuroglial stem or progenitors' cells give origin to GBM. According to the presence of mutations in the isocitrate dehydrogenase (IDH) 1 and IDH2 genes GBM is subdivided by the WHO into two major types. In particular, GBM is divided into glioblastoma, IDH-wildtype (about 90 % of cases), which corresponds to the most frequent type that has clinically defined as primary or de novo glioblastoma; glioblastoma IDH-mutant (about 10 % of cases), which closely corresponds to the so called secondary glioblastoma characterized by a history of a prior less aggressive form of WHO grade II diffuse astrocytomas and WHO grade III anaplastic astrocytomas (i.e., secondary GBM)[10,11], and to glioblastoma NOS, a diagnosis that is reserved for those tumors for which full IDH evaluation cannot be performed[6,9,10].

Primary GBM is typically diagnosed at an older age and has a worse prognosis while secondary GBM are less common and affect people under the age of 45[10–14].

1.1.2 Treatment

The standard care for GBM is maximal surgical resection, which allows for accurate histological diagnosis, tumor genotyping, and a reduction in tumor volume. This is followed by radiotherapy with concomitant adjuvant chemotherapy such as the oral alkylating agent, temozolomide (TMZ), and further 6 cycles of maintenance TMZ, according to Stupp protocol.[13,15–17] Upon this treatment combination, GBM shows a median Overall Survival of about 15 months[11,13,16,18]. TMZ is an oral alkylating agent, it works by methylating DNA, which also results in inhibited DNA and cellular replication. This drug acts nonspecifically and affects both cancerous and normal cells alike[19].

Radiotherapy has long been used to improve both local control and survival, and it remains an important modality. Conventional radiotherapy after surgery delivers 60 Gy in 2-Gy fractions over 6 weeks in combination with TMZ. Furthermore, hypofractionated radiotherapy in combination with concurrent and adjuvant TMZ has demonstrated improved OS compared with hypofractionated radiotherapy alone[17,20,20,21].

The only interstitial chemotherapy treatment approved to date for malignant glioma is Gliadel + wafer. This is a biodegradable polymer containing 3.85% carmustine (1,3-Bis[2-Chloroethyl]-1-Nitroso-urea, BCNU), which is placed in the tumor resection cavity at the time of surgery[22]. However, there are limited strong, prospective data on survival outcomes, when followed by standard radiotherapy and concomitant TMZ, in newly diagnosed GBM, with safety concerns remaining [23,24].

Toxicities of TMZ include nausea and myelosuppression, especially thrombocytopenia and neutropenia[25]. The benefit from TMZ is higher for patients whose tumors had a methylated promoter for the gene encoding O-6-methylguanine-DNA methyltransferase, MGMT[16,17]. Therefore, in patients with MGMT promoter methylation, concurrent chemoradiation with adjuvant TMZ remains the treatment of choice[26].

Locoregional therapy is represented by the addition of tumor-treating fields. It is consisting of low intensity, alternating electric fields daily delivered by transducer arrays to the shaved scalp and connected to a portable device for antimitotic therapy and given during maintenance TMZ[27]. Cost, treatment compliance, and skin toxicity are additional barriers limiting the uptake of this treatment modality[28].

Moreover, TMZ can pass through the blood-brain barrier (BBB) for ~30% of the dose[29] but it is characterized by a lower killing capability[30]. For these reasons, in the present thesis, we have chosen to test other drugs such as Docetaxel (DTX)[31,32] and Paclitaxel (PTX)[33,34]. Despite the high killing efficacy, DTX and PTX have a low bioavailability of about 95%. Also, their physiochemical

proprieties do not favor the BBB crossing[35,36]. PTX is a taxane. It is a potent anticancer agent due to its capability to interfere with normal mitotic function by stabilizing the microtubule assembly from tubulin and preventing depolymerization, PTX acts by blocking cells in the G2 phase of cell cycle[37–39]. Clinically important side effects are anemia, leukopenia, neutropenia, cardiovascular events, nausea and vomiting, hypersensitivity reactions, arthralgia/myalgia, and peripheral neuropathy[40]. DTX is a semi-synthetic derivative belonging to the taxoid family[41]. DTX is an anti-tumor drug that has proven to be frequently more efficacious than PTX as a cytotoxic anti-microtubule agent[42]. DTX binds to microtubules with high affinity, thereby preventing the depolymerization of microtubules, thus resulting in a significant decrease in the free tubulin that is required for microtubule formation. DTX binding can inhibit mitotic cell division and prevent further cell proliferation[43,44]. DTX has also been reported to possess side effects such as anemia, leucopenia, neutropenia, hypersensitivity reactions, fluid retention, alopecia, cutaneous reactions, and nail changes[45]. In this regard, NBs can encapsulate a high amount of hydrophobic DTX, release the drug in a sustained manner and counteract the toxicity-related issues associated with DTX by reducing its dose.

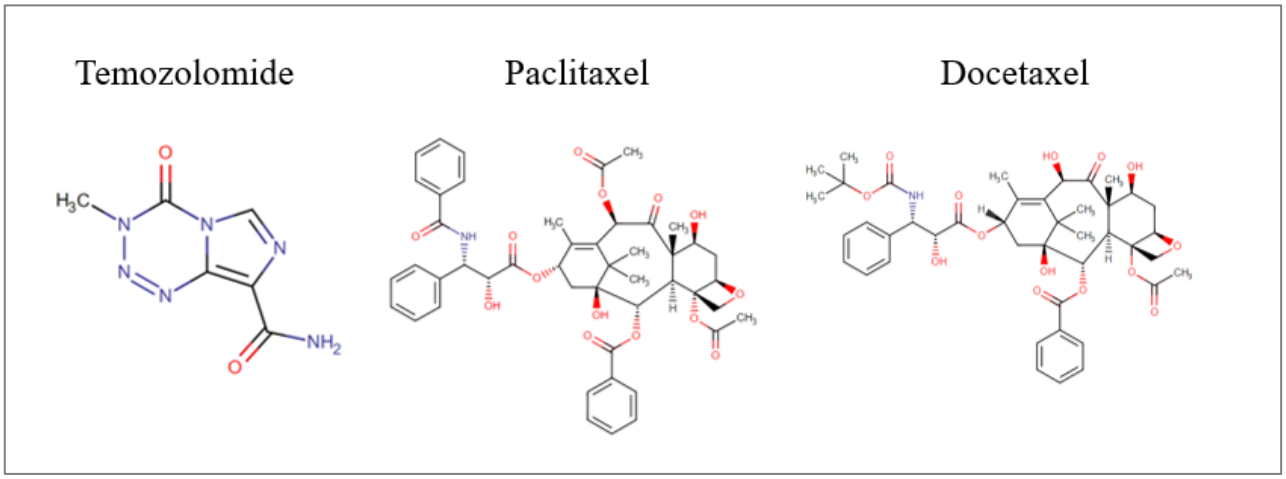

Figure 2. Chemical structure of the anticancer drugs temozolomide, docetaxel, and paclitaxel. (From *DrugBank online*)

1.2 Nanotechnology

Delivering therapeutic compounds to the desired site is a key point in the treatment of diseases. Conventional delivery of drugs is characterized by limited effect, low selectivity, poor biodistribution and so side effects in all body[46]. To overcome these limits the use of a controlling drug delivery system is a strategy for transporting drugs only in the place of action. Therefore, the use of targeted carriers loaded with drugs increases drug concentration in target cells or tissues and protects against rapid degradation or clearance of drugs. Recent advancement in Nanotechnology has shown that nanoparticles acquire great potential as drug carriers[47]. Nanotechnology is nowadays widely used for the disease diagnosis, delivery, and targeting of therapeutics for several types of cancers[48]. Nanomedicine utilizes nanotechnology in the preclusion and cure of various diseases using the nanoscale materials, such as nanoparticles (NPs) for various applications including, delivery[49], diagnosis[50], and sensory[51]. In 2004, the European science foundation defines Nanomedicine as "the science and technology of diagnosing, treating and preventing diseases and traumatic injuries, of relieving pain, of preserving and improving human health, using molecular tools and molecular knowledge of the human body"[52]. Another definition of nanomedicine that explains better the working field of that discipline is the application of the nanoscale material in medicine that takes advantage of the nanomaterial's unique properties[53]. For Food and Drug Administration (FDA) the meaning of "nanotechnology" is employed in the engineering of materials to create and manipulate materials that have at least one dimension in the size range of approximately 1 nanometer (nm) to 100 nm[54]. According to the federal US research and development program agency, the National Nanotechnology Initiative (NNI), nanotechnology involves the development of carrier's devices or systems sized in 1 to 100 nm range although this limit can be extended up to 1000 nm[55].

In the last two decades, nanotechnology has permitted the integration of therapeutic and targeting agents into NPs to detect, prevent, and treat oncological diseases[56]. Enhanced Permeability and Retention effect (EPR) is a feature of inflamed tissues, leads to an increased vascular permeability coupled to a deregulated neovascularization[57]. EPR effect was first described in tumors where discontinuous endothelium in newly formed and immature vessels are formed[58]. However, the EPR effect is a mechanism involved in inflammatory diseases, where the process of neoangiogenesis takes place (e.g., inflammatory conditions such as Rheumatoid Arthritis)[59]. Nanomedicine improves the selectivity in targeting cancers cells by the delivery of drugs to the tumor because of the EPR effect[56]. The EPR effect is the mechanism usually referred to as "passive targeting", in which the nanosystems are accumulated in cancerous tissue[60]. The EPR effect is a paradox that arises especially in solid tumors and is correlated with their pathological and anatomical characteristics, which differ from normal tissues[61]. Especially, most solid tumors have increased vessel leakiness and impaired

lymphatic function, thus permitting nanomaterials to penetrate, and accumulate there[56,60,61]. Poorly vascularized tumors, mainly prostatic, pancreatic, and liver metastatic have less EPR effect than other types of cancers[62]. Active targeting of nanosystems allows by functionalization of their surface with bioactive molecules, that recognize and interact with cancer-specific targets overexpressed on the surface of cancer cells[63]. The most frequently used targeting moieties are monoclonal antibodies, antibody fragments, antigen-binding fragments, and single-chain variable fragment[60,62,64]. Therefore, the active targeting improves the uptake of nanocarriers to the cancer cells, enhances the drug bioavailability[65,66], reducing the immunogenicity[47]. For the success of the therapeutic use of NPs, a key role is played by the clearance rate occurring in the body. The nanocarriers injected in the bloodstream are cleared, mainly by the liver for most of the nanomaterials: polymeric NPs[67], micelles[68], gold NPs[69], and quantum dots[70]. Furthermore, the physicochemical characteristics of nanomaterials like size, shape, and surface functionalization depend on the number of them that accumulate in the liver[48,64,71].

Drug delivery systems (DDS) can be divided into three generations of compounds, according to whether they were developed to target a specific molecule that is expressed on the tumor cells or in the endothelium[72]. Table 1 describes the three generations of drug delivery[72–74]. The first controlled DDS products based on the Alza Corp. definition were macroscopic designs with reservoirs of constant drug concentration enclosed in rate-controlling membranes made of polymers[75]. They are capable to accumulate by passive mechanisms[73] exploiting EPR effect[72]. Among the "first generation" of DDS, liposomes-based drug delivery is the most used in the clinic, as demonstrated by liposomal doxorubicin for breast cancer, ovarian cancer, and Kaposi's sarcoma[76]. The "second generation" of therapeutic drug delivery included "smart" DDS technologies like polymer microparticles, hydrogels, developed to enable drug delivery in response to a pH or temperature[73,77]. Moreover, they represent the natural evolution of the first generation, with additional functions including surface modification with ligands, able to bind specific biological molecules of the tumor cell[72,73,78,79]. The third generation of drug delivery (i.e., 2010–present) is made by different NPs into a single vector to build a system that can avoid the biological barrier and at the same time possess target activity and tumor cytotoxic. These nanocarriers possess the property to recognize specifically the cancerous cells through a mathematically driven recognition of the physic-chemical features (first stage). The second stage NPs are loaded into the first one and released inside the tumor by the targeting agent[72]. The strategies allowed the development of more than 200 products that have been approved or are under clinical investigation[80,81].

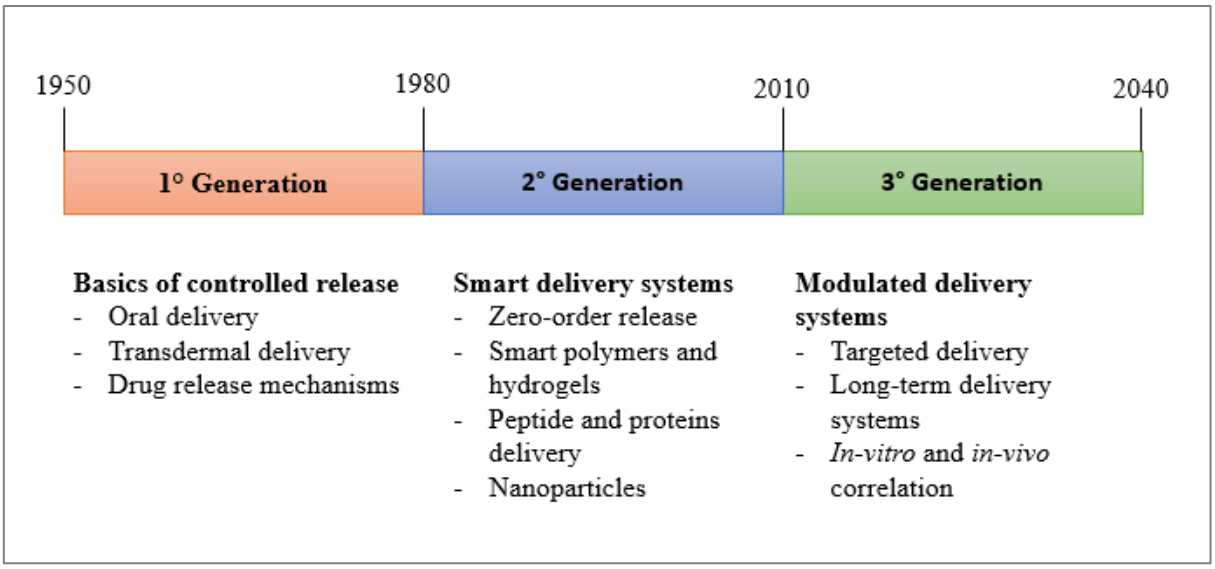

Table 1. Time intervals of the three generations of Drug Delivery Systems.

1.3 Organic NPs in Nanomedicine

Organic NPs as solid particles are composed of organic compounds (lipids, proteins, or polymers), and have been investigated for decades, providing a large variety of materials and exciting applications in nanomedicine[82].

1.3.1 Polymeric NPs

Biodegradable polymeric NPs have been considered as a potential drug delivery system for their applications in oncology[62]. Polymeric NPs consist of a biodegradable polymer that is biocompatible and not toxic[47]. Polymers are the most common materials for assembling NP-based drug carriers that can transport drugs in a controlled and targeted way through surface modification[83]. Due to their nature, there is the possibility of modifying many characteristics such as biodegradability, molecular weight, and hydrophobicity[84]. Polymeric NPs can be synthesized from natural polymers, such as albumin[85,86], chitosan[87–89], hyaluronic acid and gelatin[90], dendrimers[91,92], hyperbranched polymers[93] and from synthetic polymers, such as polyacrylic acid (PAA)[94], poly (lactic-co-glycolic acid) (PLGA)[95,96], polylactic acid (PLA)[97,98]. Different methods of synthesis of polymeric NPs are investigated depending on the application and drug type. NPs have been prepared mainly by two methods: dispersion of the performed polymers, and polymerization of monomers[99]. These methods include solvent evaporation[100,101], nanoprecipitation, and emulsion diffusion[99,101]. The drug can be loaded into the NPs by two methods: incorporating the drug at the time of NPs production or by adsorbing the drug after the formation of NPs by incubating them in the drug solution[99,102]. A large amount of drug can be encapsulated by the incorporation method compared to the adsorption. Therefore, the capacity of adsorption is related to the hydrophobicity of the polymer and the specific area of the NPs[99]. For the development of a successful formulation, drug release from NPs and their biodegradation are important factors. Drug release mechanism from polymeric NPs happens by the diffusion from the polymer matrix, desorption of the adsorbed drug, degradation of the polymer matrix, and biodegradation of the polymer matrix due to the hydrolytic degradation[99,103].

Albumin is one of the most abundant proteins in plasma, and it is an ideal candidate for NPs preparation due to its biodegradability, non-toxicity, availability, non-immunogenicity, and ease of, preparation and reproducibility[85]. Albumins have an extraordinary ligand binding capacity for different drugs due to multiple drug-binding sites[85,104]. Albumin has many different functional groups and therefore can bind to significant amounts of the drug. The structure of albumin allows the binding of various drugs to NPs by electrostatic interaction on the surface of NPs by the presence of surface functional groups, such as carboxyl groups, amine, and, thiols[105,106]. Albumin is successfully applied as a nanocarrier in clinical. ABI-007 was the first drug formulation of this category approved by the

FDA in 2005. Abraxane (Abraxis Biosceince/AstraZeneca) is an albumin-bound (nab) paclitaxel formulation. It was developed to improve the bioavailability of the therapeutic benefits of the drug but concomitantly eliminate the toxicities associated with the emulsifier Cremophor EL in the paclitaxel formulation (Taxol). Abraxane can enhance drug delivery by passive targeting of the tumor tissue and showed the reduction of cardiotoxicity compared to the free drug[60,85,107,108].

Chitosan (CS), derived from chitin by deacetylation, is the second most abundant naturally occurring biopolymer and a major structural polysaccharide found in the exoskeleton of crustaceans such as crab and shrimp[109]. CS consists of a linear polysaccharide composed of two types of monomers, that is, N-acetyl-D-glucosamine and β-(1,4)-linked D-glucosamine. Thus, it comprises copolymers of glucosamine and N-acetyl glucosamine[109–111]. The excellent biocompatible, biodegradable, and mucoadhesive proprieties of CS make it useful in drug delivery applications[109–112]. There are four methods for the preparation of CS-NPs as microemulsion, ionotropic gelation, emulsification solvent diffusion, and polyelectrolyte complex[113]. Also, CS is the most widespread polycationic[109] biopolymer to bind to nucleic acids, so it can be used for cell transfection[111]. The structure of CS is more easily functionalized with its primary hydroxy and amino groups that improve the physical and biological proprieties during conjugation. Also, the CS hydrophilic nature helps an easy conjugation of the hydrophobic moiety to form self-assembled NPs[112]. Chitosan-shelled nanobubbles (NBs) functionalized with anti-CD1a antibodies to target dendritic cells (DCs) were developed for the loading of DNA vaccines. The DC-targeted CS-NBs loaded with tumor vaccine demonstrated the capability to induce activation of DCs both in human and mouse models and elicit a specific immune response able to delay tumor growth *in-vivo* in mice. Moreover, the DC-targeted CS-NBs loaded with tumor vaccine may provide an attractive nanotechnology approach for the future immunotherapeutic treatment of cancer[114].

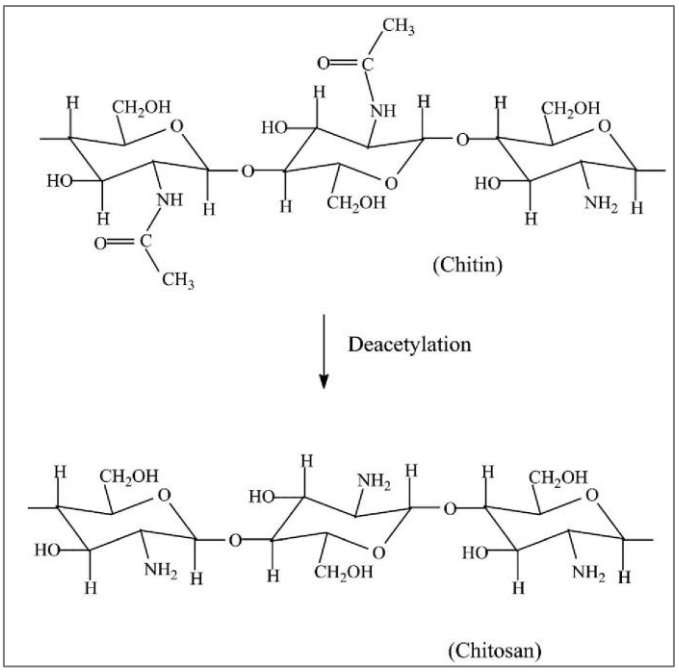

Figure 3. Chemical structure of chitosan derived from deacetylation of chitin. (From Gomathysankar et al., *APS* 2014)

Among the synthetic polymers, PLGA and PLA are commonly used in drug delivery in tumors due to their biocompatibility and controlled release through the hydrolysis of ester bonds[93,113,115]. PLGA is one of the most used nanosystems for the development of nanomedicine for its propriety, it undergoes spontaneous hydrolysis in the body to produce the biodegradable metabolite monomers: lactic acid and glycolic acid (Figure 4)[113,116].

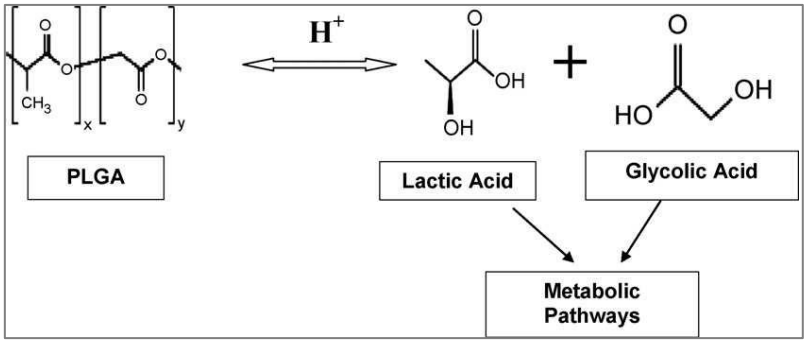

Figure 4. Chemical structure of poly (lactic-co-glycolic acid) and its monomers. (From Kumari et al., *Colloids Surf. B* 2010)

PLGA "structures/scaffolds" were developed for use in surgical implants and tissue repair in the 1960s, they have been for various biomedical applications, including bone implants abdominal mash,

and controlled drug release[103,115]. PLGA NPs have been used to develop the proteins and peptides nanomedicine, NPs-based gene delivery system, nano-antigen, nano-vaccines, and offer a platform for multifunctional imaging in cancer diagnostics[99,111–113,117,118]. Ganipineni et al.[119] found that magnetically targeted paclitaxel- and SPIO-loaded PLGA-NPs increased cellular uptake in GBM compared to the non-targeted carriers. In addition, co-treatment with PEG-PLGA NPs functionalized with CRT peptide and loaded with docetaxel increased the ability of NPs to overcome the BBB *in-vitro* and improved the survival rate *in-vivo*[120].

PLA can be obtained by the polycondensation of lactic acid or by ring-opening polymerization (ROP) of lactide, a cyclic ester of lactic acid[121,122]. ROP of lactide needs catalyst but results in PLA with controlled molecular weight[123]. PLA has gained a key role in the biomedical field for a wide range of applications: suture threads, graft materials for artificial organs bone fixation screws, devices for drug delivery[121,124,125].

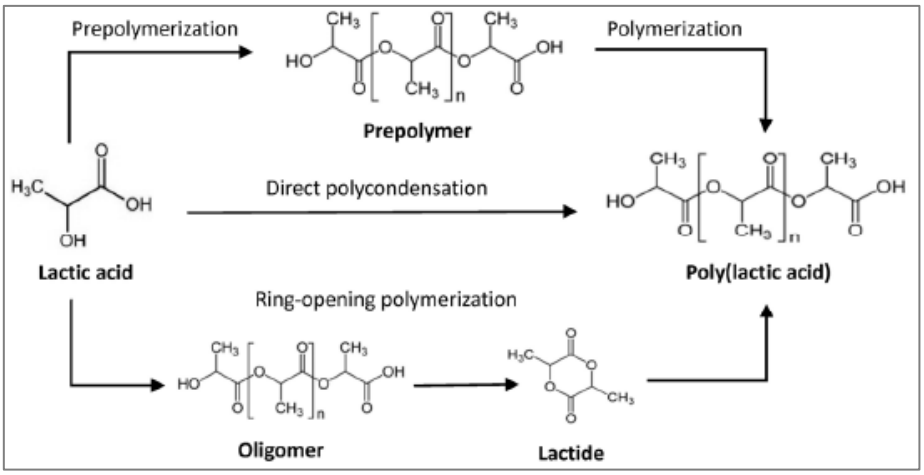

Figure 5. **Route of PLA synthesis from lactic acid.** (From Hu et al., *Materials* 2016)

PLA has been proposed for improving the oral bioavailability of poorly water-soluble drugs. And PLA-NPs enhanced protection for plasma enzymes, alternative routes of administration, and prolonged gene delivery efficacy[115,126].

1.3.2 Liposomes

Liposomes attained great attention during the last few decades in biomedicine, especially as a drug delivery system for antitumor drugs. Since their discovery by Alec Bangham and colleagues in 1961[127], liposomes became an important choice for many drugs formulations. Liposomes are spherical lipid vesicles with a hydrophilic core enclosed by lipid bilayers of amphiphilic phospholipids[128]. Liposome has both a hydrophilic and a hydrophobic region, permitting the encapsulation and transport of both therapeutic and diagnostic agents[129]; hydrophobic drugs can be enclosed within the phospholipid bilayers, while hydrophilic drugs can be entrapped in the hydrophilic cavity[130]. To avoid the recognition by RES system and prolong their circulation in the bloodstream, stealth liposomes can be covered with polymers (e.g., PEG, PLGA)[131]. They can be inserted into the liposomes to form a hydrated layer on the liposome surface[132,133]. Liposomes can be classified according to their lamellarity (uni- and multilamellar), size (small ≤ 100 nm, Intermediate 100-250 nm, and large ≥ 250 nm), and surface charge (anionic, cationic, or neutral)[134,135]. Liposomes represent versatile and advanced nano delivery systems for a wide range of biologically active compounds. They can be conjugated to antibodies, ligands, peptides, proteins, carbohydrates to enhance target specificity[133].

Indeed, more than 2000 liposome formulations are under clinical trials in 1990 Ambisome® (liposomal amphotericin B), the first liposomal drug formulation, was approved by FDA and in 1995 was approved the first anticancer liposome formulation (Doxil®)[136]. Doxil® is the principal example of formulation of liposomal doxorubicin, and also another example is Daunoxome® (Gilead Sciences), in which the drug incorporated is daunorubicin[133,137,138].

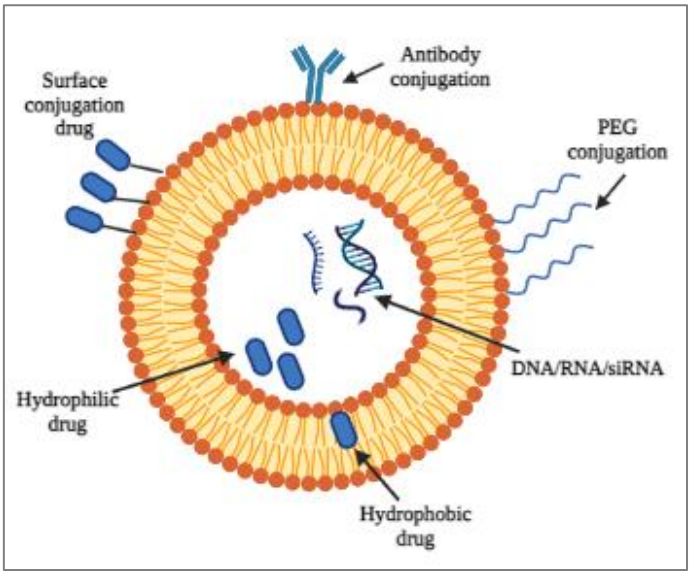

Figure 6. Structural design of liposomal drug delivery systems. (Image adapted from Çağdaş et al., *IntechOpen* 2014)

1.3.3 Micelles

Micelles are colloidal particle dispersions formed by amphiphilic molecules (block copolymers or surfactants) that self-assemble in water containing both hydrophobic and a hydrophilic segment small diameter (ranging from 5 to 100 nm)[139–141](Figure 7). They can be composed of a fatty acid, a salt of a fatty acid, phospholipids[142].

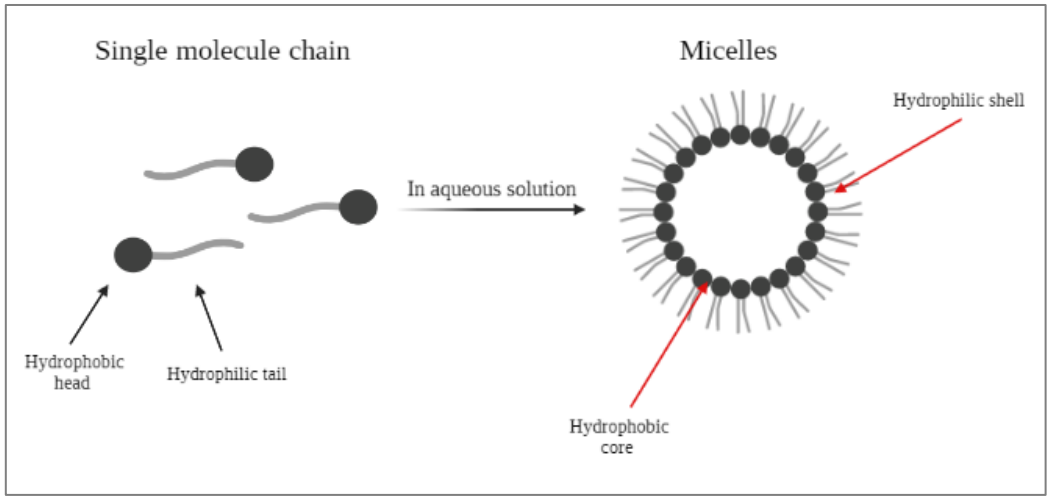

Figure 7. Assembling of Micelle structure in aqueous solution. (Image adapted from Hanafy et al. *Cancers (Basel)* 2018)

The formation of micelles in an aqueous solution occurs when the concentration of the block copolymer increases above a concentration named critical micelle concentration (CMC). At the CMC, the hydrophobic segments of block copolymers are associated to reduce the contact with water molecules, making a vesicular or core-shell structure [130,140]. According to the quality of solvent, length of blocker chain, nature of the blocker, and temperature, micelles can be assembled in different structures, such as spheres, rods, tubules, lamellae, and vesicles[143,144]. According to the types of amphiphilic molecules, they can be divided into lipid, polymeric and lipid-polymeric hybrid micelles. Lipid micelles have two limitations: a low drug loading encapsulation due to the small hydrophobic core, and faster dissociation when diluted in body fluids or cell culture medium[145]. Drug delivery applications of polymeric micelles include the encapsulation of hydrophobic anti-infectives such as amphotericin B and cancer drugs like paclitaxel, doxorubicin, and cisplatin[146]. To load a drug in an amphiphilic micelle there are two methods: drug conjugation and drug encapsulation. Drug conjugation utilizes a non-water-soluble drug as a hydrophobic core of the micelle, which is conjugated to the hydrophilic polymer backbone[147]. The drug encapsulation of hydrophobic drugs into the core of a core-shell nanostructure can occur by self-assembly process via hydrophobic interactions[146].

1.3.4 Nanobubbles

Polymeric nanobubbles (NBs) are spherical core/shell nanostructures filled by gas or vaporizable compounds (i.e., perfluorocarbons) with a nanometre order size[114,148]. Initially, NBs were designed as contrast agents[149,150] being efficient reflectors of ultrasound (US) energy, producing asymmetric oscillations when exposed to acoustic fields. Also, NBs were studied for diagnostic imaging, gene, and drug delivery for a targeted release[114,148,151–153]. NBs nanotechnology revealed extraordinary potential as a drug delivery system phase-change system that combines the advantages of NPs with the acoustic properties of NBs. This concept was pioneered by Rapoport and uses perfluorocarbons that can remain liquid at room and body temperatures but can vaporize upon application of US[148,154]. To increase the longevity of NBs, inert gas with very poor aqueous solubility for core composition is used, such as perfluorocarbons (PFCs) (i.e., perfluorobutane, perfluoropentane), thus reducing the dissolution rate of internal gas from NBs. Notably, the solubility of the gas used plays an important role in the stability of bubbles in the bloodstream. The encapsulation of PFCs can increase the half-life of various bubble systems. Firstly, PFCs have been studied to obtain phase-change contrast agents[155]. PFCs are biologically inert, safe, and their *in-vivo* excretion route is via the pulmonary capillaries[156,157]. Furthermore, for PFCs with the boiling points near-physiological temperatures (i.e., perfluoropentane), which allow liquid droplet generation at room temperature; their exposure to physiological temperatures could result in superheated droplets[148].

NBs are liquid droplets with a PFC (or oxygen, air, sulfur hexafluoride) core stabilized with a lipid, protein, polymer (chitosan, PLGA, PEG, PCL, dextran), or particle-based shell[148,158] (Figure 9). The composition of the NBs coating is a crucial factor to obtain spherical systems. Because of this, a key factor to consider in NBs formulation is shell composition, its thickness, elasticity that determine NBs stability. The shell of NBs consists of lipids or polymers for stability enhancement against gas loss, dissolution, and NBs coalescence[148]; also giving more opportunities for functionalization and targeting of the NBs[159].

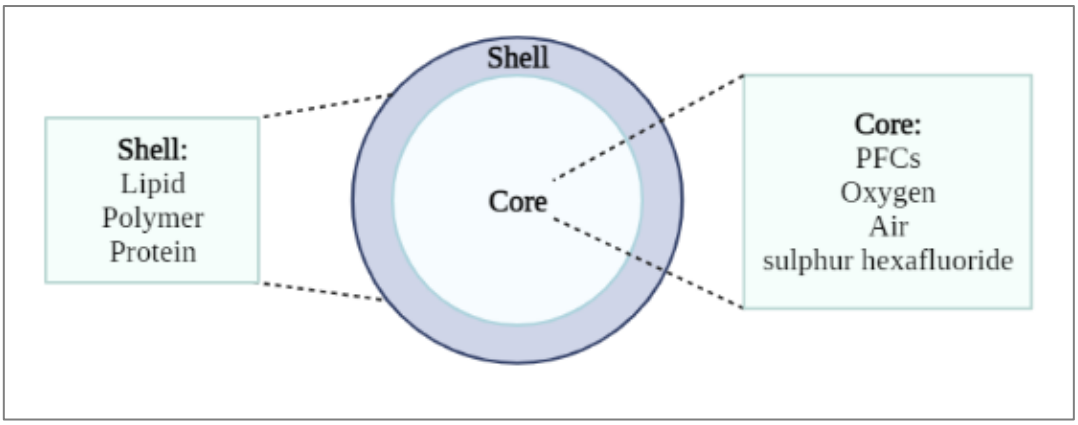

Figure 9. Schematic representation of nanobubble structure.

There are several NBs loading strategies, such as encapsulated drugs into NBs core, or incorporating drugs within the shell through covalent or noncovalent interactions (Figure 10) and the encapsulation of the drug attached to the NBs surface[148,159–161].

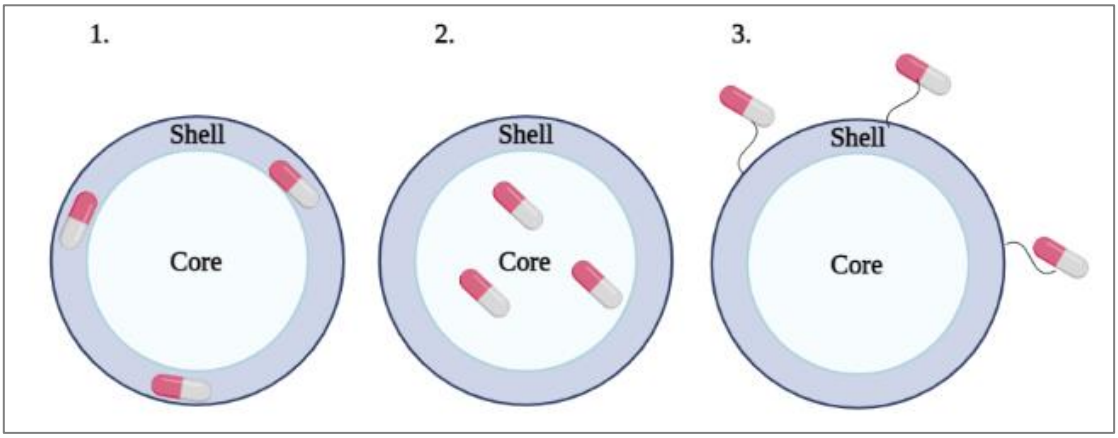

Figure 10. Simplified sketch of the main drug-loading techniques in NBs. Drugs can be embedded in the shell (1), incorporated in the core, in the case of gases or molecules soluble in PFCs (2), covalently attached to the surface (3).

By electrostatic interaction, the drug is associated with the NBs shell. Using this technique, a hydrophobic drug or charged components (such as nucleic acids) can be easily combined electrostatically with the shell when anionic/cationic lipids or polymers are present. This method has been used for gene delivery. The problem of electrostatic loading is the early release in the body. However, to overcome these limitations multilayer systems have been proposed. When the physicochemical properties of the drug allow its solubilization, the NBs core can act as a reservoir. Therefore, lipophilic drugs can be dissolved in PFCs. Otherwise, drugs can be previously loaded into a nanostructure, which can then be linked to the NBs surface. Loading on the NBs shell can also be achieved using ligand-receptor interactions[148,159–161].

Targeted NBs

Targeted NBs is an efficient drug delivery system, which is due to their capability in achieving the highest accumulation of cytotoxic agents in a specific site. This approach modifying drug pharmacokinetics and biodistribution can improve the effectiveness of treatment, and limit side effects. Targeted delivery may be achieved passively or actively[148]. With active targeting, the NBs are modified on the surface to enhance their tumor selectivity and reduce nonspecific toxicity.

Jiang et al. designed a novel Herceptin-targeted NBs for diagnosing and evaluating the treatment response of Her-2-positive breast cancer, so the NBs-Her binding tumor cells *in-vitro* therefore with a long-acting contrast enhancement[162]. NBs were conjugated with the tumor-targeting monoclonal anti-HLAG antibody (mAbHLA-G), exhibited targeted efficiency on tumor tissues, and enhanced tumor-targeting ultrasound imaging[163]. NBs conjugated with specific target asparagine–glycine–arginine peptide (NGR) -containing cell-penetrating peptide (CPP) decorated DOX and CPP decorated c-myc siRNA were constructed. NGR-modified NBs containing CPP-DOX and CPP-siRNA can realize time- and spatial-controlled drug delivery in the tumour[164].

Chitosan NBs loaded with perfluoropentane were designed for the delivery of doxorubicin into anaplastic thyroid cancer cell lines. The combined treatment with NBs loaded with doxorubicin and extracorporeal shock waves (ESWs) caused an approximate 40% reduction in drug GI50[165]. Zhou et al. have studied doxorubicin (DOX)-loaded chitosan NBs in breast cancer and assessed their drug delivery capacity. The results showed that DOX-NBs effectively delivered DOX into cancer cells and the US irradiation promoted the release of DOX from DOX-NBs *in-vitro*[166]. Oxygen-loaded nanodroplets (OLNDs), filled with oxygen-solving 2H,3H-decafluoropentane, and shelled with polysaccharides were proposed as a promising tool to counteract hypoxia by releasing oxygen amount in a time-sustained manner. Low weight chitosan emerges as the best biopolymer for OLND application as a skin device to treat chronic wounds[167]. Chitosan NBs can be considered as a tool to ultrasound-responsive formulations for targeting DNA delivery. Indeed, Cavalli et al 2012, have produced DNA-loaded chitosan NBs to gene delivery system. The in-vitro and *in-vivo* anticancer effects of a formulation of-cyclodextrin nanosponges containing DOX (BNS-DOX) were evaluated in breast cancer. BNS may be a strategy to deliver DOX in the treatment of breast cancer since it improves the anti-cancer efficacy[168]. Argenziano et al. have studied the NBs functionalized with anti-CD1a antibody to target dendritic cells (DCs) in immunotherapeutic treatment of cancer. The antiCD1a-NBs showed the capability to induce activation of DCs and stimulate a specific immune response able to delay tumor growth *in-vivo*[114].

1.4 Inorganic NPs in Nanomedicine

Inorganic NPs are investigated both in preclinical and clinical studies for therapeutic and diagnostic purposes, especially in oncology[60,112,169,170]. Inorganic NPs exhibit different material proprieties, such as optical and magnetic proprieties, fluorescence, near-infrared (NIR) absorption, and Raman enhancement making them extremely useful in image-guided therapies. Therefore, inorganic NPs are suitable in magnetic resonance (MRI), compound tomography (CT), position emission tomography (PET), surface plasmon resonance (SPR), and as image contrast agent[112,171]. Inorganic NPs (gold and iron oxide) increased effectiveness both as a nanocarriers for antimicrobic drugs and as nanobiocides due to intrinsic antimicrobial proprieties[172,173]. NanoThermr magnetic fluid is an aqueous colloidal dispersion of iron-oxide NPs is a therapeutic formulation approved in Europe for GBM treatment for enhancing the chemotherapy[60]. Functionalized gold NPs with PEG and coumarin were found to show efficient incorporation capacity into breast cancer without toxicity in normal cells[174].

Carbon nanotubes (CNTs) are the hexagonal arrangement of carbon atoms that leads to cylindric nanostructure formation and capped at one or both ends by buckyball[47,112]. CNTs can be classified into two categories: single-walled (SWNTs), which consist of one sheet of cylinder graphene, and multi-walled (MWNTs), which have some concentric graphene layers[112,175]. SWCNTs are used as contrast agents in several imaging modalities, such as MRI, Raman spectroscopy, PET, NIR, and radionuclide-based imaging[175]. Due to the unique properties of CNTs, such as their ultrahigh surface area and electrical mechanical, the CNTs can be integrated into their walls and tips peptides, drugs, and nucleic acids. Functionalized CNTs with a specific ligand for surface proteins expressed in cancer cells, can bring chemotherapeutic drugs more effectively into the cells, which makes CNTs an ideal candidate for drug delivery and image applications[175,176].

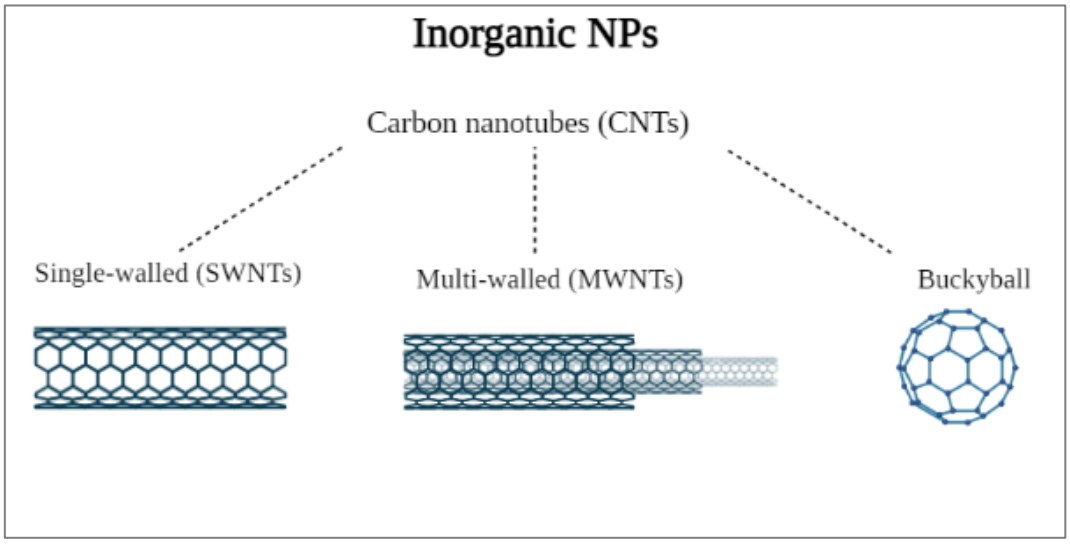

Figure 8. Schematic representation of the different types of carbon nanotubes.

1.5 NPs in GBM

Regarding the potential use of a nanoparticle-based approach for GBM treatment, nanotechnology has provided us with a promising tool that can be used to enhance the uptake of drugs across the BBB[177]. Moreover, despite our improved understanding of the molecular characteristics of GBM, treatments targeting specific molecular pathways remain limited[178]. Tumor-associated antigens (TAAs) have gradually become a GBM research hotspot. TAA is peptides present on a tumor that can also be presented on other non-malignant tissues[179]. TAAs can be overexpressed or downregulated and regulate many features of GBM such as proliferation, migration, vascularization, immune evasion, and therapeutic limitation[180]. Therefore, TAAs can also be targeted in the clinical setting if they are overexpressed on tumor cells[179]. Hence, identify potential new tumor antigens in primary brain tumors that were not previously defined, GBM patients may benefit from active specific targeting. Regarding GBM treatment, Nance et al. demonstrated that PEGylated PTX-loaded NPs significantly delayed GBM growth following local administration, as compared to PTX-loaded PLGA NPs or unencapsulated PTX. Thus, the enhanced distribution of PTX loaded PLGA-PEG NPs to the tumor infiltrative front and the resulting reduction of tumor growth demonstrates that NPs penetration within the brain tumor parenchyma improves therapeutic efficacy[181]. Other authors developed transferrin-functionalized PEGylated NPs (Tf-NPs) that can be used to deliver TMZ and bromodomain inhibitor JQ1 across the BBB in orthotopic mouse GBM models. TF-NPs with combination therapy showed a decrease of tumor burden and prolonged survival compared to mice treated with free drug combinations or TMZ and JQ1 in non-functionalized NPs, thus demonstrating the potential use of this DDS to deliver novel combination therapies to gliomas[182]. Moreover, Ramalho et al. developed receptor-mediated TMZ-loaded PLGA NPs for GBM functionalized with OX26 anti-Transferrin R (TfR). The cellular internalization of TMZ-PLGA-OX26 NPs was enhanced compared to PLGA NPs without functionalization[183]. To maximize the therapeutic effect of chemotherapeutic drugs and their accumulation in glioma, a specific ligand (RVG29 peptide) that can combine with acetylcholine receptor was conjugated with PEG-PLGA NPs loaded with DTX. RVG29-PEG-PLGA NPs displayed good penetrating ability and accumulation in glioma tissue *in-vivo*[32]. Gao et al. developed a new formulation DTX-loaded albumin-lipid NPs (DNPs) for GBM treatment. *In-vitro* DNPs showed apoptotic induction and cell proliferation inhibition. *In-vivo* imaging indicated that DNPs localize and accumulate in GBM, these NPs resulted in lower toxicity and conducted greater effect anti-GBM compared to free drug[43]. Ephrin type-A receptor 3 (EPHA3) tyrosine kinase antibody-modified PLGA NPs were developed to target GBM. *In-vitro* cell cytotoxicity and cellular uptake of NPs demonstrated the anti-EPHA3modification could enhance GBM targeting. *In-vivo* studies of NPs showed that EPHA3-modified NPs exhibited high

accumulation in GBM tissue, and it caused the increased tumor cell apoptosis and prolonged the median survival time of rats[184]. Because of the upregulated expression of neuropilin (NRP) in both GBM and endothelial cells of angiogenic blood vessels, the ligand of NRP, tLyp-1 peptide was functionalized to the surface of PLA-NPs to mediate the penetration into the GBM. tLyp-1-NPs exhibited enhanced cellular uptake in both endothelial and Rat C6 cells, increased cytotoxicity of the loaded PTX, improved penetration, and growth inhibition in C6 GBM spheroids[185].

1.6 NPs across the BBB

Drug delivery and tumor uptake are affected by biochemical parameters such as shape, size, charge, polarity, lipophilicity, biocompatibility, stability, and systems via EPR effect[119,186,187]. In literature has highlighted the main characteristics that must have the nanocarrier to overcome the BBB, such as high lipophilicity and the size (~30–100 nm in diameter). Whereas NPs with diameters> 200–300 nm were also able to extravasate into tumors due to differences in vascular permeability, they showed a lower capability to pass the BBB. Moreover, the NPs can be functionalized with molecular ligands that can facilitate the transport across the BBB[36,188–190]. Ohta et al. have investigated the widening of BBB tight junctions via focused ultrasound (FUS) offer a promising approach for enhancing the delivery of gold NPs (AuNPs) into the brain. FUS exposure significantly increased permeation across an *in-vitro* BBB model, and the permeability was higher with a smaller diameter (3 nm). However, *in-vivo* results showed that medium-sized particles (15 nm) were the highest delivery efficiency into the brain[191]. Another group has studied venlafaxine (VLF)-loaded poly (lactic-co-glycolic acid) (PLGA) NPs were surface-functionalized with two ligands against transferrin receptor to enhance access to the brain. In-vitro studies showed that encapsulated VLF was not affected by P-gP pump efflux increasing its concentration in the basolateral side after 24 h. *In-vivo* studies demonstrated that empty NPs travel via a direct nose-to-brain route whereas functionalized NPs reach the brain by receptor-mediated endocytosis[192]. Another study was focused on synthesizing a novel type of dendrimer with poly (propylene imine) core and maltose-histidine shell (G4HisMal) assessing if the maltose-histidine shell can improve the ability to cross the BBB. *In-vivo* studies suggested that a G4HisMal shell can be used to improve biocompatibility and ability to cross the BBB of dendrimers[193]. Kadari et al. in this study, angiopep-2, a ligand for the lipoprotein receptor-related protein 1 (LRP 1) receptor, was grafted on the surface of SLNs for the delivery of DTX. *In-vitro* studies of the peptide-functionalized NPs (A-SLN) showed increased cytotoxicity and enhanced cellular internalization than that of unconjugated NPs. *In-vivo* studies of pharmacokinetics and biodistribution showed selective targeting with higher accumulation of A-SLN in the brain, and the

mean animal survival time of the animals was significantly enhanced compared to free DTX[45]. Moreover, another group studied different kinds of PLGA NPs modified with a mutated form of diphtheria toxin (CRM197) covalently coupled PLGA with different fluorescent probes and different ligands (g7 and CRM197) tested *in-vivo* to assess their behavior and trafficking cross the BBB. The results highlighted that CRM-197 modified NPs and g7-NPs can cross the BBB at a similar extent[194].

1.7 Glypican family

Glypicans (GPC) are members of a larger HSPGs (membrane-bound heparan sulfate proteoglycans) family[195–197] which includes the glycerophosphatidylinositide (GPI)-anchored type, which is at the surface of the membrane (such as glypicans), the transmembrane type (such as syndecans), and the extracellular matrix type (such as perlecan)[196]. The structure of GPCs is consisting of three key features: a core protein, HS chains, and a GPI linkage that anchors GPCs to the exocytoplasmic surface of cellular membranes[198].

They can be classified according to the structure of protein cores. Their structural heterogeneity can be generated through specific heparan sulfate (HS) chain modification during their biosynthesis. Therefore, the nature of the core proteins and modifications of HS-GAG chains can determine the specificity and function of HSPGs[199].

GPCs are composed of six glypican members in the human genome (GPC1 to GPC6). They are structured as GPI-anchored core proteins substituted with three chains of HS near its C-terminus[196,197,200,201]. The structure of GPCs is highly conserved within the family[198]. Based on sequence comparisons, GPCs are divided into two subfamilies: one composed by GPC1, GPC2, GPC4, and GPC6 and a second composed by GPC3 and GPC5 There is about 25% of amino acid identity between the groups[196,197,201,202].

Gene name	Location	Gene accession number (GenBank)	Number of amino acids
Human			
GPC1	2q35-37	NM_002081	558
GPC2	7q22,1	NM_152742	579
GPC3	Xq26	NM_004484	580
GPC4	Xq26.1	NM_001448	556
GPC5	13q32	NM_004466.3	572
GPC6	13q32	NM_005708.2	555

Table 2. Glypicans in humans. (Adapted from Filmus et al., *Genome Biol.* 2008)

The mature forms of GPCs have a core protein of 60 to 70 kDa in size and are around 550 amino acids in length. It is comprised of an N-terminal secretory signal peptide, 14 evolutionarily conserved cysteine residues in a 50 kDa domain, and a hydrophobic domain for the addition of the GPI anchor at the C-terminus (Figure 11)[197,200–203]. HS chain attachment sites are located close to the c-terminal

of the core protein (Figure 11). HS chain synthesis is initiated at the serine residues, which are a part of a Ser-Gly consensus sequences group present near each other[195,203].

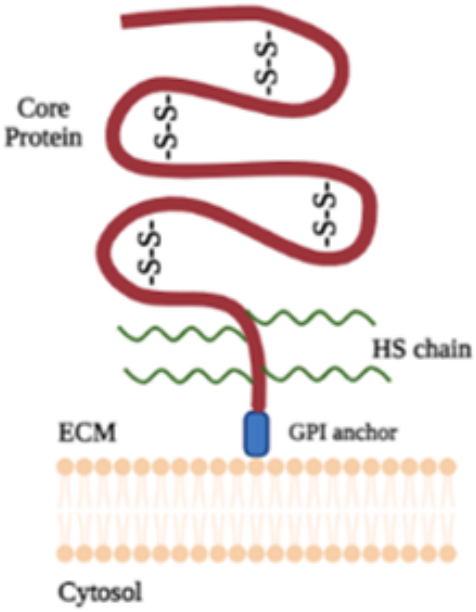

HSPG	No of HS attachment sites	Attachment site on protein core
GPC1	3	
GPC2	2	
GPC3	2	Ser-Gly dipeptides
GPC4	3	
GPC5	4	
GPC6	4	

Figure 11. Schematic representation of glypican structure showing the core protein, HS chain, and the GPI anchor. HS chains are covalently attached to Sr-Gly dipeptide sequences on the core protein via a tetrasaccharide linkage. The core protein is linked to the plasma membrane by the GPI anchor.

GPCs are predominantly expressed during embryonic development[204]. GPCs are involved with important roles in cellular signaling, cell adhesion, motility, proliferation, differentiation, morphogenesis, tumorigenesis, and progression of cancers[204–206].

1.7.1 Glypican-1 (GPC1)

GPC1 is a protein (of 558 amino acids) that can be found both in a membrane-anchored form (by GPI at S530) and in a secreted soluble form. The GPC1 protein is composed of an N-terminal core (residues 24–474) and a C-terminal GAG attachment region (residues 475–530), ending with a sequence of hydrophobic residues that link it to the GPI anchor (Figure 12). The GPC1 protein is decorated with two N-linked glycans at positions Asn-79 and Asn-116 and is also substituted with three chains of HS at Ser-486, Ser-488, and Ser-490[197].

The crystal structure of GPC1 core protein shows a stable α-helical domain, which is densely packed and is globular in shape[202]. The core protein structure also shows the arrangement of 14 conserved cysteine residues, forming six disulfide bonds near the N-terminus, with most linkages present in a cysteine-rich domain (CRD)[200,202].

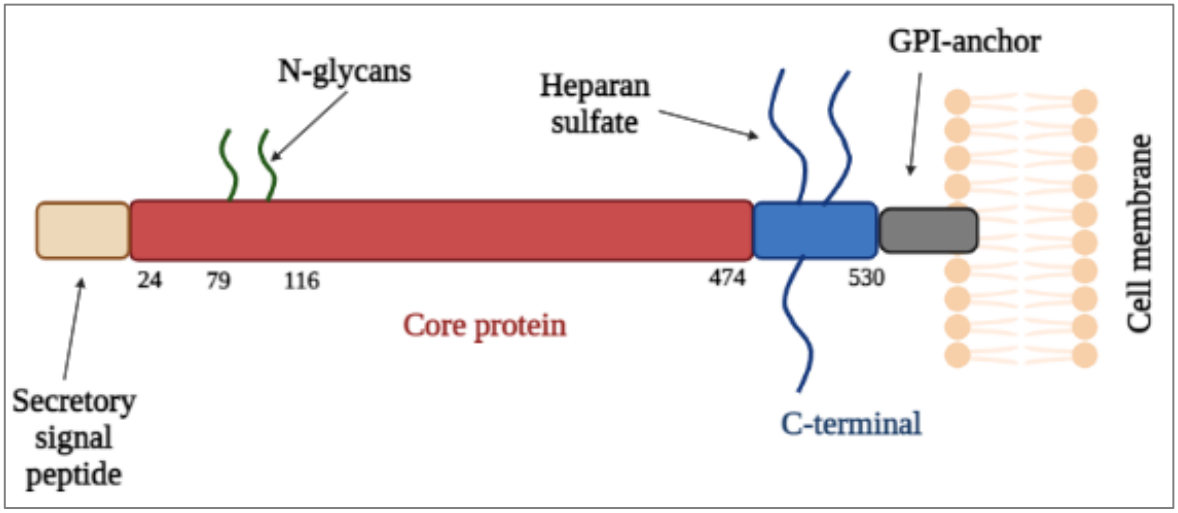

Figure 12. Schematic of GPC1 core protein linked to the cell membrane by its GPI anchor, with *N*- and *O*-glycosylation positions annotated and the Cys residues.

The heparan sulfate chains are covalently linked to the core protein, when anchored to a cell, allowing GPCs the ability to sequester and retain growth factors from the environment to signaling molecules on the cell surface[206,207].

GPC1 is normally expressed during embryonic development, it is expressed in the brain, skeletal system bone marrow, and kidney development. It is no required for normal adult tissues[196,197,204,206,208,209]. It is, overexpressed in a variety of solid tumors such as glioma[210], glioblastoma[211], pancreatic cancer[212], breast cancer[207], prostate cancer[213], esophageal squamous cell carcinoma (ESCC)[214] and epithelioid mesothelioma[215]. GPC1 regulates tumor growth, proliferation,

invasion, metastasis, and angiogenesis, through modulation of tumor cell biology as well as influence on the tumor microenvironment (TME)[196,197,203,206].

The HS chains of GPC1 interact with several factors, such as Wnt, hepatocyte growth factor (HGF), fibroblast growth factor (FGF), transforming growth factor-β (TGF-β), vascular endothelial growth factor A (VEGF-A), and regulates various pathways associated with tumor progression[196,203,206].

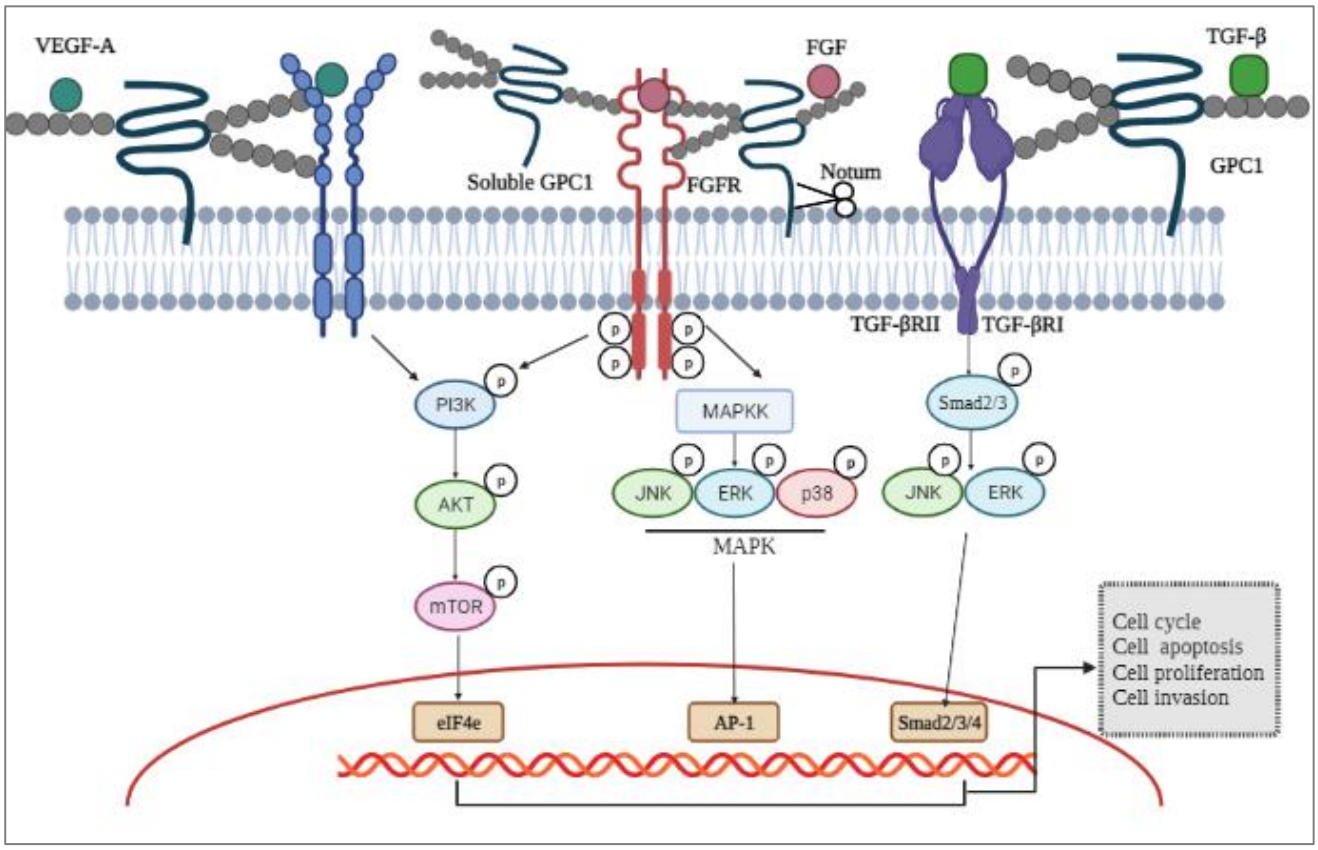

Figure 13. GPC1 modulates signaling pathways in cancer progression. The HS side chains of GPC1 bind both growth factors (such as VEGF-A, FGF-2, and TGF-β) and their receptors, to facilitate their assembly for enhanced signaling in PI3K/AKT, MAPK, Smad pathways. GPC1 can be cleaved by Notum and then released into the extracellular space, which can compete with the GPC1 anchored on the cell membrane to inhibit its function. (Adapted from Wang et al., *Front. Oncol* 2019)

Regarding the interaction of GPC1 and Wnt, it has been shown that the overexpression of GPC1 inhibited Wnt signaling, therefore exerting a negative regulatory role on Wnt signalling[216]. Also, GPC1 acts as a co-receptor for FGF-2 and heparin-binding growth factors (HBGFs) signaling pathway[209], influencing the mitogenic response of tumor cells and tumor growth[217]. GPC1 also modulates the TGF-β signaling pathway. Gene expression of GPC1 is upregulated when tumor cells are stimulated with Wnt and TGF-β in combination. Wnt signaling known to be regulated by GPC1 is critically involved in angiogenesis, through regulation of VEGF transcription[196,203,206].

1.7.2 GPC1 in GBM

GPC1 is overexpressed in human GBM. GPC1 is involved in neoplastic growth, migration, proliferation, and chemotherapy resistance in GBM. GPC1 and FGF-2 co-stimulated activity were identified as having a crucial role[210]. In particular, GPC1 overexpression in glioma vessel endothelial cells contributes to FGF-2 responsiveness and tumor angiogenesis[218]. Overexpression of GPC1 resulted in increased angiogenesis and radiation resistance in brain GBM[196,218]. The overexpression of GPC1 in GBM cells enhanced FGF-2-stimulated proliferation of cells by enhancing FGF-2 signaling, whereas knockdown of GPC1 reduced cellular growth and proliferation. These findings demonstrated that GPC1 overexpression promotes the proliferation of GBM cells[219]. Listik et al. by generating GPC1-silenced clones in GBM cells showed that the transcriptional profiles of β-catenin and MMP9 were affected by GPC1 expression in GBM cells. By downregulating GPC1, β-catenin expression was reduced, which may indicate a reduction in canonical Wnt signaling in GBM. These findings also suggest that GPC1 directly affects β-catenin expression[220]. Moreover, it has been shown that GPC1 influences GBM cellular migration and adhesion. When GPC1 was silenced, migration activity was highly reduced or almost abolished. Therefore, it has been suggested a fundamental role of GPC1 in tumoral cells' migration is the migration one of the primary factors associated with the proliferation of GBM[220,221]. By downregulating the expression of GPC1, was impeded the tumor growth, indicating GPC1 is a vital element in GBM tumorigenesis[220]. GPC1 expression is significantly correlated with the occurrence of dissemination and shorter overall survival (OS) for patients with GBM treated with radiotherapy and TMZ. Also, GPC1 may be associated with resistance mechanisms of alkylating agents in GBM[220,222]. GPC1 expression is strongly correlated with tumor dissemination and may be important for predicting OS in patients with GBM[211]. Annexin A2 (ANXA2) increased the expression of GPC1 via c-Myc, and the upregulated GPC1 further promotes the c-Myc level, thus creating a positive feedback loop, which enhanced the proliferation of glioma cells. Therefore, the combination of ANXA2 and its downstream target GPC1 can be used for improved prognostic evaluation in glioma patients[219].

1.8 Protein production from Hybridomas

In the present thesis, the Hybridoma technology has been used (Figure 14) to produce specific antibodies against the GPC1 protein. It is a multi-step process that takes advantage of a host animal's natural ability to produce highly specific and functional (monoclonal antibody) mAbs. A host animal is immunized with the specific immunogenic antigen (GPC1) for several weeks. Later, B lymphocytes of the spleen of mice (that produces antibodies) are collected, in turn, fused with immortal B cancer cells, myeloma, to produce hybridoma cells that have the same features of mothers' cells, the propriety to secreting a specific mAb anti-GPC1 and the immortality. The fused cells are then selected on a hypoxanthine-aminopterin-thymidine (HAT) medium. The myeloma cells are sensitive to the HAT medium as they lack the hypoxanthine-guanine phosphoribosyltransferase (HGPRT) gene required for nucleotide synthesis by the de novo or salvage pathways, while the unfused B cells die as of short lifespan. In this way, only the hybridoma cells survive since they have the functional HGPRT gene from the B cells[223,224].

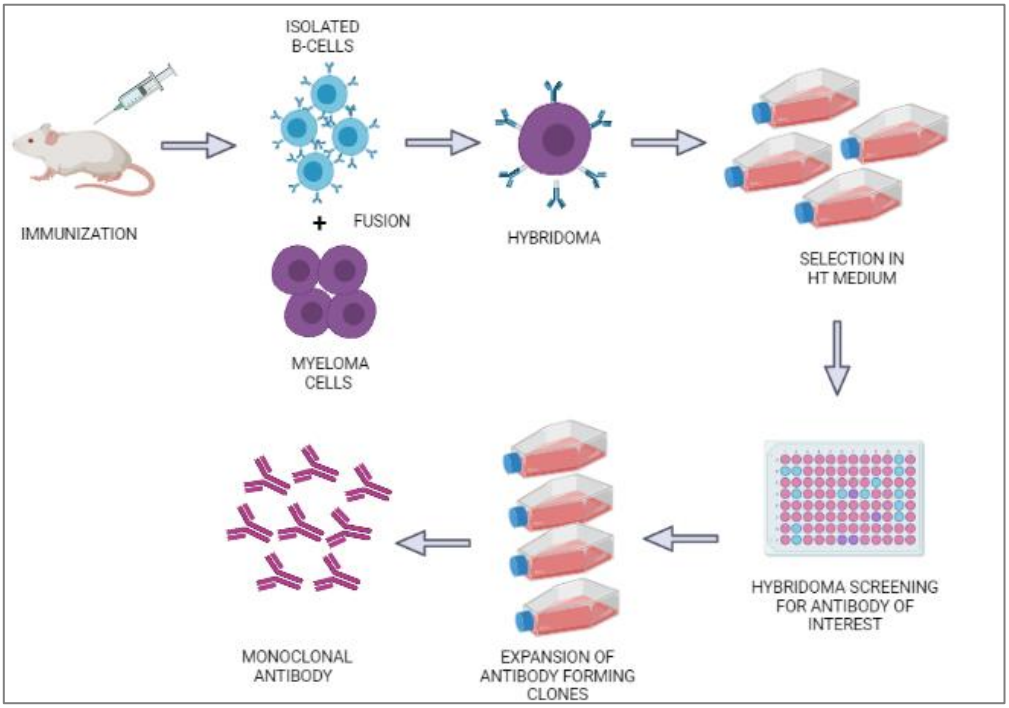

Figure 14. Graphical summary of the Hybridoma Technology flowchart. Generation of mAb anti-GPC1 by immunizing animals with GPC1. The somatic fusion of B lymphocytes of the spleen with immortal myeloma cells gives rise to hybridoma cells. These last are selected in HAT media and finally, cells will be secreting mAb against specific GPC1. (Adapted from Parray et al., *Int Immunopharmacol*. 2020)

2. Aim

GPC1 is overexpressed in breast, pancreatic, esophageal cancers, and GBM whereas it is not expressed or expressed at negligible levels in healthy tissues.

For these reasons, the GPC1 represents a specific tumor-associated antigen, is expressed in GBM tumors, therefore anti-GPC1 antibody can be used for the functionalization of nanoparticles specifically directed only to the GBM cells. In this context, chitosan, a natural polycationic polysaccharide, can be used as a component of nanoparticles, including NBs, for its biocompatibility, biodegradability, low toxicity, and no immunogenicity. Specifically, NBs, spherical nanosized core/shell structures filled by gas or vaporizable compounds, can be particularly useful for the delivery of drugs.

Thus, the main goal of this project is to use highly biocompatible chitosan NBs conjugated with an anti-GPC1 antibody loaded with docetaxel as a chemotherapeutic agent, for GBM treatment. This approach will allow major challenges in the context of GBM treatment, including overcoming the BBB, allowing the therapeutic release exclusively to tumor cells, and minimizing the possible toxic side effects in cancer patients, as well as reducing the treatment resistance.

The specific aims of this study are:

- Evaluation of GPC1 as a useful target for drug delivery with NBs.
- Production and characterization of a specific anti-GPC1 antibody.
- *In-vitro* characterization and efficacy of anti-GPC1 NBs loaded with docetaxel in GBM cell lines.
- *In-vivo* test the biodistribution of anti-GPC1 NBs in GBM mice models.

3. Materials and Methods

3.1 Reagents and Cell Culture Conditions

The glioblastoma multiforme cell line (T98G) and the U87MG likely glioblastoma cell line (provided by ATCC) were grown as indicated by the suppliers. Hepatocellular carcinoma cell line (Huh-7) was cultured in a DMEM medium (Sigma-Aldrich, Milan, Italy). Acute T cell leukemia (Jurkat) was cultured in RPMI-1640 medium (Sigma-Aldrich, Milan, Italy).

3.2 Evaluation of GPC1 expression

For the evaluation of GPC1 expression on cells, the anti-GPC1 polyclonal antibody (PA5-28055, Invitrogen, USA) was used. The anti-vinculin antibody (E-AB-27406) (Elabscience, USA) was used to evaluate Vinculin as the housekeeping gene. Secondary antibodies were from Abcam: anti-rabbit HRP (Abcam, Cambridge, UK), anti-mouse HRP (Abcam, Cambridge, UK). Secondary antibodies were from Thermo Fisher Scientific (MA, USA) anti-mouse Alexa Flour 488, anti-mouse, and anti-rabbit Alexa Flour 594 (Bethyl).

3.2.1 Western Blot

The cell pellets (from 2 x 10^6 cells) were resuspended into RIPA buffer supplemented with a protease inhibitor mixture (Complete-EDTA, Roche, Switzerland) for protein extraction. And 25μg of proteins were run in 8% denaturing polyacrylamide gel. After electrophoresis, the proteins were transferred to the nitrocellulose membrane (Whatman International Ltd, UK). The membranes were blocked with 5% milk in Tris-buffered saline Tween-20 solution (TBS-T) and incubated overnight with primary antibodies. After washing, the membranes were incubated for 1 h with secondary antibodies in 5% milk TBS-T at RT. The membranes were developed with ECL solution (Euroclone, Italy) and visualized with the ChemiDoc Imager instrument (Bio-Rad Laboratories, CA, USA).

3.2.2 Flow Cytometry

To evaluate GPC1 expression in GBM cell lines, Huh-7 and Jurkat cells were incubated at the density of 50^4 cells with anti-GPC1 antibody for 1 hour in agitation at RT. Then, cells were washed twice and incubated with a secondary antibody for 1 hour in agitation, RT, and dark. All experiments were performed on FACSCanto II (BD Biosciences). The measurements, 10,000 events were acquired by FACSCanto II (BD Biosciences), and flow cytometry data were analyzed by CELLQuest software (Becton Dickinson).

3.2.3 Immunofluorescence

GBM cells were seeded at a density of 25 x10^3 cells on poly-lysine coated coverslips. After fixed in 4% paraformaldehyde (Sigma-Aldrich) in PFA for 15 min. Cells were blocked with 2% BSA in PBS for 1 h to avoid nonspecific bonds. Samples were incubated with primary antibody, at 4°C ON. Samples were washed three times and incubated with a secondary antibody for 1h at RT. Then the sections were stained with DAPI (Sigma-Aldrich) for 5 min, to stain the cell nuclei, and then mounted using Prolong anti-fade mounting medium (Light AntiFADE Kit, Molecular Probes Invitrogen). The sections were then observed by a Leica fluorescence microscope (Leica DMI 4000B, Germany), photographed with a Retiga 200R digital camera (QImaging, Surrey, BC, Canada).

3.2.4 Immunofluorescence of frozen tissue section

Tumour tissues were cut with a cryostat (thickness 5–7μm) and treated with 4% paraformaldehyde (Sigma-Aldrich) diluted in PBS for 10 min at room temperature to fix the sample on the glass slides. Then, the samples were incubated with PBS with Triton X100 0.1%for 15 min to permeabilize the tissue. The samples were then blocked with 2% BSA in PBS for 1 h, to block aspecific sites to which the primary antibody could bind. The samples were incubated with primary antibody, at 4°C ON in a humid chamber. Samples were washed four times and incubated with a secondary antibody, at 4°C in a humid chamber. Then the sections were stained with DAPI (Sigma-Aldrich) for 5 min, to stain the cell nuclei, and then mounted using Prolong anti-fade mounting medium (Light AntiFADE Kit, Molecular Probes Invitrogen). The sections were then observed by a Leica fluorescence microscope (Leica DMI 4000B, Germany) using different magnifications.

3.3 Production of a specific antibody against GPC1 protein

3.3.1 Antibody production by immunization of mice

The anti-GPC1 antibody development was performed with the group of Professor Paolo Macor (University of Trieste) and in collaboration with an external company. To produce specific anti-GPC1 antibodies recognizing the cell surface form of GPC1, it was designed and synthetized of cDNA for *in-vivo* expression of GPC1. Quality control of the expression by FACS using the commercial antibodies. After, it was proceeded to the immunization of 5 mice by genetic vaccination. To follow, hybridomas were generated from spleens antigen from mice with the highest titer. After immunization, the specificity of the obtained antibody clones was evaluated by testing serum of immunized mice by ELISA by using the GPC1 recombinant protein (LSBio) and by performing flow cytometry in GPC1-expressing cell lines and GPC1-not expressing cell lines as negative controls. Hybridomas were obtained from three different clones showing specificity for GPC1 expressing cells. The supernatant of hybridoma cultures was tested by flow cytometry to evaluate anti-GPC1 antibody production. Two (B and C) out of the 3 hybridomas were finally selected as hybridomas producing specific anti-GPC1 antibodies. The other hybridomas did not produce a sufficient amount of anti-GPC1 antibodies. Anti-GPC1 antibodies were finally purified by the supernatant of the hybridomas.

The capability of the purified anti-GPC1 antibodies (B and C) to recognize GPC1 was evaluated in the GPC1 expressing cell lines T98G and U87-MG by flow cytometry and immunofluorescence. After this first validation, the B antibody was selected. The capability of the purified B antibodies to recognize GPC1 was also evaluated in tumor masses grown in the GBM xenograft murine model obtained by injecting U87-MG cells in athymic nude mice. Finally, the specificity of anti-GPC1 B was evaluated in GBM primary tumor tissues and normal tissues by immunofluorescence.

3.4 Cytotoxic assays

3.4.1 Cell viability assays

Cells were seeded in 96-well plates (Becton Dickinson, NJ, US) at a density of 50^3 cells/well and incubated for 24 h to allow attachment of cells. The cells were incubated with the drugs or nanoparticles at the same concentrations for 48 h. After 48 h, cell viability was determined by CellTiter-Glo® Luminescence assay (Promega, Madison, Wisconsin, US) with an Infinite 200 PRO instrument (Tecan Trading AG, Switzerland) (Figure 15).

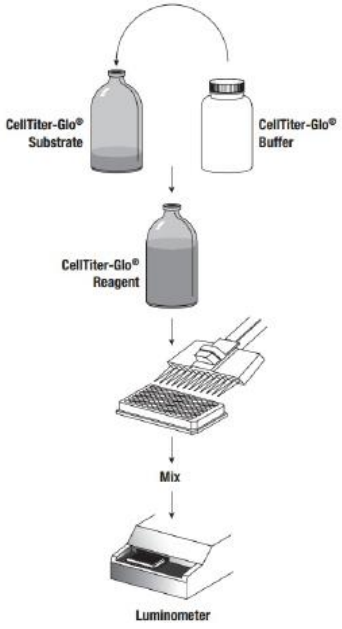

Figure 15. Flow diagram showing preparation and use of CellTiter-Glo® Reagent.

The CellTiter-Glo® Assay relies on the properties of a proprietary thermostable luciferase (Ultra-Glo™ Recombinant Luciferase), which generates a stable "glow-type" luminescent signal. The luciferase reaction for this assay is shown in (Figure 16).

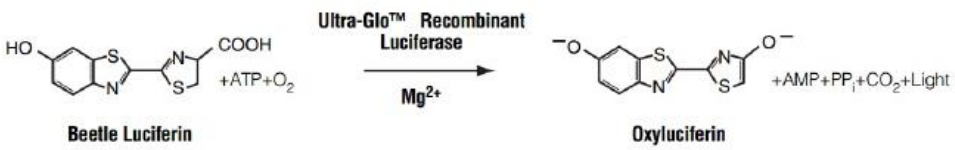

Figure 16. The luciferase reaction. Mono oxygenation of luciferin is catalyzed by luciferase in the presence of Mg2+, ATP, and molecular oxygen.

3.4.2 Annexin V and 7AAD assay

Annexin V and 7AAD assay was used for the detection of apoptotic and necrotic cells. Annexin V is Ca 2+ dependent affinity for phosphatidylserine that can be used to detect and measure apoptosis. 7-Amino-actinomycin-D (7AAD) is a nucleic acid dye that can be used for the exclusion of nonviable cells.

3.5 Nanoparticles

3.5.1 Preparation of chitosan NBs

Chitosan nanobubbles were obtained thanks to the collaboration with the group of Professor Roberta Cavalli of the University of Torino. Chitosan NBs were obtained using medium molecular weight chitosan (170,000 Da, degree of deacetylation 75%–85%) for the shell and a perfluorocarbon for the core. Briefly, to prepare the chitosan NBs, an ethanol solution containing Epikuron 200 (1% w/v) and palmitic acid was added to perofluoropentane and ultrapure water under stirring. Then, to obtain the NBs, a 2.7% w/v chitosan solution at pH 5.0 was added dropwise, whilst the mixture was homogenized using an Ultra-Turrax SG215 homogenizer (IKA, Konigswinter, Germany) for 3 minutes at 13,000 rpm. The NBs were then purified by ultra/diafiltration using a TCF2 instrument (Millipore) with a membrane cut-off at 100,000. To obtain DTX-loaded NBs, DTX was dissolved in the perfluoropentane core using ethanol as co-solvent, facilitating drug dissolution. The system was incubated for 30 minutes and subsequently characterized. Then, docetaxel was added to the blank NBs nanosuspension to obtain DTX loaded NBs (NB-DTX) at a concentration of 125µg/mL.

3.5.2 Docetaxel encapsulation and quantification in NBs

A weighted amount of freeze-dried NB-DTX was dispersed in 5 mL of ethanol and sonicated for 15 min. The sample was then centrifuged (10 min, 15,000 rpm) and after the supernatant was analyzed by High-Performance Liquid Chromatography (HPLC), to determine the DTX concentration in the NB.

The HPLC system consisted of a Perkin Elmer pump (Perkin Elmer PUMP 250B, Waltham, MA) equipped with a spectrophotometer detector (Flexar UV/Vis LC spectrophotometer detector, Perkin Elmer, Waltham, MA). A reverse-phase Agilent TC C18 column was used (150 cm ×4.6 mm, pore size 5µm: Agilent Technologies, Santa Clara, CA, USA). The column was eluted with acetonitrile/water (60:40) at a flow rate of 1 ml/min. Docetaxel was detected with a UV/vis detector at 230 nm. The drug concentration was calculated using an external standard method from a calibration curve. The linear calibration curve was obtained over the concentration range of 0.5-25 µg/ml with a regression coefficient of 0.998. The loading capacity of NB-DTX was calculated according to Loading capacity (%) = [amount of DTX/weight of NB-DTX] × 100. The encapsulation

efficiency of NB-DTX was determined using the formula: Encapsulation efficiency (%) = [amount of DTX loaded/total amount of DTX] × 100.

3.5.3 NBs conjugation with Cy 5.5

Fluorescent NBs were prepared binding cyanine 5.5 (Cy5.5, 10nmol/ml, FluoroLinkTM Cy5.5 Monofunctional Dye, GE Healthcare Bio-Sciences AB, Uppsala, Sweden) to the chitosan shell of NBs. The labeling of NBs with Cy5.5 was made by incubating the chitosan NBs with a Cy5.5 DMSO solution under magnetic stirring in the dark for 1 hour. The amount of Cy5.5 associated with the NBs surface was quantified by spectrophotometric methods. Molar extinction coefficients of 250,000 M^{-1} cm^{-1} at 678 nm for the Cy5.5 dye was used.

3.5.4 Evaluation of antibody concentration bounded to the NBs

The B antibody concentration bound to the NBs was measured by the Pierce BCA Assay protein Kit (Thermo Scientific, Rockford, IL USA). That Kit is a detergent-compatible formulation based on bicinchoninic acid (BCA) for the colorimetric detection and quantification of total protein. One mL of the BCA reagent was added to 100 µL of the sample and reacted for 30 min at 37 °C. After cooling to room temperature, the chromogenic product was measured by a UV-Vis spectrophotometer at 562 nm. The antibody concentration was calculated referring to a calibration curve obtained analyzing standard solutions in the concentration range between 0 – 200 µg/mL.

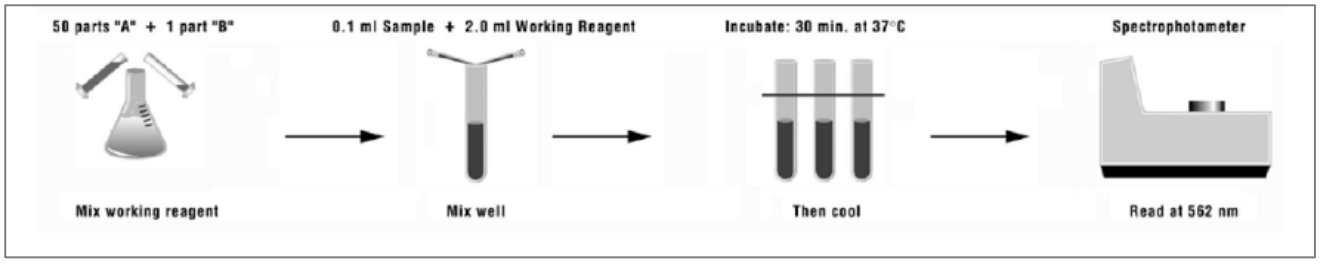

Figure 17. Flow diagram showing preparation and use of Pierce BCA Assay protein Kit.

3.5.5 NBs conjugation with anti-GPC1 antibody

The anti-GPC1 antibody (B) was oxidized by periodate oxidation and conjugated by reductive amination to chitosan amino groups using sodium cyanoborohydride to transform the reversible imine bonds (R−CH=N−R) into permanent amine bonds (R−CH2−NH−R).

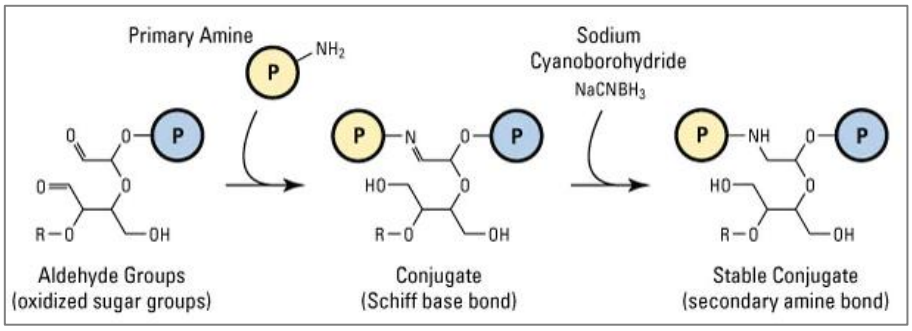

Figure 19. Reductive amination, the conjugation of aldehydes and primary amines. The initial reaction results in a weak, reversible Schiff base linkage. Reduction with sodium cyanoborohydride creates a stable, irreversible secondary amine bond.

3.6 Nanobubbles characterization

3.6.1 Dynamic Light Scattering

The size, polydispersity index (PDI), and zeta potential of NBs were measured by dynamic light scattering (DLS) 90 Plus Particle Size Analyzer (Brookhaven, NY, USA). The analyses were performed at a scattering angle of 90°C and a temperature of 25°C. The samples were diluted with water (1:30 v/v) immediately before the measurements.

3.6.2 Transmission electron microscopy

Transmission electron microscopy (TEM) analysis was performed using a Philips CM 10 (Eindhoven, NL) to observe the morphology of NBs. The NB nanosuspensions were sprayed on Formvar coated copper grid and air-dried before observation.

3.6.3 Nano Tracking Analysis

Nanobubble concentration and size distribution were determined by Nanosight –Nanoparticle Tracking Analysis (NTA). An NS300 NanoSight (Malvern Instrument, Worcestershire, UK) fitted with an NS300 flow-cell top plate, and a 532 nm laser was used. Data were analyzed on the NTA software 3.2 (Malvern Instrument, Worcestershire, UK). NB formulations were diluted with Milli-Q water 1:10000 immediately before analysis and loaded into the sample chamber before video recordings.

3.6.4 Cell Uptake Studies of NBs

T98G and U87-MG cells (30^3 cells/well) were seeded on Corning® cover glasses (Sigma-Aldrich) in a 6-well plate. The day after, the cells were incubated with NB-B-Cy 5.5 and NB-Cy 5.5 for 1 and 3 h. Then, the cells were washed with PBS, fixed with 4% PFA at RT for 15 min. Finally, coverslips were mounted, and the image acquisition was performed with a Leica SPE confocal microscope (Leica, Wentzler, Germany), with a 63× oil-immersion objective.

3.7. Animal studies

AthymicNude-Foxn1nu mice (immunodeficient mice) were purchased from Envigo (Udine, Italy). The experimental procedures were approved by the Italian Ministry of Health n° 788/2015-PR and performed in accordance with the institutional guidelines. We utilized female mice of 4-6 weeks of age. Data are reported as the mean and standard error of the mean.

The xenograft GBM model was obtained by injecting $5x10^6$ U87MG cells subcutaneously on the flank of nude mice with a 29G syringe needle in a volume of 100µl. When tumors reached a measurable size (> 50 mm^3), mice were treated intravenously (i.v.) with 1nmol of NBs-Cy 5.5 NBs-B-Cy5.5 or saline solution as a control. Tumour volumes were measured with a caliper instrument and calculated using the formula: (length×width2)/2.

3.7.1 In-vivo analysis

Biodistribution studies were used to evaluate NBs-Cy 5.5 and NBs-B-Cy 5.5 biodistribution in a localized model of GBM mice. All *in-vivo* studies were acquired by Xenogen IVIS Spectrum (PerkinElmer, Milan, Italy) and elaborated by Living Image Software. *In-vivo* biodistribution studies were performed before (background) and after 1, 24, 48, 72, and 96 hours from NB injection by Xenogen IVIS Spectrum (PerkinElmer, Milan, Italy). Two-dimensional regions of interest (ROIs) were selected, and laser power, integration time (repetition time of the excitation per raster point), and scan step size were optimized according to the emitted signal. The data were recorded as temporal point-spread functions and the images were reconstructed as fluorescence intensity maps.

3.7.2 Ex-vivo analysis

At the end of *in-vivo* biodistribution studies (96 h), mice were sacrificed, and organs and tumor mass were analyzed by *ex-vivo* optical imaging with the Xenogen IVIS Spectrum as previously described.

Organs of GBM mice were collected in O.C.T. embedding medium at -80°C. Frozen sections were cut with a cryostat (thickness 5–7µm) (Leica). For each biopsy, the section was performed at a thickness of 5µm for hematoxylin and eosin (H&E) staining and immunofluorescence analysis. The tissues were analyzed with the fluorescence microscope (Leica DMI 4000B, Germany) using different magnifications.

3.7.3 Toxicity

Toxicity was evaluated by analyzing AST and ALT in blood samples from treated animals using Integrated System Dx 880 (Beckman Coulter, Brea, CA, USA). Analysis of blood samples was made in collaboration with Professor Paolo Macor (University of Trieste).

3.8 Statistical Analysis

The statistical significance was determined using a two-tailed *t*-test. A p-value less than 0.05 was considered significant for all comparisons done. Bars represent the standard error of the mean. All other bars are standard deviations.

4. Results

4.1. Evaluation of GPC1 as a useful target for drug delivering with nanoparticles in GBM.

Previous studies defined GPC1 as a useful tumor-associated antigen (TAA) for drug delivery approaches for GBM treatment[210,220]. To confirm the potential use of GPC1 in the proposed drug delivery approach, GPC1 expression was assessed in the GBM cell lines T98G and U87-MG. First, GPC1 protein expression levels were investigated by Western blot in GBM cell lines (T98G, U87-MG) and the other cell lines as a negative control (Huh-7) using the commercially available antibody (a-GPC1c) specific to GPC1. The expression of vinculin was evaluated as housekeeping protein expression. As expected, results showed that GPC1 expression was detected in GBM cell lines T98G and U87-MG but not in non-GBM Huh-7 cell line. The expression of Vinculin in the cell extracts confirmed the results, as expected (Figure 20 A-B). To further confirm GPC1 expression in GBM cell lines, immunofluorescence (IF) was used to assess the antigens' localization. The expression of GPC1 was detected on the cell surface and in the cytoplasm of GBM cell lines whereas it was lacking in the negative control cells (Figure 20 C). Finally, flow cytometry analysis confirmed these data showing a GPC1 expression in U87-MG cells (MFI 109; median 48%, range 35-60% of positive cells) and T98G cells (MFI 230; median 70%, range 56-71% of positive cells). On the other hand, as expected GPC1 expression was negligible/absent in Huh-7 cells (MFI 70; 8%, range 6-10% of positive cells) (Figure 20 D).

These results were in keeping with the previous studies[210,211,219].

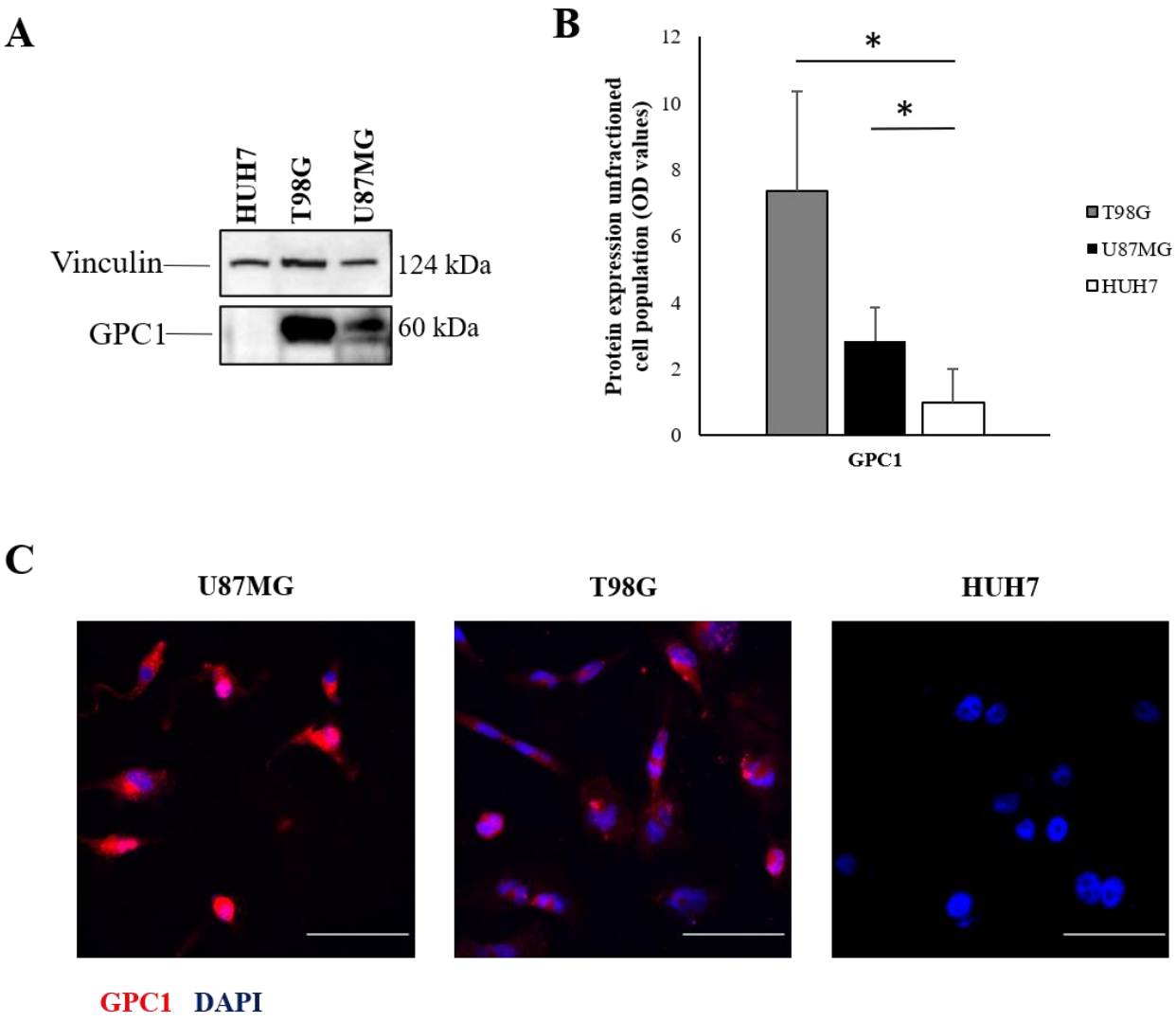
A
HUH7
T98G
U87MG
Vinculin
124 kDa
GPC1
60 kDa
B
Protein expression unfractioned cell population (OD values)
12
10
8
6
4
2
0
*
*
GPC1
T98G
U87MG
HUH7
C
U87MG
T98G
HUH7
GPC1 DAPI

D

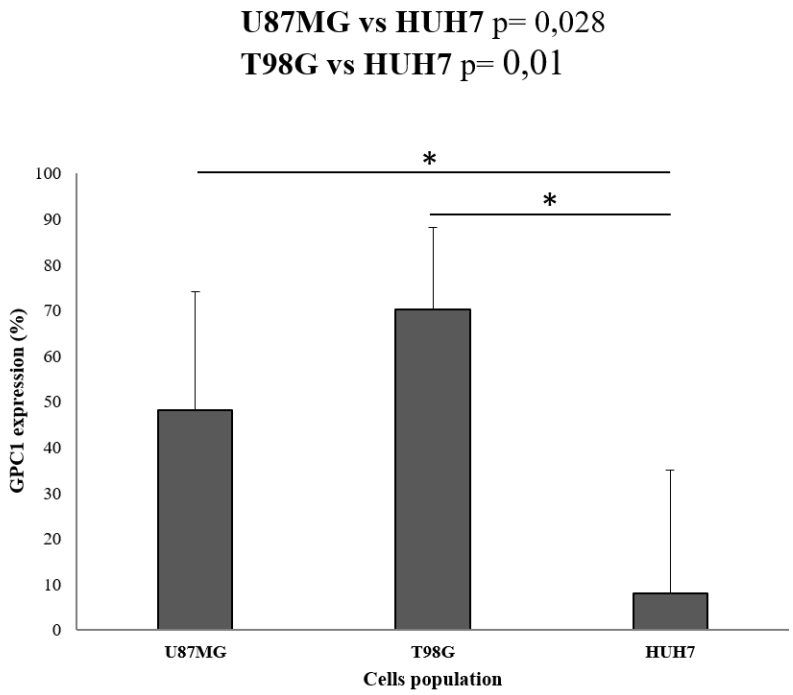

	a-GPC1c % positive	MFI
U87MG	48	109
T98G	70	230
HUH7	8	70

Figure 20.
Panel A: Representative western blot of GPC1 protein levels of U87-MG, T98G, and Huh-7.
Panel B: Densitometric measurements (relative GPC1/Vinculin OD values) of western blot values (means ±SD). Analyses were performed using ImageJ software.
Panel C: Representative immunofluorescence of GPC1 protein localization of U87-MG, T98G, and Huh-7. Blue represents nuclei and in red GPC1. Scale bar = 50µm.
Panel D: Flow cytometric expression of GPC1 surface antigens in U87-MG, T98G, and Huh-7 cells. Gray histograms indicate specific fluorescence. (* p-*value* < *0.05*, p-*value* was calculated by using paired *t*-test).

4.2. Production and characterization of the anti-GPC1 antibody.

To obtain specific anti-GPC1 antibodies, in collaboration with the group of Professor Paolo Macor (University of Trieste) and an external company, an immunization in mice was performed. To produce specific anti-GPC1 antibodies recognizing the cell surface form of GPC1, it was designed and synthetized of cDNA for *in-vivo* expression of GPC1. Quality control of the expression by FACS using the commercial antibodies. After, it was proceeded to the immunization of 5 mice by genetic vaccination. To follow, hybridomas were generated from spleens antigen from mice with the highest titer. The serum of immunized mice was tested to detect GPC1 specific clones by ELISA versus a recombinant full-length GPC1 protein or by flow cytometry using the U87-MG and T98G GBM cell lines as positive control and the Huh-7 cell line as a negative control. After validations, hybridomas were produced for three different anti-GPC1 specific clones (A, B, and C). The expression of GPC1 was analyzed by flow cytometry in U87-MG, T98G cells to evaluate the efficacy of the three hybridomas to produce specific anti-GPC1 antibodies, in terms of amount antibody production, the growth rate of hybridoma cells, and the capability of hybridoma supernatants to recognize GPC1. GPC1 was analyzed by flow cytometry in U87-MG, T98G cells. GPC1 expression was detected in U87-MG and T98G cells by using the supernatants of the B and C clones (B MFI 776, median B 59%, C MFI 684, median C 57%, GPC1c MFI 103, median a-GPC1c 39% in U87-MG; B MFI 937 median B 65%, C MFI 697 median C 74%, a-GPC1c MFI 168 median a-GPC1c 49%in T98G, Figure 21). On the contrary, the A clone was not capable to recognize GPC1 by flow cytometry (A MFI 95 median A 2% in U87-MG, A MFI 153 median A 7% in T98G, Figure 21). The validity of the anti-GPC1 clones was also confirmed by evaluation in Huh-7 cells, in which GPC1 expression was not detected. Thus, the expression of GPC1 evaluated with B and C antibodies followed the same trend of expression that can be obtained when the commercially available antibody a-GPC1c is employed (Figure 21). Moreover, among the three clones, B and C showed the best binding affinity for GPC1expressed on the cell surface. For this reason, supernatants of B and C clones were purified to obtain specific anti-GPC1 monoclonal Abs.

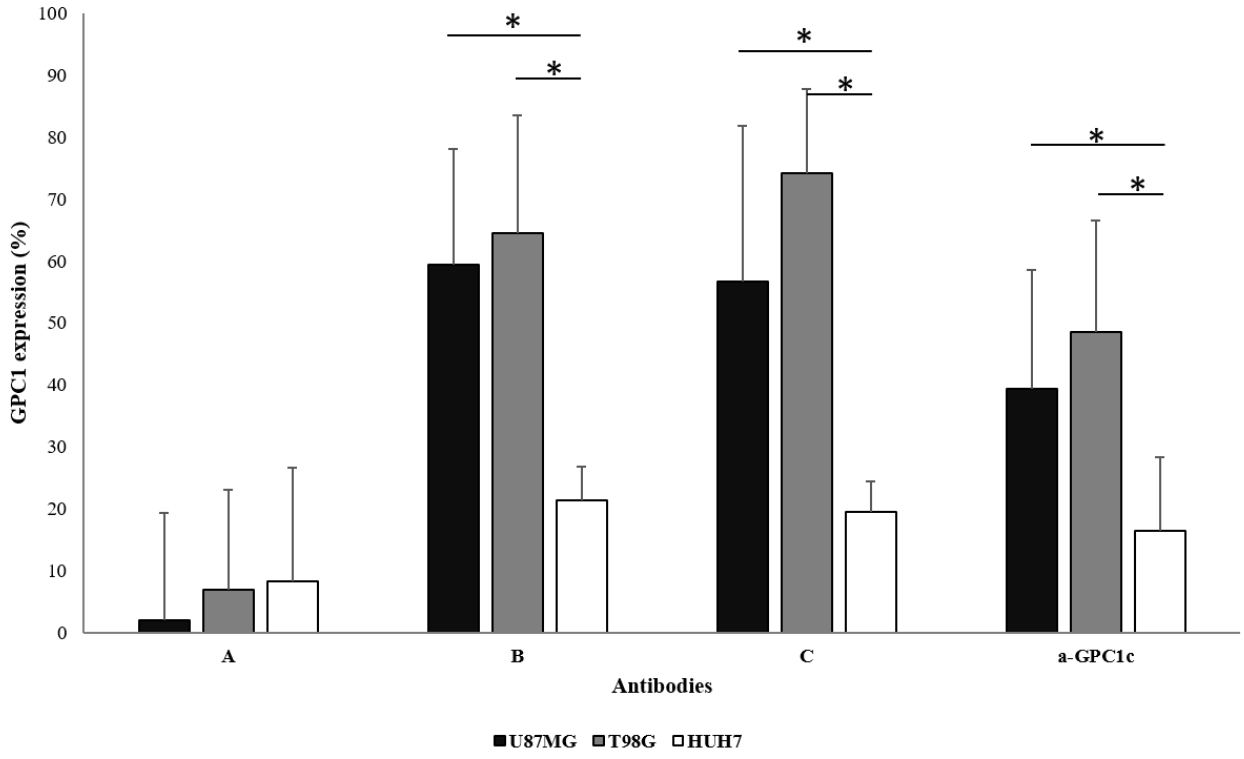

U87MG	% positive	MFI
A	2	95
B	59	776
C	57	684
a-GPC1c	39	103

T98G	% positive	MFI
A	7	153
B	65	937
C	74	697
a-GPC1c	49	168

HUH7	% positive	MFI
A	8	115
B	21	139
C	19	218
a-GPC1c	16	75

Figure 21.
Representative flow cytometric expression of GPC1 in U87-MG, T98G GBM cells, and Huh-7 cells as a negative control using A, B, C clones not purified and compared to a-GPC1c antibody.
Black histograms indicate specific fluorescence of U87-MG, grey of T98G, and white of Huh-7. (* p-*value* < *0.05*, p-*value* was calculated by using paired *t*-test).

The two obtained purified anti-GPC1 monoclonal antibodies (B, C) were tested for their capability of recognizing GPC1 by flow cytometry in GPC1-expressing GBM cell lines. GPC1 expression was assessed both in GBM cell lines (e.g., U87-MG, T98G) and in other tumor cell lines as negative control (Jurkat). We observed a high expression of GPC1 in GBM cell lines compared to the negative control (B MFI 2.209; B 98.5%, MFI 1.307; C 95.5% in T98G and MFI 1.811; B 97.4%, MFI 1.406; C 90.4% in U87-MG of the total cell population compared to MFI 40; B 14.2%, MFI 24; C 3.4% of cell population in the Jurkat cell line). Moreover, GPC1 expression levels detected with the two purified antibodies followed the same expression trend obtained with the commercially available a-GPC1c (MFI 117; 80.1% in T98G and MFI 98; 41.7% in U87-MG) (Figure 22). In keeping with the results obtained by flow cytometry, GPC1 expression was observed by immunofluorescence analysis in T98G and U87-MG (Figure 23 A, B).

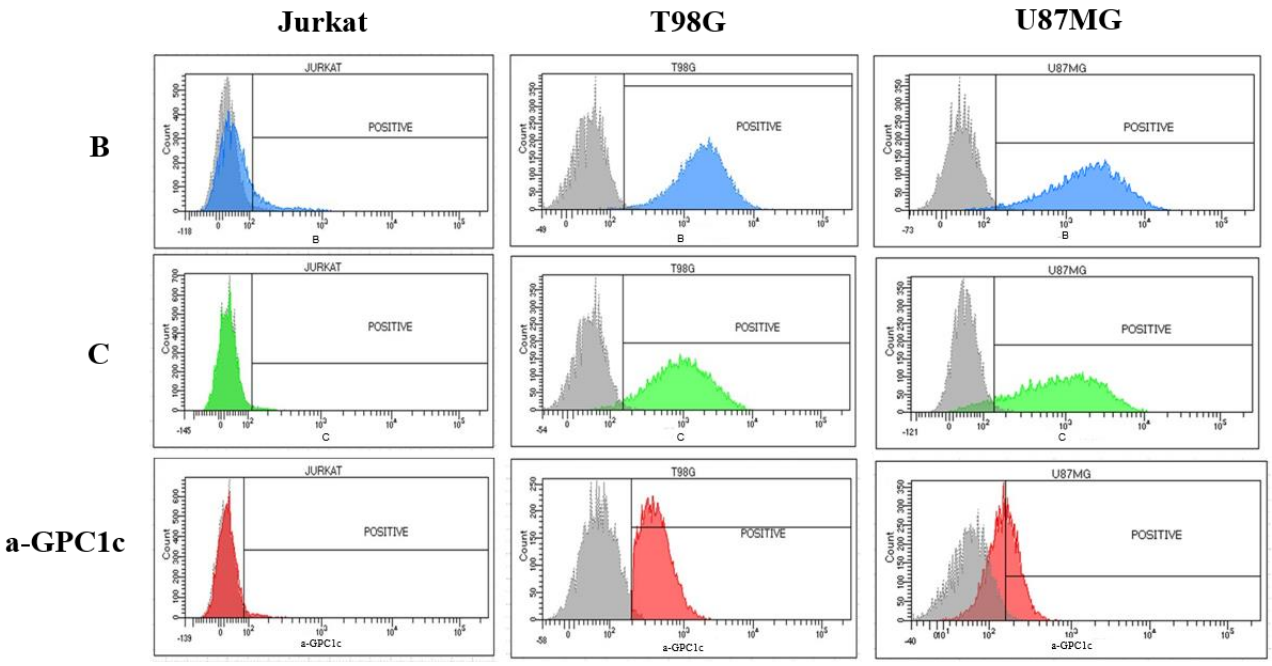

JURKAT	% positive	MFI
B	14,2	40
C	3,4	24
a-GPC1c	5,9	13

T98G	% positive	MFI
B	98,5	2.209
C	95,5	1.307
a-GPC1c	80,1	117

U87MG	% positive	MFI
B	97,4	1.811
C	90,4	1.406
a-GPC1c	41,7	98

Figure 22.
Representative flow cytometric expression of GPC1 in U87-MG, T98G GBM cells, and Jurkat cells as a negative control using purified anti-GPC1 monoclonal antibodies B, C and compared to a-GPC1c antibody. Blue, green, and red histograms indicate specific fluorescence; Dotted histograms isotype-matched irrelevant Ab, negative control.

A

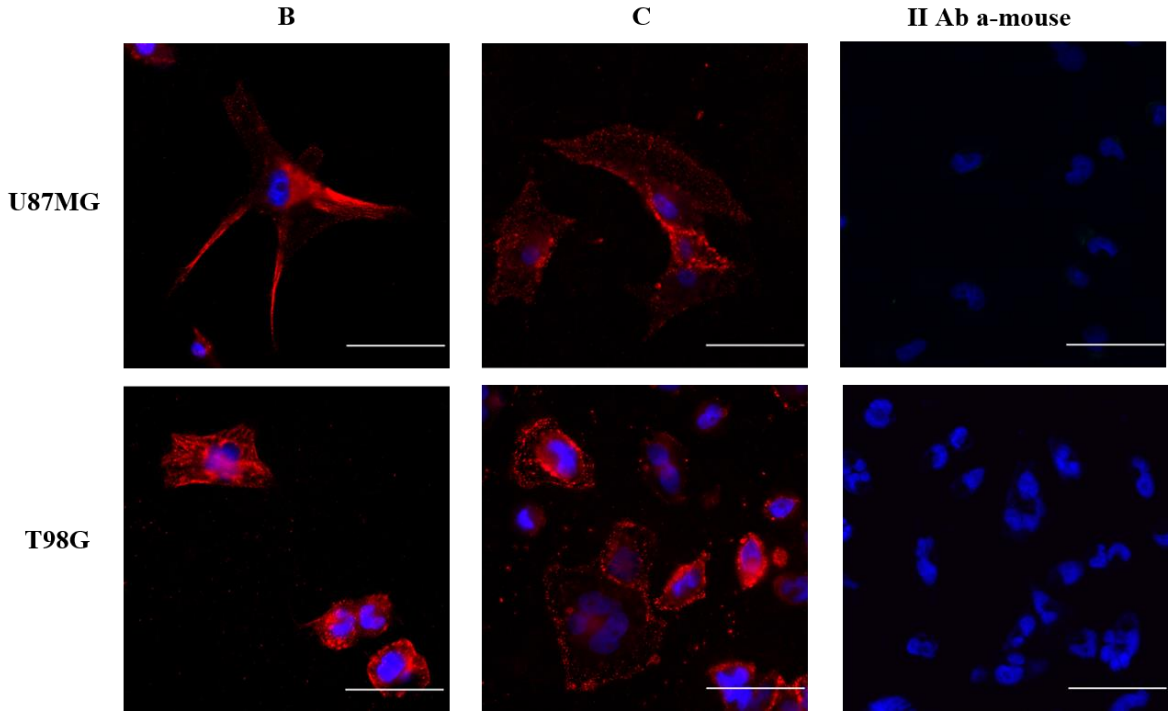

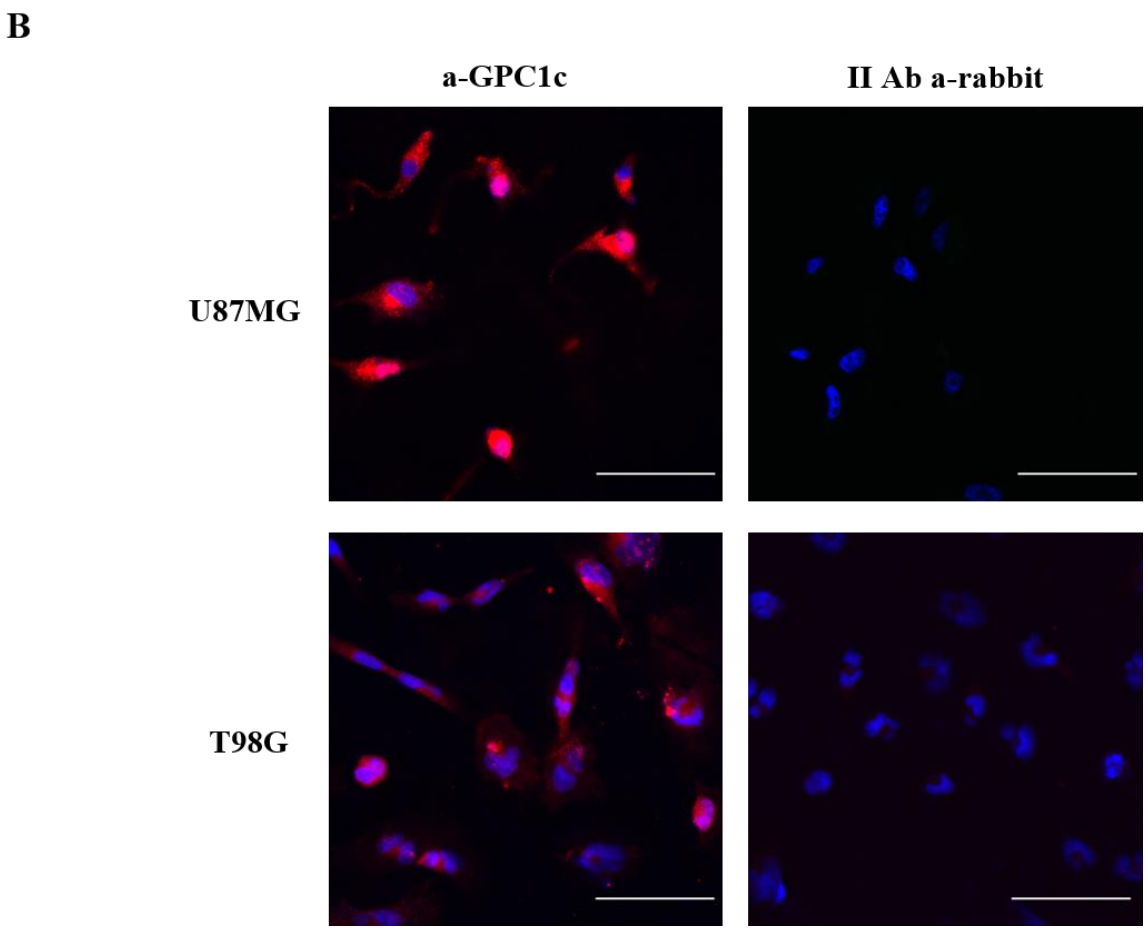

Figure 23.
Panel A: Representative immunofluorescence of GPC1 protein in GBM cell lines U87-MG and T98G using anti-GPC1 antibody B, C. Blue represent nuclei and in red GPC1. Scale bar = 50µm.
Left panel: Corresponding negative controls with secondary hybridization only.
Panel B: Representative immunofluorescence of GPC1 protein in GBM cell lines U87-MG and T98G using anti-GPC1 antibody a-GPC1c. Blue represents nuclei and in red GPC1. Scale bar = 50µm.
Left panel: Corresponding negative controls with secondary hybridization only.

The capability of the B and C anti-GPC1 antibodies to recognize GPC1 expressing cells was also evaluated in frozen primary GBM tumor samples and healthy tissues (e.g., liver, lung) as control. Of note, GBM tumor specimens were positive for GPC1 expression by using the B and C antibodies. On the contrary, as expected, no signal was detected in healthy tissues by using these two antibodies (Figure 24, 25). Of note, as previously observed for T98G and U87-MG cell lines, a similar pattern of expression for the GPC1 protein was observed by using the B and C antibodies compared to that obtained by using the commercially available anti-GPC1 antibody (Figure 24, 25).

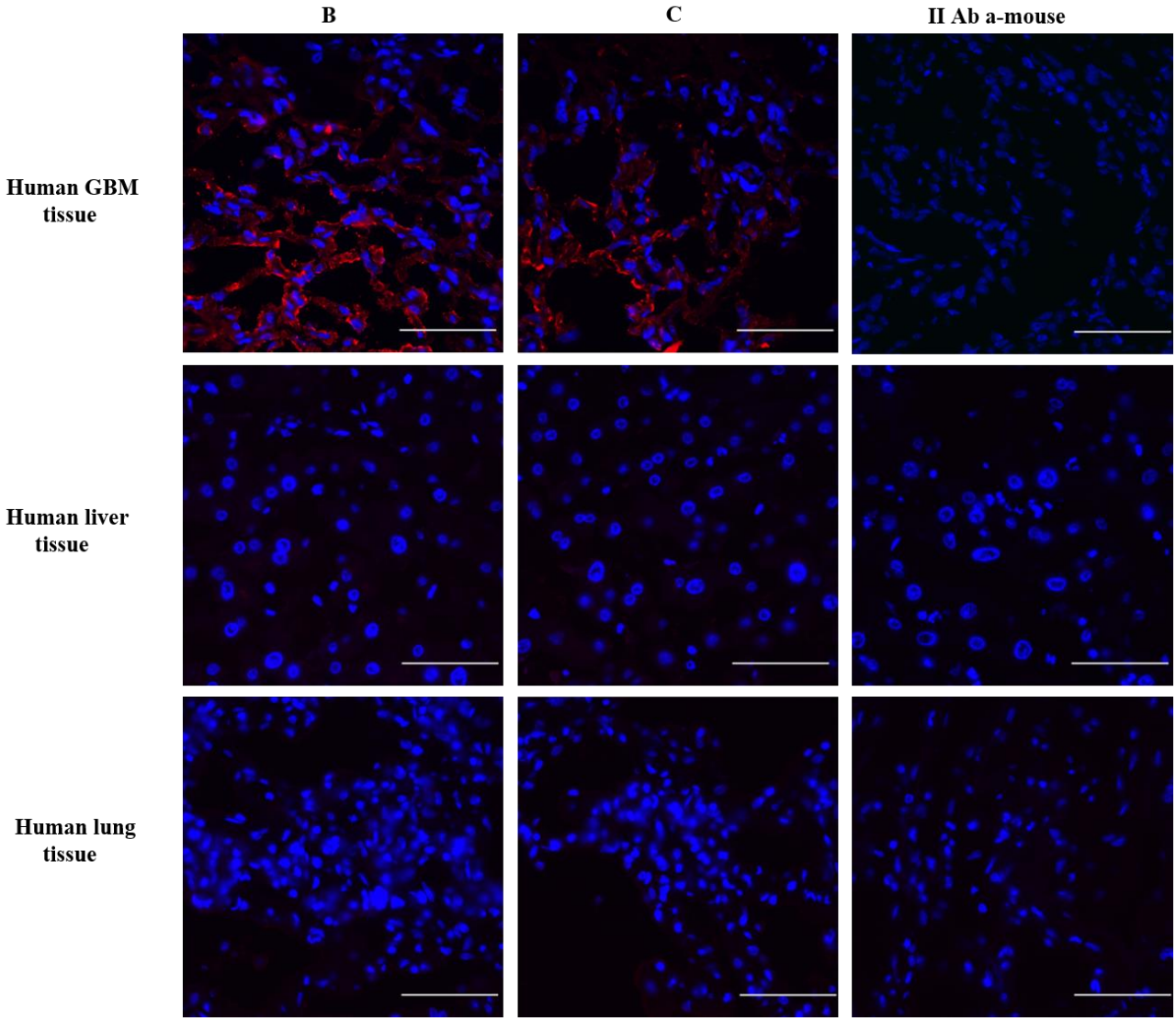

Figure 24.
Representative immunofluorescence of GPC1 protein in frozen primary GBM tumor samples and healthy tissues (e.g., liver, lung) using anti-GPC1 antibody B, C.
Left panel: corresponding negative controls with secondary hybridization only. Nuclei are reported in blue and GPC1 is reported in red. Scale bar = 50µm.

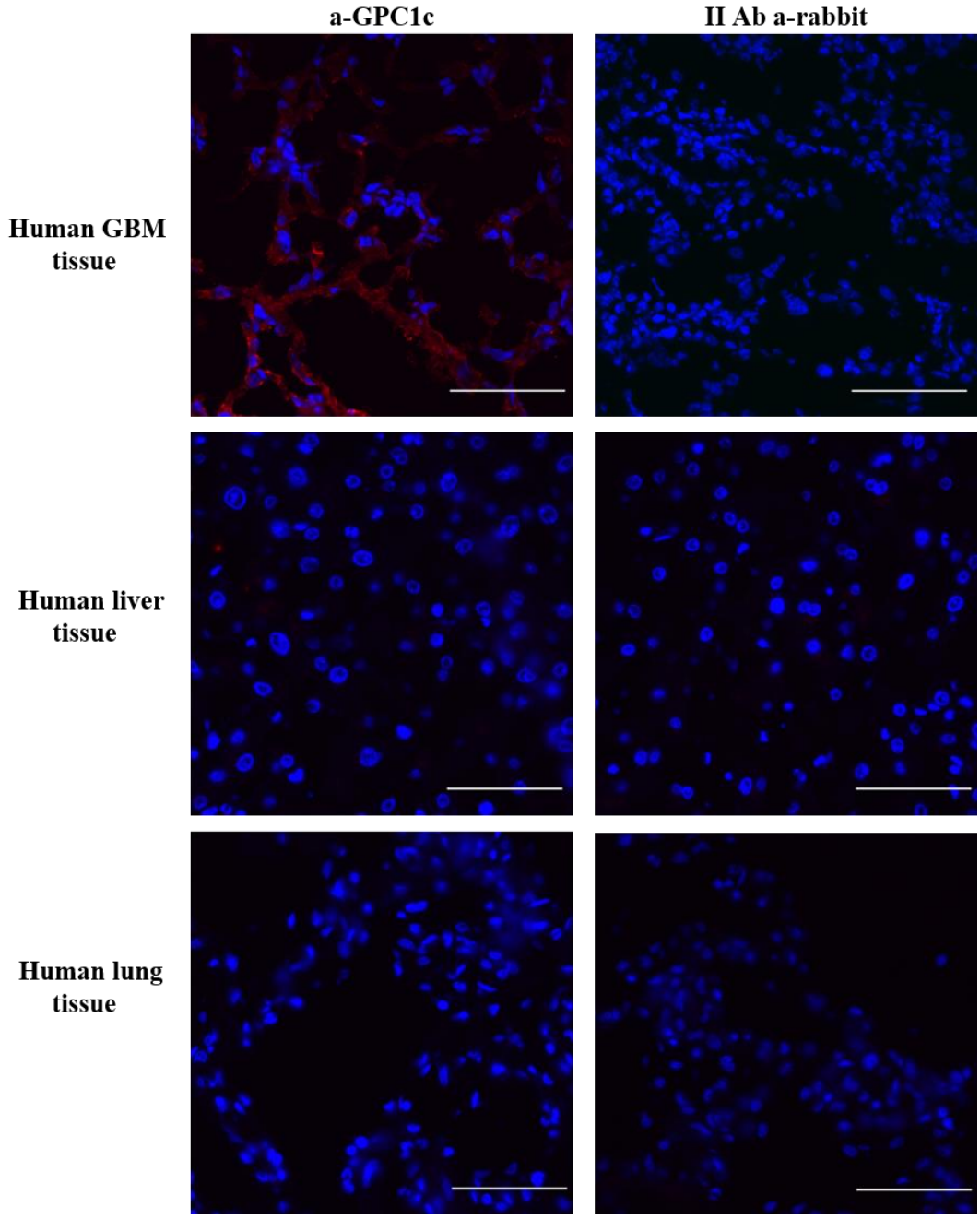

Figure 25.
Representative immunofluorescence of GPC1 protein in frozen primary GBM tumor samples and healthy tissues (e.g., liver, lung) using a-GPC1c.
Left panels: Representative immunofluorescence of GPC1 protein in frozen primary GBM tumor samples and healthy tissues (e.g., liver, lung) using a-GPC1c. Nuclei are reported in blue and GPC1 is reported in red.
Right panels: Corresponding negative controls with secondary hybridization only. Nuclei are reported in blue. Scale bar = 50µm.

According to the results obtained by flow cytometry and immunofluorescence analyses, the B antibody appeared to be more efficient than the C antibody. Therefore, the B clone was chosen to be bound to the NBs to develop the active drug delivery strategy.

4.3. Establishment of GBM xenograft model.

To perform in-vivo validations of the proposed active drug delivery strategy, a GBM xenograft mouse model was established. To do this, $5x10^6$ U87-MG cells were subcutaneously injected in the flank of athymic nude mice. After a median time, interval of 30 days, GBM-like tumor masses of about 250 mm^3 were obtained. By immunofluorescence analysis, GPC1 expression was detected in slices from tumor masses both by using both B and C anti-GPC1 antibodies (Figure 26). These results confirmed that the established GBM xenograft model was useful to characterize the proposed active drug delivery approach. As you can see also in IF of mouse tissue, the staining of the B antibody is more efficient looks than the C antibody. indeed, the B clone was chosen to be bound to the NBs to develop the active drug delivery strategy.

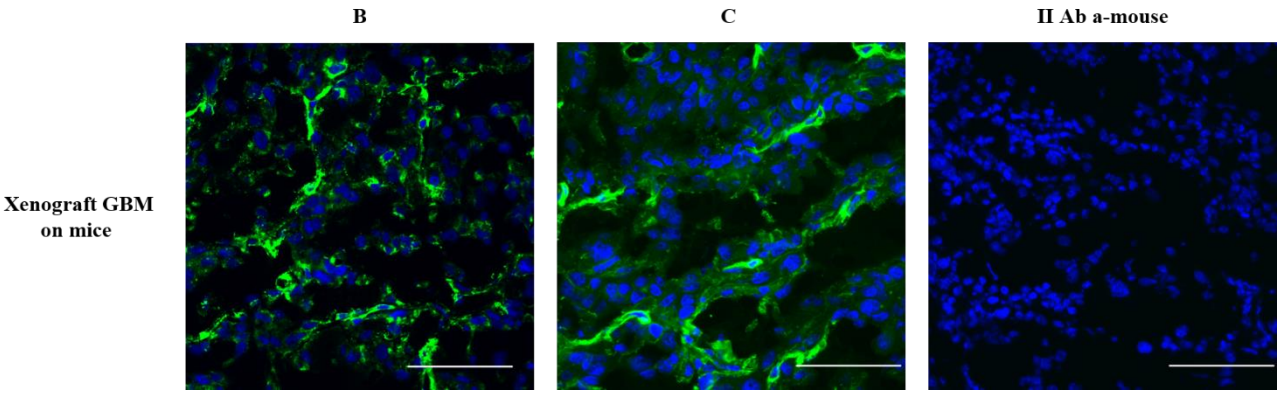

Figure 26.
Representative immunofluorescence of GPC1 protein in GBM mass tissues of xenograft GBM mice using anti-GPC1 antibody B, C. Left panel: Corresponding negative controls with secondary hybridization only. Nuclei are reported in blue GPC1 is reported in green. Scale bar = 50μm.

4.4. *In-vitro* evaluation of killing capability of chemotherapeutic drugs in GBM cell line models.

The current standard treatment for GBM is tumor resection followed by radiotherapy and chemotherapy with Temozolomide (TMZ). TMZ can pass through the blood-brain barrier (BBB) for ~30% of the dose[29] but it is characterized by a low killing capability[30]. For these reasons, we have chosen to test other drugs such as Docetaxel (DTX)[31,32] and Paclitaxel (PTX)[33]. Compared to TMZ, despite the high killing efficacy, DTX and PTX are characterized by a low bioavailability[225]. Their administration could be facilitated by an active drug delivery approach employing polymeric NBs conjugated with the B anti-GPC1 antibody.

To select the drug to be loaded in the NBs, the killing capability of TMZ, PTX and DTX were evaluated in GBM cells (U87-MG, T98G). IC_{50} (half maximal inhibitory concentration) was determined by treating GBM cell lines with a scalar dose of drugs (100, 10, 1, 0.1, 0.01µM, ctrl) at different time points (24, 48 h). Cell viability (reported as a percentage of viable cells) was quantified by CellTiter 96 proliferation assay. The IC50 of TMZ, PTX, and DTX, as reported in Table 3 A, B, showed that TMZ at 24h and 48h timepoints have the highest IC_{50} in both GBM cell lines (at 24h 900µM and 48h 500 µM in U87-MG; at 24h 1000µM and 800µM in T98G) compared to the other chemotherapeutic tested drugs, highlighting that TMZ had the lower killing capability among the 3 tested drugs at the different time-points. On the other hand, DTX had a higher killing capability compared to PTX (PTX at 24h 80µM and 48h 20µM in U87-MG; at 24h 50µM and 10µM in T98G; DTX at 24h 30µM and 48h 5µM in U87-MG; at 24h 28µM and 48h 0.5µM in T98G). Results from FACS analysis at the time point of 48 h, by using FITC-labelled recombinant human Annexin V-7AAD assay, allowed us to obtain comparable IC_{50} values. In particular, results from FACS analysis, showed that DTX after 48 hours of treatment in GBM cell lines has the highest killing capability compared to PTX (T98G p=0,46891, U87-MG p=0,01618) and TMZ (T98G p=0,03694, U87-MG p=0,0274, Figure 27 A, B). According to the obtained results, we have chosen the DTX for the encapsulation of chemotherapeutic drugs in the NBs.

A

Cell lines	IC_{50} TMZ		IC_{50} PTX		IC_{50} DTX	
	24h	48h	24h	48h	24h	48h
U87MG	900µM	500µM	80µM	80µM	30µM	5µM
T98G	1000µM	800µM	50µM	10µM	28µM	0.5µM

B

Cell lines	IC_{50} TMZ 48h	IC_{50} PTX 48h	IC_{50} DTX 48h
U87MG	500µM	100µM	1µM
T98G	800µM	5 µM	0.5µM

Table 3. (A, B) Half maximal inhibitory concentration (IC_{50}) of TMZ, DTX, and PTX.

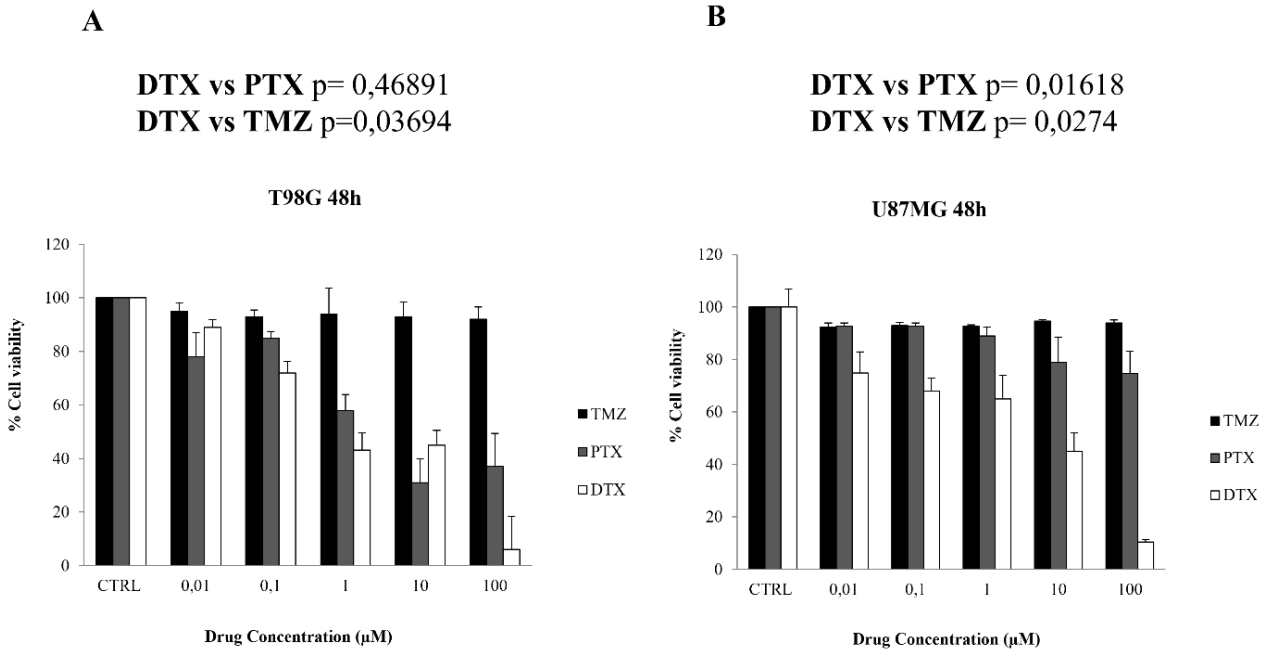

Figure 27.
Panel A, B: Percentage of cell survival following TMZ, PTX, and DTX treatment. (A) T98G and (B) U87-MG human GBM cell lines were treated with increasing concentrations of the drugs for 48 h. Results are expressed as % of viable cells of control shown as mean ± SEM (n = 3). (p-*value* was calculated by using paired *t*-test).

4.5. Chitosan nanobubbles characterization and stability.

The chitosan NBs were prepared by the group of Professor Roberta Cavalli (University of Torino) in the context of a collaborative project. In particular, the following different types were prepared: blank NBs, NBs conjugated with Cy 5.5, NBs conjugated with Cy 5.5 and with anti-GPC1 antibody (B), NBs loaded with DTX, and NBs loaded with DTX and conjugated with B (Figure 28). The *in-vitro* characterization of the prepared NBs was performed for all the NB preparations. DLS showed the according to my knowledge average diameter of about 350 nm and a positive charge. The NB concentration determined by NTA analysis was $1 \cdot 10^{12}$ NB/ml. The *in-vitro* results are listed below. Table 4 reports the physicochemical characteristics of blank NBs, NBs conjugated with Cy 5.5, NBs conjugated with Cy 5.5, and with anti-GPC1 antibody (B), NBs loaded with DTX, and NBs loaded with DTX and conjugated with B. NBs nanoformulations displayed similar sizes. DTX was incorporated in the nanostructure to a good extent. Indeed, the loading capacity and encapsulation efficiency of NBs-DTX were 5.60% and 89.5%, respectively). Notably, the drug loading did not affect the physicochemical parameters of NBs and the physical stability of the nanosuspensions. The physical stability of all formulations stored at 4°C was confirmed for up to 1 month. The spherical morphology and their nanometric sizes were shown by Transmission electron microscopy (TEM) analysis (Figure 29). We showed the TEM image of NB-DTX because this formulation is the basis of the cytotoxic *in-vitro* test. Indeed, as you can see from the DLS test there isn't a large increase in the diameter when we conjugate the Cy 5.5 or the antibody with NBs.

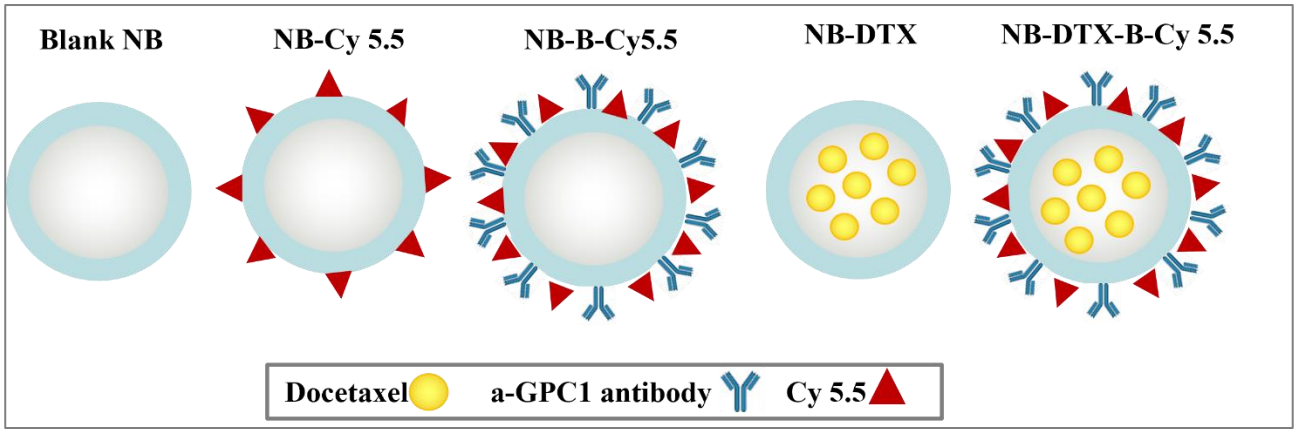

Figure 28.
Schematic representation of blank NBs, NB-Cy 5.5, NB-B-Cy 5.5, NBs containing docetaxel (NBs-DTX), and NB-DTX-B-Cy 5.5.

Formulation	Average diameter ± SD (nm)	PDI	Z-Potential ± SD (mV)	Drug concentration (µg/ml)
Blank NBs	360.5 ± 11.2	0.238	30.11 ± 1.56	-
NBs-Cy5.5	358.6 ± 9.4	0.230	28.86 ± 2.14	-
NBs-B12-Cy5.5	355.4 ± 12.3	0.225	27.64 ± 2.06	-
NBs-DTX	402.3 ± 13.6	0.240	29.97 ± 1.85	125
NBs-DTX-B12-Cy5.5	398.8 ± 18.2	0.245	26.13 ± 1.94	125

Table 4. Physicochemical characteristics of blank NBs, NB-Cy 5.5, NB-B-Cy 5.5, NBs-DTX and NB-DTX-B-Cy 5.5, and drug concentration.

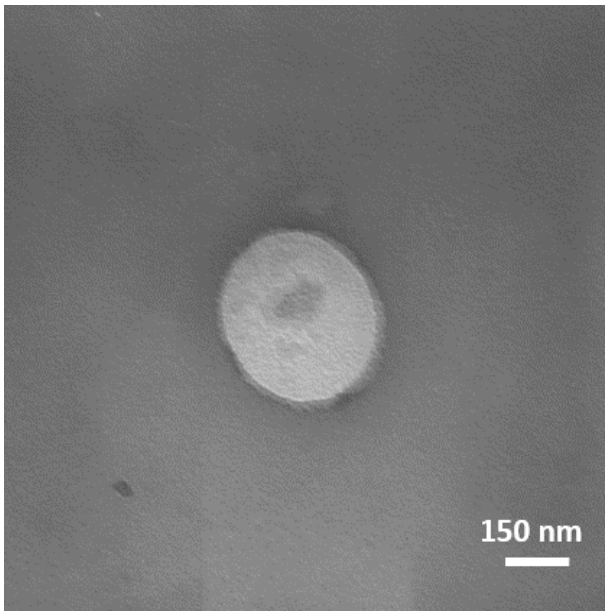

Figure 29.
Transmission electron microscopy image of NBs-DTX (scale bar 150 nm). Original magnification 28500×.

To demonstrate the specific binding of NBs conjugated with B antibody, we performed immunofluorescence of T98G cell line treated with NB-Cy 5.5 and NB-B-Cy 5.5 at different time-point (30 min and 2 h). Figure 30 shows that both NB-Cy and NB-B-Cy 5.5 were localized in the proximity of T98G cells. Of note, at the time point of 2 h, a higher amount of NB-B-Cy 5.5 appeared to be bound to T98G cells compared to the quantity of NBs in T98G cells treated with NB-Cy 5.5.

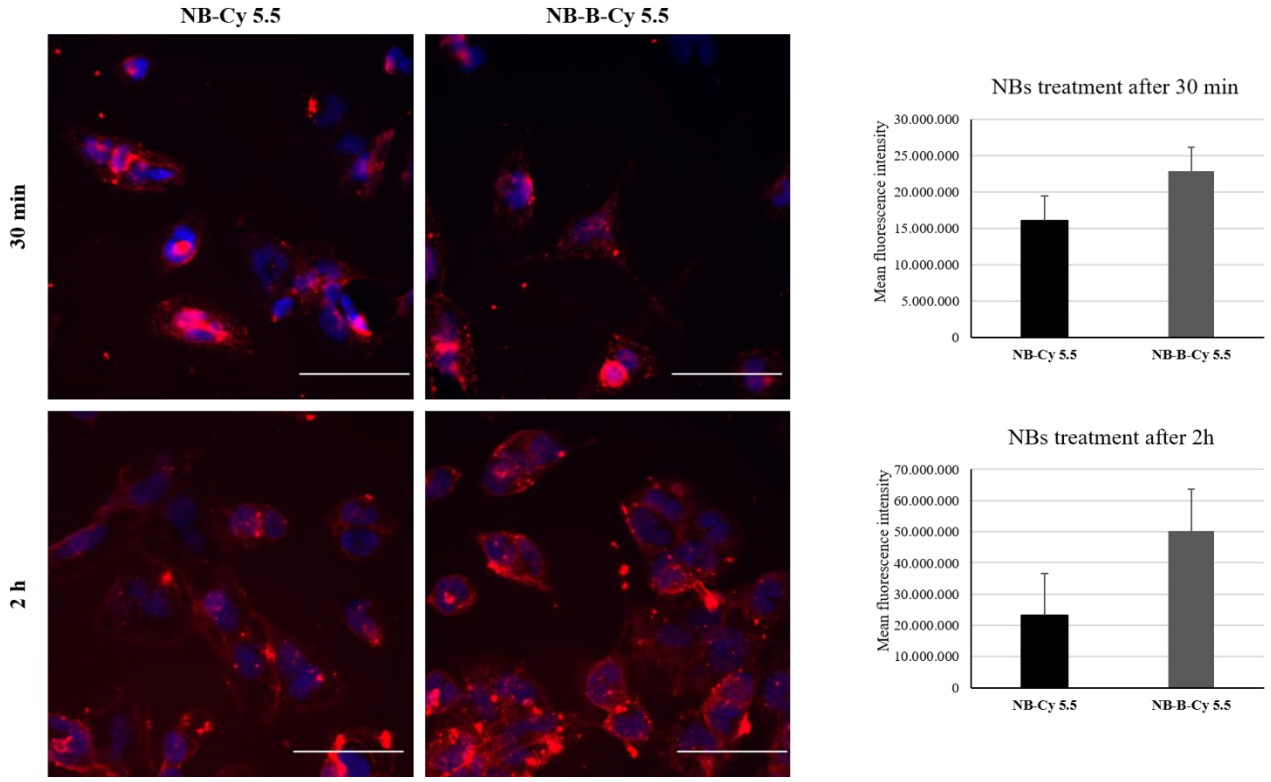

Figure 30.
Relative immunofluorescence image of T98G treated with NB-Cy 5.5 and NB-B-Cy 5.5 at different time-point 30 min and 2h. Nuclei are reported in blue, and NBs are reported in red. Scale bar = 50µm.
Right panels: Histogram represented the quantification of the mean fluorescence intensity of NBs. Images are representative of four fields per condition (n = 4). Analyses were performed using ImageJ software. Data are expressed as means ± standard deviation of three independent experiments.

To further confirm these data, we evaluated the cellular uptake of NBs-B-Cy5.5 and NBs-Cy 5.5 (in blue) in U87-MG and T98G cells by using confocal microscopy. Confocal microscopy showed that NBs-B-Cy5.5 were internalized in cells. Specifically, figure 31 reports the confocal microscopy images after 1 h of incubation of NBs. In detail in each image, we have the magnification of the image in the three planes (x, y, z), in which the localization of NBs-B-Cy 5.5 in the cell cytoplasm around the nucleus is shown. Moreover, the amount of NBs seems to be higher inside for the cells treated with NBs-B-Cy 5.5 compared to the amount of NBs in the cells treated with unconjugated NBs (NBs-Cy 5.5) (Figure 31).

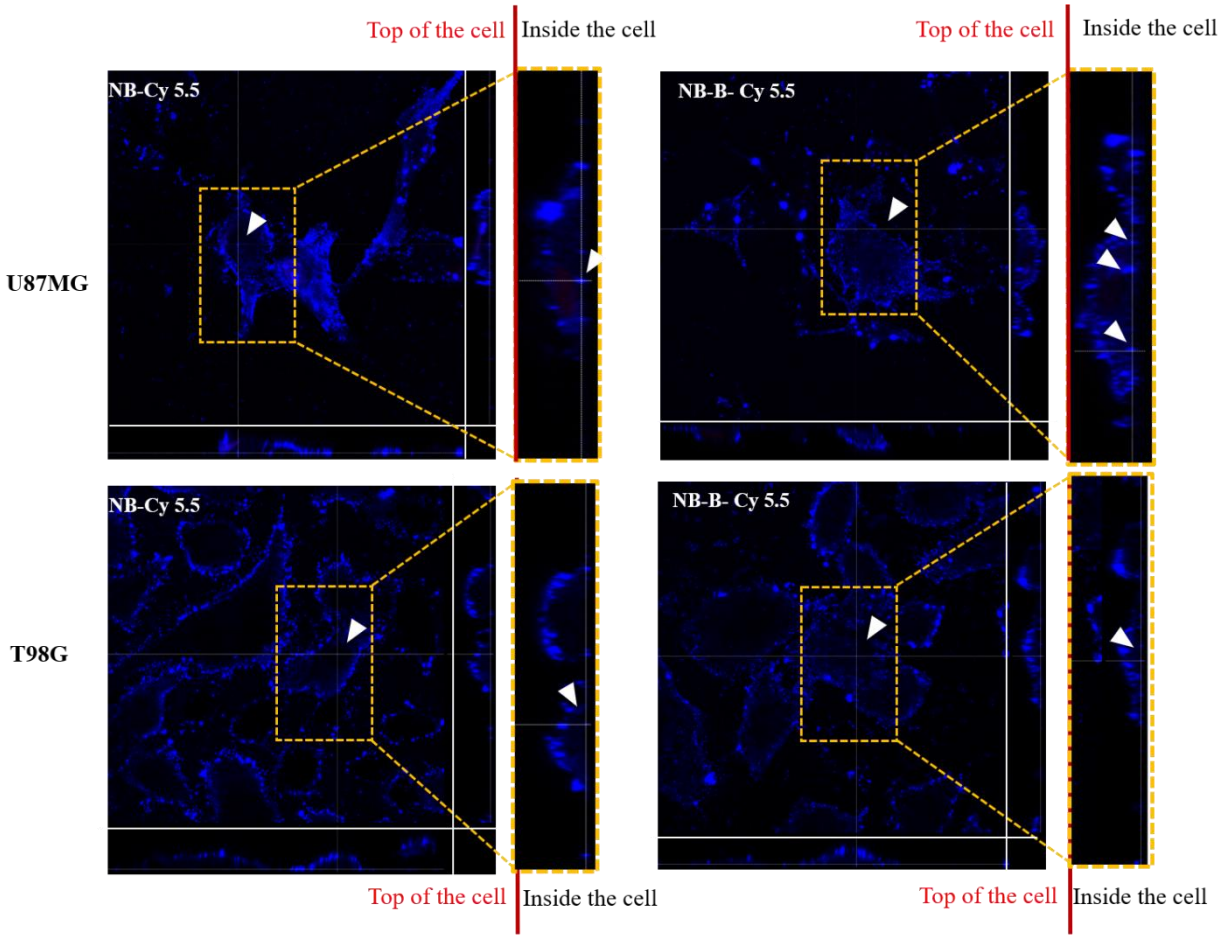

Figure 31. Cellular uptake studies.
NBs-B-Cy 5.5 and NBs-Cy 5.5 were incubated with U87-MG and T98G cells for 1 h. The cells were incubated with NBs-B-Cy 5.5 and NBs-Cy 5.5 (Blu). On the right of each image, we have the magnification of the image in the three planes (x, y, z). Red bars represent the division form inside and outside the cell. The cells were fixed and analyzed with Leica SPE confocal microscopy using a 63× oil lens. Images are representative of three fields per condition (n = 3).

4.5.1 *In-vitro* evaluation of killing capability of loaded anti-GPC1 NBs in GBM cell lines.

To test *in-vitro* the cytotoxic effect of blank NBs, NB-Cy5.5, NB-B-Cy5.5, NB-DTX, NB-DTX-B-Cy5.5, free DTX on cell viability, T98G and U87-MG cells were seeded in 96-well plates at a density of 5000 cells/well. After 24 h, T98G and U87-MG cells were incubated with different concentrations of NBs (100, 50, 25, 12.5, 10, 6.2, 3.1, 1, 0.1µM, ctrl) to obtain the appropriate dilutions of the formulations or left untreated. After 48 h, cell viability was determined by the CellTiter 96 Proliferation Assay Kit. NB-DTX, NB-DTX-B-Cy 5.5 showing a killing capability correlated with the concentration in each concentration point, with cell viable levels similar to those free DTX for some concentrations especially for T98G (Figure 32 A, B).

Figure 32 A, B showed that T98G and U87-MG cell lines, NB-DTX has significantly higher killing ability than blank NBs in both cell lines (NB-DTX vs free DTX: T98G p=0,00348, U87-MG p= 0,00157). The histograms show also that the free DTX has a major killing capability compared to NB-DTX into the cells probably because of the more immediate availability of the drug for the cells, compared to NB-DTX where the drug is encapsulated in the chitosan shell eventually slowing down the drug release.

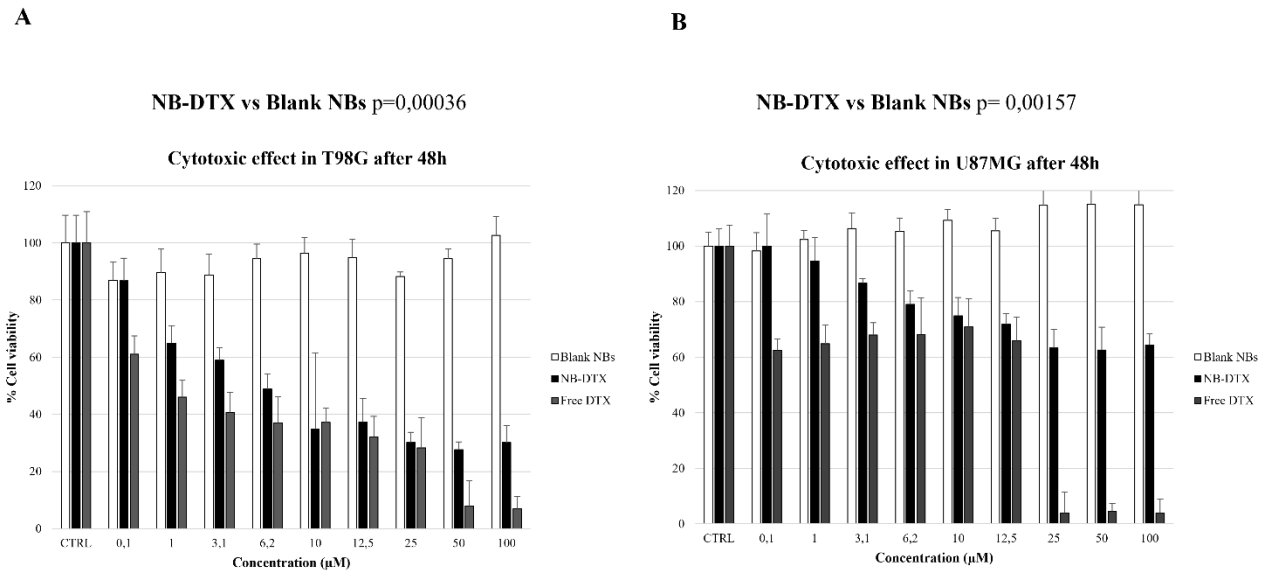

Figure 32.
Cytotoxic effect in GBM cells after 48 h of treatment.
Panel A, B: T98G and U87-MG human GBM cell lines were treated with increasing concentrations of f Blank NBs, NB-DTX, and free DTX. Results are expressed as % of viable cells of control shown as mean ± SEM (n = 3). (p-*value* was calculated by using paired *t*-test).

On the other hand, as expected, blank NBs, NB-Cy 5.5, NB-B-Cy 5.5 were not toxic at all tested concentrations (Figure 33 A, B). Therefore, is not significant the difference between the blank NB and NB-Cy 5.5 groups (T98G p=0,17371, U87-MG p=0,15307) and blank NBs and NB-B-Cy 5.5

(T98G p=0,82449, U87-MG p=0,05768). These results demonstrated that the conjugation with a Cy 5.5 for the visualization of NBs *in-vivo* and *ex-vivo* tests as well as the conjugation with the B antibody do not elicit any toxicity into the cells.

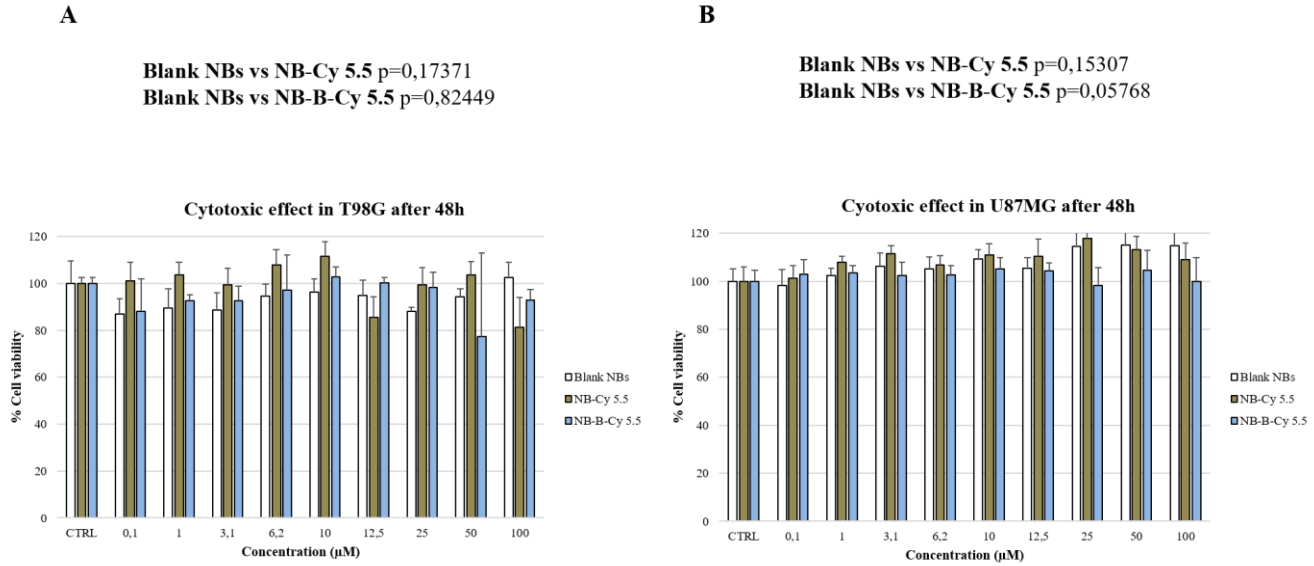

Figure 33.
Cytotoxic effect in GBM cells after 48 h of treatment.
Panel A, B: T98G and U87-MG human GBM cell lines were treated with increasing concentrations of Blank NBs, NB-Cy 5.5, NB-B-Cy 5.5. Results are expressed as % of viable cells of control shown as mean ± SEM (n = 3). (p-*value* was calculated by using paired *t*-test).

In Figures 34 A, B we reported that the NBs-B-DTX-Cy 5.5 has significantly higher killing ability than blank NBs (NBs-B-DTX-Cy 5.5 vs blank NBs: T98G p=0,000696, U87-MG p=0,000643) and then NBs-Cy 5.5 (T98G p=0,000072, U87-MG p=0,000216).

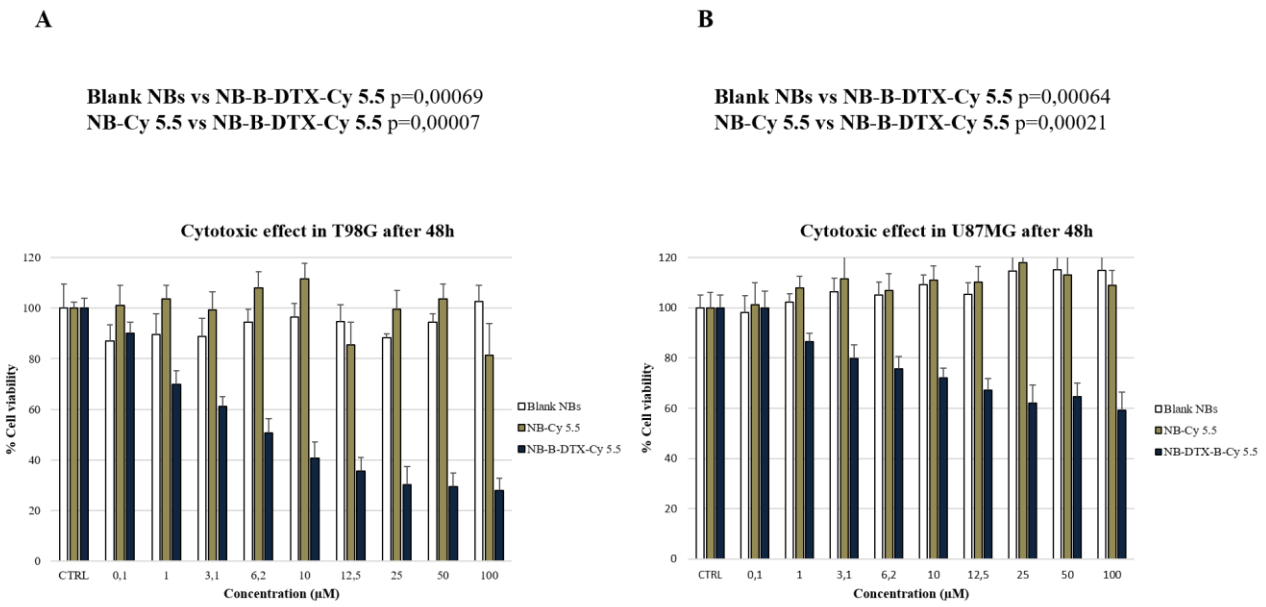

Figure 34.
Cytotoxic effect in GBM cells after 48 h of treatment.
Panel A, B: T98G and U87-MG human GBM cell lines were treated with increasing concentrations of Blank NBs, NBs-Cy 5.5, NBs-B-DTX-Cy 5.5. Results are expressed as % of viable cells of control shown as mean ± SEM (n = 3). (p-*value* was calculated by using paired *t*-test).

In Figures 35 A, B we compared the NBs-B-DTX-Cy 5.5 to NB-DTX. Both NBs have similar behavior in both GBM cell lines. Therefore, the killing capability of these NBs seems to be the same because both have encapsulated the drug therefore the drug inside is preserved, and the conjugation with B antibody did not seem to significantly increase the killing capability.

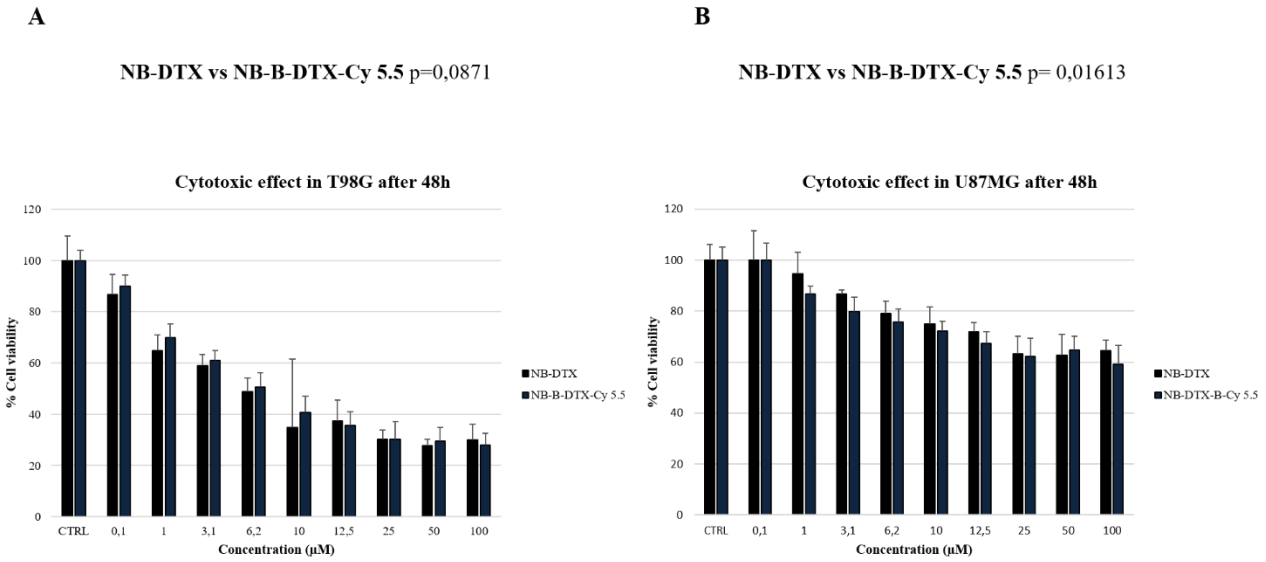

Figure 35.
Cytotoxic effect in GBM cells after 48 h of treatment.
Panel A, B: T98G and U87-MG human GBM cell lines were treated with increasing concentrations of NBs-DTX and NBs-B-DTX-Cy 5.5. Results are expressed as % of viable cells of control shown as mean ± SEM (n = 3). P-value was calculated by using a paired *t*-test.

4.6. *In-vivo* evaluation of biodistribution of anti-GPC1 NBs.

To characterize NBs' biodistribution pattern, we take advantage of the GBM xenograft mouse model prepared using the U87-MG (Figure 26). To do this, we evaluated the distribution of NBs-B compared to NBs without conjugation by using IVIS Imaging (PerkinElmer). An amount of NB-B-Cy 5.5 (NB-B-Cy 5.5 group: n=4) or NB-Cy 5.5 (NB-Cy 5.5 group: n=4) corresponding to 1 nmol of Cy 5.5 bonded to the NBs, were intravenously injected in GBM mice compared with negative control was represented by saline solution (negative control group: n=4). After the treatments, mice were followed at different time points (24, 48, 72, 96 h). Figure 36 A shows the experimental flow chart. Figure 36 B shows different images, corresponding to the different time points, of a representative mouse for each of the three groups of mice. After intravenous injection of NBs-B-Cy 5.5, (in the NB-B-Cy 5.5 group) or NBs-Cy 5.5 (in the NB-Cy 5.5 group), the contrast between tumor and surrounding tissue increased slowly and was significantly higher than pre-contrast within the first 24 hours, allowing for a clear delineation of the subcutaneously injected tumor tissue from the surrounding background tissue in the NB-B-Cy 5.5 group and the NB-Cy 5.5 group (Figure 36 B). At 48 hours after treatment with NBs (NBs-B-Cy 5.5, NBs-Cy 5.5) a peak of NBs accumulation in the U87-MG tumor mass was shown both in the NB-B-Cy 5.5 group and in the NBs-Cy 5.5. The fluorescence signals were higher in the NBs-Cy 5.5 than in the negative control group although without reaching a statistical significance. More interestingly, by considering the Cy 5.5 fluorescence intensity, NBs-B-Cy 5.5 group yield improved signal-to-background ratios in comparison to NBs-Cy 5.5 group ($p=0,02541$) within the tumor site, taking into account the entire series of fluorescence intensity values from 24 hours until 96 hours after injection (Figure 36 B, C). Moreover, it is notable that the retention time of NBs-B-Cy 5.5 was higher than NBs-Cy 5.5 when tested in mice sacrificed at the 96h time-point although without reaching a significant difference. Overall considered, these results showed that the presence of the conjugation with the B antibody allows a major accumulation of the injected NBs in the tumor as well as a higher retention time at least until the last time point of 96 h of treatment.

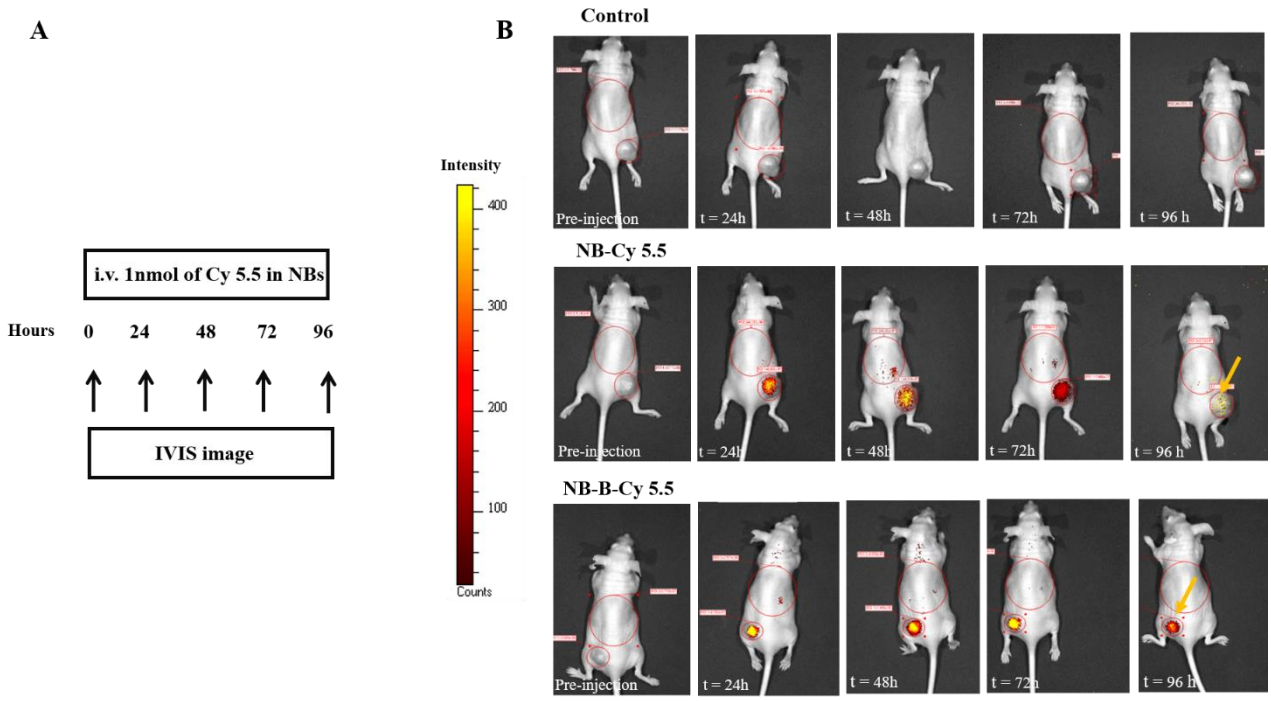

C

CTRL vs NB-Cy 5.5 p=0,07549
CTRL vs NB-B-Cy 5.5 p=0,02364
NB-Cy 5.5 vs NB-B-Cy 5.5 p= 0,02541

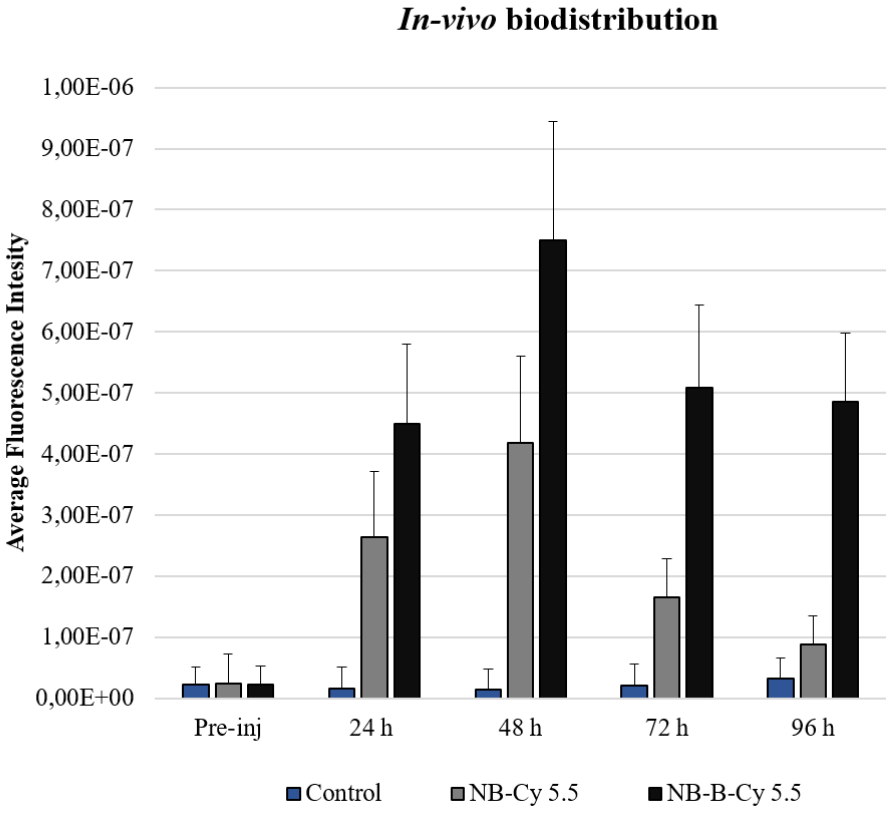

Figure 36. *In-vivo* analysis.
Panel A: Schematic representation of the experiment of imaging by IVIS of *in-vivo* and *ex-vivo*.
Panel B: Biodistribution of NB-B-Cy5.5, NB-Cy 5.5 (1 nmol of Cy5.5) injected intravenously via the tail vein in a mouse model subcutaneously transplanted with the U87-MG cells and control as mice that injected only physiologic solution in mouse model subcutaneously transplanted with the U87-MG cells. A whole-body scan of a representative mouse is shown; fluorescence intensity images were acquired at the indicated time pre-injection and different time-point (24h, 48h, 72h, 96h) and are displayed in normalized counts. The circles enclose the tumors.
Panel C: Whole-body fluorescence intensity distribution in a representative U87-MG mouse at different time-point (24h, 48h, 72h, 96h) -injection of NBs-B-Cy5.5 and untargeted NBs displayed in the normalized count. Data are expressed as means ± SEM (n = 4). (p-*value* was calculated by using paired *t*-test).

4.7. *Ex-vivo* evaluation of biodistribution of anti-GPC1 NBs.

To further highlight the importance of the B conjugation of NBs to allow a high tumor targeting efficiency, we performed the *ex-vivo* analysis of explanted U87-MG tumor masses and mice organs (Figure 37 A, B). *Ex-vivo* evaluation at 96 hours of Cy 5.5 average fluorescent intensity analysis by IVIS of the tumor masses and explanted organs (tumor mass, brain, heart, kidney, liver, spleen, lung) showed NBs accumulation in tumor mass, as well as in the liver and kidney that are organs of excretion (Figure 37 A, B). Moreover, as shown in Figure 37 B, the average Cy 5.5 fluorescence intensity of the tumor tissues explanted was higher in the NBs-B-Cy 5.5 group compared to the NBs-Cy 5.5. Thanks to the conjugation with the antibody, after 96h of treatment with NB-B-Cy 5.5, these NBs remain more time in the tumor and organs compared to the mice treated with unconjugated NB-Cy 5.5. Thus, we have demonstrated that the use of a specific monoclonal antibody anti-GPC1 increases the retention time of NBs in the GBM tumor. As expected, both NBs-B-Cy 5.5 and NBs-Cy 5.5 signals were higher than those of the signal of the control group mice although without reaching a significant difference.

The selective localization of NB-B-Cy 5.5 in tumor masses and the liver was further confirmed by evaluating the presence of the NBs-B-Cy 5.5 using fluorescent microscopy. In keeping with the IVIS images, the analyses of U87-MG tumor tissue and liver cryosections isolated from mice sacrificed at 96 hours revealed a non-homogeneously distributed fluorescence signal, consistent with the presence of the NB-B-Cy 5.5 (Figure 38). These results confirmed the accumulation of NB-B-Cy 5.5 in the tumor and liver.

Finally, at the end of the treatments at 96 h, there were no macroscopic signs of organ injury and no systematic changes in organ weight.

To assess the potential liver toxicity of the administered NBs, considering their elimination in this organ, the levels of serum alanine transaminase (ALT) and aspartate-aminotransferase (AST) from the sera of mice after 96 hours of treatments were determined compared to the control mice. After the treatments with NBs, the levels of ALT and AST have not increased compared with the control group.

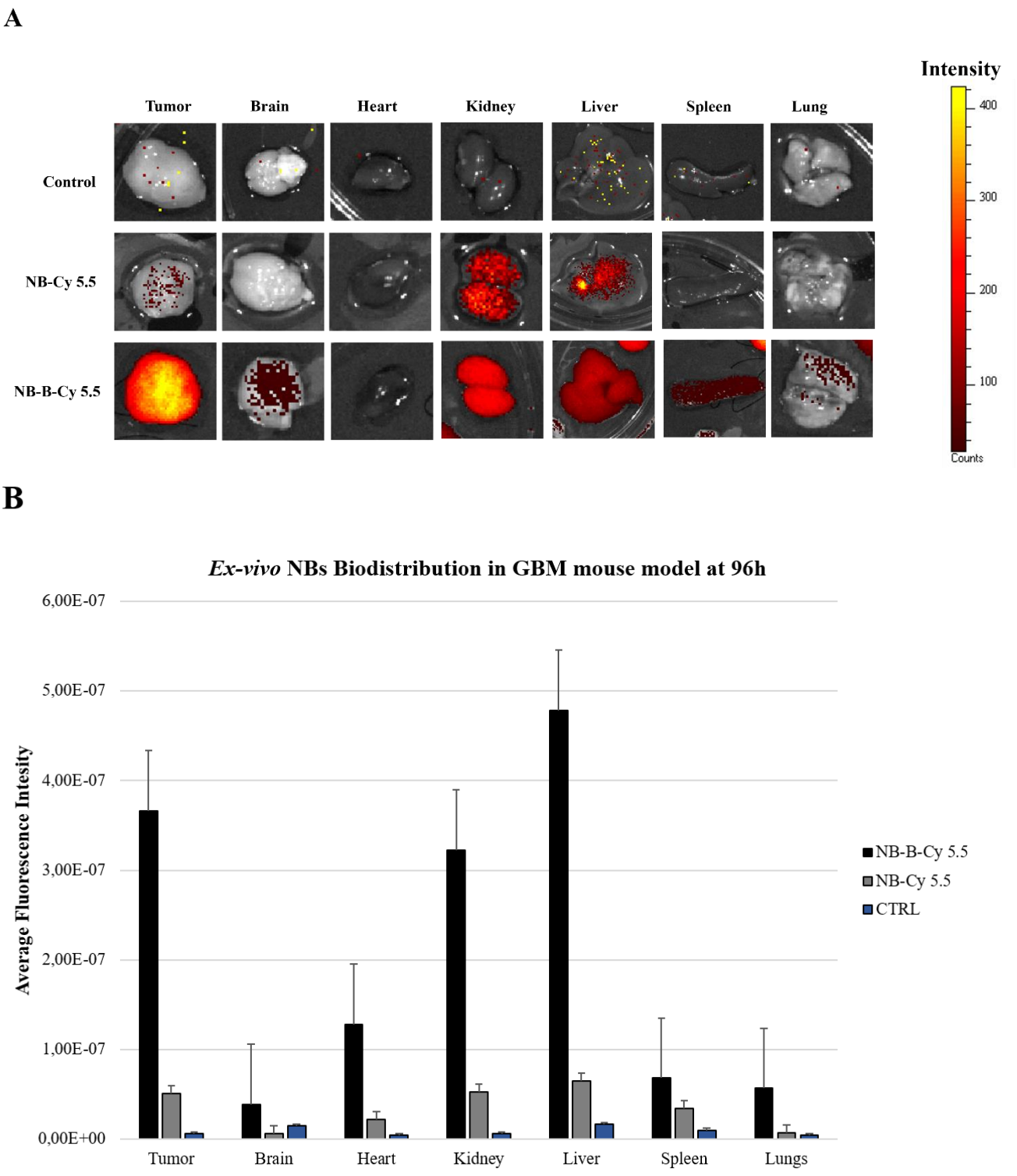

Figure 37. *Ex-vivo* analysis.
Panel A: *Ex-vivo* optical imaging of organs explanted at 96 hours after treatment with NB-B-Cy5.5 and Cy5.5-untargeted NBs administration are shown 1: tumor; 2: brain, 3: heart, 4: kidney, 5: liver, 6: spleen, 7: lung.
Panel B: Histogram representation of the average fluorescence intensity over tumor, brain, heart, kidney, liver, spleen, lung, and liver tissues explanted at 96 h after NB-B-Cy 5.5 and NBs-Cy 5.5 administration and control group. Data are expressed as means ± standard deviation of four independent experiments. (p-*value* was calculated by using paired *t*-test).

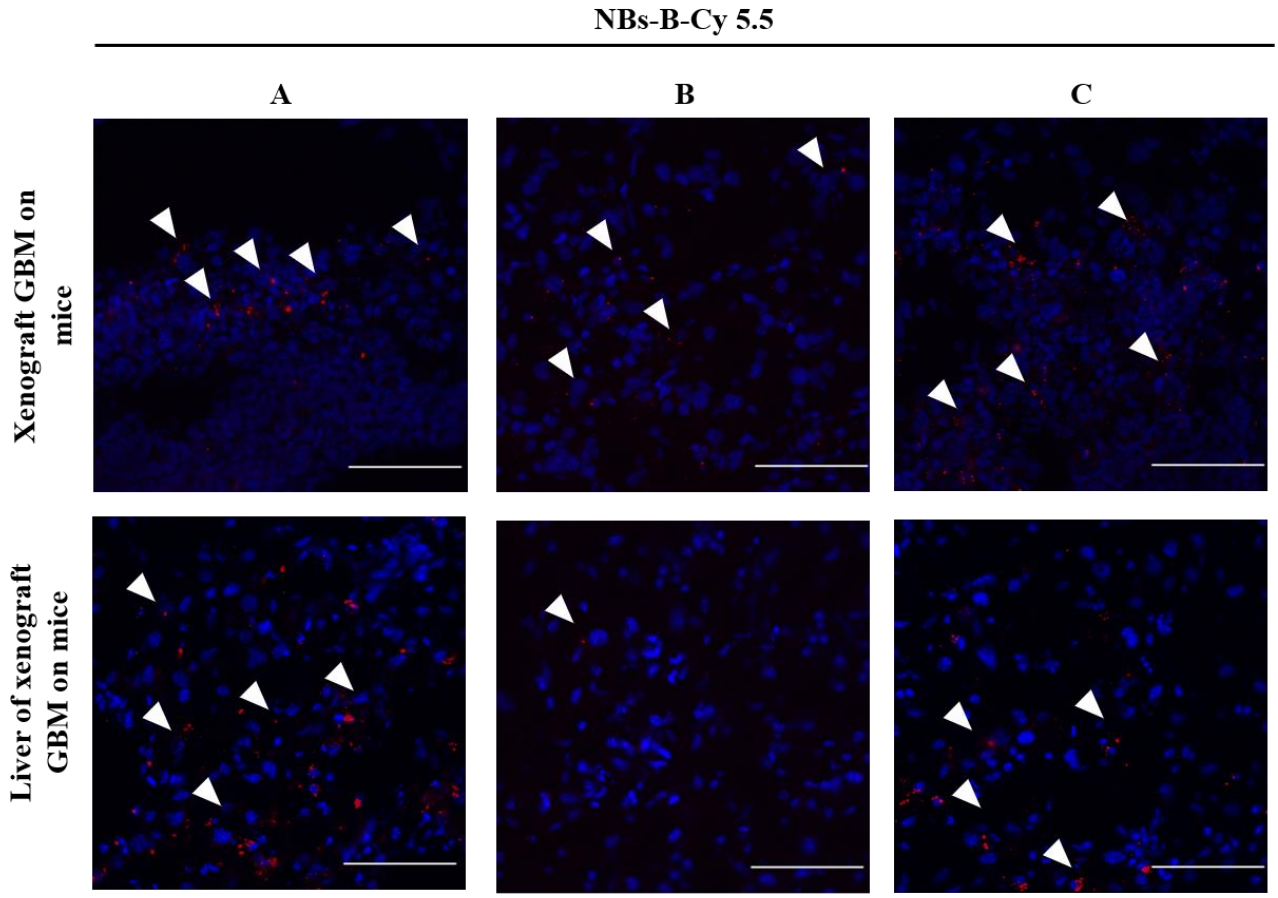

Figure 38. ***Ex-vivo*** **analysis.**
Fluorescence microscopy images of explanted three tumor mass' and three liver's cryosections were obtained from NBs-B-Cy5.5 injections into mice. Nuclei are reported in blue and in red Cy 5.5 to visualize NBs-B-Cy 5.5. Scale bar = 50μm.

5. Discussion

In this research project, we developed a drug delivery strategy using chitosan NBs loaded with DTX and conjugated with the B anti-GPC1 antibody for the treatment of GBM. We demonstrated that the proposed strategy could kill GBM cell line cells *in-vitro*. Moreover, we also demonstrated that the proposed NB formulation is capable to reach the tumor cells in GBM xenograft mouse models. In the last decade, many strategies using nanotechnologies have been proposed for the treatment of cancers, both for hematological malignancies and solid tumors to increase the efficacy of the treatments and concomitantly reduce the side-toxicity[131,226]. In this context, the proposal of active strategies in which an antibody is employed to allow the specific targeting of tumor cells appears to be more efficient in reaching the tumor side especially in the case of solid tumors. The presence of cellular heterogeneity in GBM can be stunning, genetic, and phenotypic heterogeneity, the remaining of GSCs, and the drug delivery issues created by the BBB, all of which make the likelihood of treatment for GBM unlikely. Therefore, in GBM there is a clinical need to identify a new molecular target that is expressed in GBM tumors and not in normal tissue. In such a way, the identification of a specific molecular target can also be targeted in the clinical setting if they are overexpressed on tumor cells. therefore, identify potential new tumor antigens in primary brain tumors that were not previously defined, GBM patients may benefit from active specific targeting. For this reason, we have developed a new antibody direct against a protein overexpressed in GBM and not in normal tissue. Nevertheless, the efficiency of the antibody-based active drug-delivery strategy is surely dependent on the specificity of the employed antibody. Indeed, for many tumors associated with antigens that have been identified as potential targets of anticancer pharmaceutical compounds the proposed active drug delivery strategy lacked in killing efficiency for the poor binding capability of the employed antibody[227]. In the approach proposed in the present project, the proteoglycan GPC1 has been used as a specific drug-delivery target, being specifically expressed in GBM tumor tissue cells, and not expressed in healthy tissues[210,211,220]. Nevertheless, the glypican family is characterized by a high degree of glycosylation as well as there is a high degree of homology among glypican family components[202]. For these reasons, few treatment strategies have been so far proposed using antibodies specifically targeting glypicans for the treatment of solid tumors including GBM. An accurate analysis of the GPC1 protein structure has been performed to obtain an antibody with a higher affinity and specificity for GPC1, also not recognizing the other members of the glypican family whose expression is peculiar of other hematological malignancies and solid tumors. Moreover, the anti-GPC1 antibody has been developed by using an approach with mouse immunization by transfecting a specific part of the GPC1 protein in which the homology among GPC1 and the other Glypican family members was lower. Finally, the two anti-GPC1 antibodies selected among those produced by the hybridomas were carefully tested

with different strategies to define the more efficient one. This fine-tuned methodological approach was used to maximize the efficiency of the proposed anti-GPC1 antibody-driven drug delivery strategy.

Standard of care first-line treatment of GBM is constituted by maximal surgical resection (complete resection is performed quite rarely because of the presence of diffuse infiltrations), followed by radiotherapy with concomitant and adjuvant chemotherapy such as the oral alkylating agent, temozolomide (TMZ) (Stupp protocol). Nevertheless, upon this treatment combination, the increase of patient survival is small and GBM tumors invariably recur after TMZ, showing a median OS of about 15 months[3,8,11,228,229]. Moreover, the efficiency of GBM treatment is surely affected by the presence and integrity of the BBB. The brain is distinguished from the other organs by the presence of the BBB that provides a selective barrier between the systemic circulation and the brain, thus representing a limit for the delivery of many therapeutic agents[230,231]. The composition of the extracellular matrix of the normal brain is distinctive, with specific tissue-resident cell types such as neurons, astrocytes, and microglia. Moreover, specialized endothelial cells, pericytes, and astrocytic foot processes, dictating junctional integrity, are the elements that constitute the BBB. BBB integrity can be also regulated by microglia, being these cells capable of repairing the BBB. The BBB physically protects the extracellular matrix from inflammation[232,233]. The most common component of the brain extracellular matrix is hyaluronic acid which is localized in the intraparenchymal region[234]. The haptotactic cues from the vascular basement membrane, the enrichment of vascular-derived chemotactic cues, as well as interconnected axon tracts can determine the therapeutic resistance of GBM cells in the perivascular space further providing haptotactic cues for cellular invasion[235–237]. However, a loss of BBB integrity could be displayed in the presence of cancer, during cancer progression. This seems to be the reason why several agents that are known to be not capable of penetrating the BBB, have however shown to some extent a clinical efficacy. In this context, TMZ is known to be able to pass the BBB although its efficiency in GBM treatment has been demonstrated to be still not sufficient. In the present project, we proposed DTX as a pharmaceutical compound employed to kill the GBM tumor cells. In our proposed approach, the lower capability of DTX to pass the BBB compared to TMZ should be overcome by the loading into NBs. This could allow for the higher killing capability of DTX compared to TMZ but also allow a higher capability to pass the BBB of the proposed NB formulation. However, this issue remains to be demonstrated by using other *in-vivo* xenograft models such as orthotopic mouse models.

In this project, to allow the selective delivery to GBM cells, DTX was encapsulated in the purposely tailored anti-GBM targeted chitosan NBs. These NBs are spherical nanosized core/shell structures

filled by a gas that has been fine-tuned to be efficiently loaded with drugs, such as DTX[148,163,238]. The biocompatibility, biodegradability, low toxicity, and no immunogenicity of chitosan, which is a natural polycationic polysaccharide, was the reason for its selection as a component of the NB shell[110,112,148,166]. The chitosan complexation capability has been exploited to design different nanocarriers such as nanoparticles, micelles, nanocapsules[239,240]. Intriguingly, chitosan has been proposed for the manufacturing of polymer-shelled NBs, showing a great capacity to be loaded with different drugs, due to the cationic properties of the shell [241,242]. Moreover, the NB chitosan surface offers the possibility to function with specific target ligands for an active targeted delivery such as the anti-GPC1 B antibody as proposed in the present research project. In particular, the results of both *in-vitro* biocompatibility and cytotoxicity experiments and biodistribution experiments performed *in-vivo* in the xenograft mouse models confirmed the above-mentioned characteristics of chitosan. Overall considered, the results showed in the project demonstrate that chitosan is an efficient compound for the development of nanocarriers aimed at the delivery of pharmaceutical compounds such as DTX[45,243]. Moreover, both targeted and untargeted NB formulations can bind GBM tumor cells. In the *in-vivo* experiments, NBs demonstrated the capacity to accumulate in the tumor microenvironment in a relatively short period (about 24h), maintaining their concentration for several days until at least 96h, with a peak at 48h for anti-GPC1 conjugated NBs. In this context, the shape, size, and surface charge of the proposed chitosan, NBs are key parameters affecting their accumulation in the GBM tumor tissue. However, the results showed that the targeting agent (e.g., the B anti-GPC1 antibody) seems to be required to enhance the binding and the internalization of the proposed nanosystems further experiments will be performed to confirm these data. However, a critical factor that hampers progress in GBM treatment is the lack of suitable and reliable *in-vitro* models that should drive the choice of subsequent more comprehensive and sophisticated *in-vivo* GBM animal models. Indeed, recent developments in the implementation of innovative 3D tumor models have revealed that this novel approach could mirror more closely than 2D systems the real in the vivo tumor microenvironment. In addition, we obtained little difference *in-vitro* tests when we tested NBs internalization because they depend on the complexity of the cell model applied. Nanoparticle features such as electrostatics strength, the covalent bond between NBs and antibodies, and the surface charge may interfere within a 2D culture model, that does not recapitulate the natural *in-vivo* environment. Another strategy for recapitulation of human GBM features and accurately the response to the drug therapy is the use of patient-derived (PDX) xenograft orthotopic models. But, PDX models have certain disadvantages, establishing a PDX line is not always successful and is dependent on the experience of the lab. Also, as each PDX model is derived from a different patient sample, there can be significant variability between different individual models, limiting their

reducing the reproducibility of experimental results. On the other hand, the killing capability of the proposed anti-GPC1 conjugated NBs loaded with DTX remains to be demonstrated in the xenograft GBM model. The proposed NB formulation also allows loading the NBs with more than a pharmaceutical compound. This is an opportunity that remains to be investigated also in our proposed anti-GPC1 drug delivery strategy. Of note, due to their vaporizable core (i.e., perfluoropentane), NBs can be activated by ultrasound that induces the liquid-to-vapor transition via acoustic droplet vaporization (ADV) phenomenon[244]. This could carry out other possibilities of employment of the proposed NB-based drug delivery system as a multifunctional theragnostic agent potentially utilizable for ultrasound imaging and spatiotemporal control of the payload delivery being these NBs sensitive to ultrasounds.

6. Conclusions

In this research project, we developed an active drug delivery strategy based on the use of chitosan-made NBs conjugated with an anti-GPC1 antibody and loaded with DTX for the treatment of GBM. GBM, the most frequent and aggressive primary central nervous system tumor, is still a disease for which a curative treatment has not been yet obtained. In this context, polymeric nanoparticle-based formulations could represent useful pharmaceutical compounds for the development of active drug-delivery strategies for the treatment of GBM. In this project, we proposed GPC1 as a useful TAA to specifically target GBM tumor cells being specifically overexpressed in GBM tissues and not expressed or expressed at negligible levels in healthy tissues. GPC1 is a proteoglycan member of the glypican family that is characterized by a high degree of homology among the different family members. Moreover, the carbossi-terminal region of these glypican proteins is the less homologous one of the protein structures. For these reasons, we developed homemade antibodies by mouse immunization by transfecting a specific part of the GPC1 protein. This strategy allows us to obtain at least one specific and efficient anti-GPC1 antibody (B). We think that the approach employed for the development of the anti-GPC1 antibody could at least in part overcome the lack of efficiency of other anti-tumor treatment strategies in which antibodies targeting Glypicans have been employed that could be allegedly attributed to the high degree of homology among glypican members as well as to the complex glypican structure with a high degree of glycosylations. To treat GBM cells, we synthesized chitosan NBs conjugated with the B clone and loaded with DTX. The capability of chitosan-made NBs to reach the tumor site is dependent on key parameters such as shape, size, and surface charge. We demonstrated that the produced NBs are biocompatible and, when loaded with DTX, are capable to kill GBM cell line cells. We also developed a GBM xenograft mouse model to evaluate the behavior of the B conjugated NBs *in-vivo*. We demonstrated that the B conjugated NBs are capable to reach the tumor masses when injected into the mouse tail. Moreover, we also demonstrated that the conjugation of NBs with the B antibody allows increasing the number of NBs capable to reach the tumor mass. On the other hand, further studies are needed to define the *in-vivo* killing capability of GBM cells of the proposed anti-GPC1 driven drug delivery strategy, and its clinical potential remains to be clarified. In conclusion, in the present research project, we developed an anti-GPC1-driven NB-based active drug delivery strategy based on the use of B conjugated NBs loaded with DTX. The proposed approach could be useful to increase the efficiency of GBM treatment but also to avoid or limit the side-effect toxicity.

Bibliography

1. Adamson, C. *et al.* Glioblastoma multiforme: a review of where we have been and where we are going. *Expert Opin Investig Drugs* **18**, 1061–1083 (2009).

2. Glaser, T., Han, I., Wu, L. & Zeng, X. Targeted Nanotechnology in Glioblastoma Multiforme. *Front Pharmacol* **8**, 166 (2017).

3. Stupp, R. *et al.* Effects of radiotherapy with concomitant and adjuvant temozolomide versus radiotherapy alone on survival in glioblastoma in a randomised phase III study: 5-year analysis of the EORTC-NCIC trial. *Lancet Oncol* **10**, 459–66 (2009).

4. Louis, D. N. *et al.* The 2016 World Health Organization Classification of Tumors of the Central Nervous System: a summary. *Acta Neuropathol* **131**, 803–20 (2016).

5. Mendes, M., Sousa, J., Pais, A. & Vitorino, C. Targeted Theranostic Nanoparticles for Brain Tumor Treatment. - Abstract - Europe PMC. *Pharmaceutics* https://europepmc.org/article/pmc/pmc6321593 (2018).

6. Altmann, C., Keller, S. & Schmidt, M. H. H. The Role of SVZ Stem Cells in Glioblastoma. *Cancers* **11**, 448 (2019).

7. Ostrom, Q. T. *et al.* CBTRUS Statistical Report: Primary Brain and Other Central Nervous System Tumors Diagnosed in the United States in 2012-2016. *Neuro Oncol* **21**, v1–v100 (2019).

8. Di Cintio, F. *et al.* The Molecular and Microenvironmental Landscape of Glioblastomas: Implications for the Novel Treatment Choices. *Frontiers in Neuroscience* **14**, 1220 (2020).

9. Nam, J. Y. & de Groot, J. F. Treatment of Glioblastoma. *J Oncol Pract* **13**, 629–638 (2017).

10. Louis, D. N. *et al.* The 2016 World Health Organization Classification of Tumors of the Central Nervous System: a summary. *Acta Neuropathol.* **131**, 803–820 (2016).

11. Ohgaki, H. & Kleihues, P. The definition of primary and secondary glioblastoma. *Clin Cancer Res* **19**, 764–772 (2013).

12. Brennan, C. W. *et al.* The Somatic Genomic Landscape of Glioblastoma. *Cell* **155**, 462–477 (2013).

13. Di Cintio, F. *et al.* The Molecular and Microenvironmental Landscape of Glioblastomas: Implications for the Novel Treatment Choices. *Front Neurosci* **14**, 603647 (2020).

14. Doetsch, F., Caillé, I., Lim, D. A., García-Verdugo, J. M. & Alvarez-Buylla, A. Subventricular zone astrocytes are neural stem cells in the adult mammalian brain. *Cell* **97**, 703–716 (1999).

15. Stupp, R. *et al.* Radiotherapy plus Concomitant and Adjuvant Temozolomide for Glioblastoma. *New England Journal of Medicine* **352**, 987–996 (2005).

16. Stupp, R. *et al.* Effects of radiotherapy with concomitant and adjuvant temozolomide versus radiotherapy alone on survival in glioblastoma in a randomised phase III study: 5-year analysis of the EORTC-NCIC trial. *Lancet Oncol* **10**, 459–466 (2009).

17. Tan, A. C. *et al.* Management of glioblastoma: State of the art and future directions. *CA: A Cancer Journal for Clinicians* **70**, 299–312 (2020).

18. Canoll, P. & Goldman, J. E. The interface between glial progenitors and gliomas. *Acta Neuropathol* **116**, 465–477 (2008).

19. Wesolowski, J. R., Rajdev, P. & Mukherji, S. K. Temozolomide (Temodar). *AJNR Am J Neuroradiol* **31**, 1383–1384 (2010).

20. Hingorani, M., Colley, W. P., Dixit, S. & Beavis, A. M. Hypofractionated radiotherapy for glioblastoma: strategy for poor-risk patients or hope for the future? *Br J Radiol* **85**, e770–e781 (2012).

21. Mann, J., Ramakrishna, R., Magge, R. & Wernicke, A. G. Advances in Radiotherapy for Glioblastoma. *Front Neurol* **8**, 748 (2018).

22. Westphal, M. *et al.* Gliadel® wafer in initial surgery for malignant glioma: long-term follow-up of a multicenter controlled trial. *Acta Neurochir (Wien)* **148**, 269–275 (2006).

23. Dixit, S., Hingorani, M., Achawal, S. & Scott, I. The sequential use of carmustine wafers (Gliadel®) and post-operative radiotherapy with concomitant temozolomide followed by adjuvant temozolomide: a clinical review. *Br J Neurosurg* **25**, 459–469 (2011).

24. Pallud, J. *et al.* Long-term results of carmustine wafer implantation for newly diagnosed glioblastomas: a controlled propensity-matched analysis of a French multicenter cohort. *Neuro Oncol* **17**, 1609–1619 (2015).

25. Gilbar, P. J., Pokharel, K. & Mangos, H. M. Temozolomide-induced aplastic anaemia: Case report and review of the literature. *J Oncol Pharm Pract* **27**, 1275–1280 (2021).

26. Malmström, A. *et al.* Temozolomide versus standard 6-week radiotherapy versus hypofractionated radiotherapy in patients older than 60 years with glioblastoma: the Nordic randomised, phase 3 trial. *The Lancet Oncology* **13**, 916–926 (2012).

27. Hottinger, A. F., Pacheco, P. & Stupp, R. Tumor treating fields: a novel treatment modality and its use in brain tumors. *Neuro Oncol* **18**, 1338–1349 (2016).

28. Taphoorn, M. J. B. *et al.* Influence of Treatment With Tumor-Treating Fields on Health-Related Quality of Life of Patients With Newly Diagnosed Glioblastoma: A Secondary Analysis of a Randomized Clinical Trial. *JAMA Oncology* **4**, 495–504 (2018).

29. Agarwala, S. S. Temozolomide, a Novel Alkylating Agent with Activity in the Central Nervous System, May Improve the Treatment of Advanced Metastatic Melanoma. *The Oncologist* **5**, 144–151 (2000).

30. Pazhouhi Mona, Reyhaneh Sariri, Mohammad Rasoul Khazaei, Mohammad Taher Moradi, & Mozafar Khazaei. Synergistic effect of temozolomide and thymoquinone on human glioblastoma multiforme cell line (U87MG). http://www.cancerjournal.net/article.asp?issn=0973-1482;year=2018;volume=14;issue=5;spage=1023;epage=1028;aulast=Pazhouhi (2018).

31. Rafiei, P. & Haddadi, A. Docetaxel-loaded PLGA and PLGA-PEG nanoparticles for intravenous application: pharmacokinetics and biodistribution profile. *International Journal of Nanomedicine* **Volume 12**, 935–947 (2017).

32. Hua, H. *et al.* RVG29-modified docetaxel-loaded nanoparticles for brain-targeted glioma therapy. *International Journal of Pharmaceutics* **543**, 179–189 (2018).

33. Wang, H. *et al.* Diagnostic imaging and therapeutic application of nanoparticles targeting the liver. *Journal of Materials Chemistry B* **3**, 939–958 (2015).

34. Ruan, D., Li, X., Li, A., Liu, B. & Xu, F. Paclitaxel inhibits growth and proliferation of glioblastoma through MMP-9- meidated p38/JNK signaling pathway. *Biomed Res* **28**, 6 (2017).

35. Urien, S. *et al.* Docetaxel serum protein binding with high affinity to alpha 1-acid glycoprotein. *Invest New Drugs* **14**, 147–151 (1996).

36. Ganipineni, L. P., Danhier, F. & Préat, V. Drug delivery challenges and future of chemotherapeutic nanomedicine for glioblastoma treatment. *Journal of Controlled Release* **281**, 42–57 (2018).

37. Jia, F., Ruan, S., Liu, N. & Fu, L. Synergistic Antitumor Effects of Berbamine and Paclitaxel through ROS/Akt Pathway in Glioma Cells. *Evidence-Based Complementary and Alternative Medicine* **2017**, 1–8 (2017).

38. Wang, B. *et al.* Improved anti-glioblastoma efficacy by IL-13Rα2 mediated copolymer nanoparticles loaded with paclitaxel. *Sci Rep* **5**, 16589 (2015).

39. Weaver, B. A. How Taxol/paclitaxel kills cancer cells. *Mol Biol Cell* **25**, 2677–2681 (2014).

40. van Eerden, R. A. G., Mathijssen, R. H. J. & Koolen, S. L. W. Recent Clinical Developments of Nanomediated Drug Delivery Systems of Taxanes for the Treatment of Cancer. *Int J Nanomedicine* **15**, 8151–8166 (2020).

41. Daraei, B., Aghvami, M., Pourahmad, J. & Dinarvand, R. A Comparison of Hepatocyte Cytotoxic Mechanisms for Docetaxel and PLGA-Docetaxel Nanoparticls. *Iran J Pharm Res* **16**, 249–265 (2017).

42. Lyseng-Williamson, K. A. & Fenton, C. Docetaxel: a review of its use in metastatic breast cancer. *Drugs* **65**, 2513–2531 (2005).

43. Gao, H. *et al.* Preparation, Characterization and Anti-Glioma Effects of Docetaxel-Incorporated Albumin-Lipid Nanoparticles. *Journal of Biomedical Nanotechnology* **11**, 2137–2147 (2015).

44. Arvind Gannimitta, Prathima Srinivas, Venkateshwar Reddy A, & Pedireddi Sobhita Rani. PREPARATION, PHYSICAL CHARACTERIZATION, AND PHARMACOKINETIC STUDY OF DOCETAXEL NANOCRYSTALS. *Asian J Pharm Clin Res* 238–244 (2019) doi:10.22159/ajpcr.2019.v12i6.32856.

45. Kadari, A. *et al.* Design of multifunctional peptide collaborated and docetaxel loaded lipid nanoparticles for antiglioma therapy. *European Journal of Pharmaceutics and Biopharmaceutics* **132**, 168–179 (2018).

46. Patra, J. K. *et al.* Nano based drug delivery systems: recent developments and future prospects. *Journal of Nanobiotechnology* **16**, 71 (2018).

47. Bhatia, S. Nanoparticles Types, Classification, Characterization, Fabrication Methods and Drug Delivery Applications. in *Natural Polymer Drug Delivery Systems* 33–93 (Springer International Publishing, 2016). doi:10.1007/978-3-319-41129-3_2.

48. Baboci, L. *et al.* The Dual Role of the Liver in Nanomedicine as an Actor in the Elimination of Nanostructures or a Therapeutic Target. *J Oncol* **2020**, 4638192 (2020).

49. Cho, K., Wang, X., Nie, S., Chen, Z. (Georgia) & Shin, D. M. Therapeutic Nanoparticles for Drug Delivery in Cancer. *Clin Cancer Res* **14**, 1310–1316 (2008).

50. Yezhelyev, M. V. *et al.* Emerging use of nanoparticles in diagnosis and treatment of breast cancer. *The Lancet Oncology* **7**, 657–667 (2006).

51. Patra, C. R., Bhattacharya, R., Mukhopadhyay, D. & Mukherjee, P. Fabrication of gold nanoparticles for targeted therapy in pancreatic cancer. *Advanced Drug Delivery Reviews* **62**, 346–361 (2010).

52. Webster, T. J. Nanomedicine: what's in a definition? *Int J Nanomedicine* **1**, 115–116 (2006).

53. Wagner, V., Dullaart, A., Bock, A.-K. & Zweck, A. The emerging nanomedicine landscape. *Nat Biotechnol* **24**, 1211–1217 (2006).

54. Guidance for Industry Considering Whether an FDA-Regulated Product Involves the Application of Nanotechnology. *Biotechnology Law Report* **30**, 613–616 (2011).

55. Bharali, D. J., Khalil, M., Gurbuz, M., Simone, T. M. & Mousa, S. A. Nanoparticles and cancer therapy: a concise review with emphasis on dendrimers. *Int J Nanomedicine* **4**, 1–7 (2009).

56. Jain, R. K. & Stylianopoulos, T. Delivering nanomedicine to solid tumors. *Nat Rev Clin Oncol* **7**, 653–664 (2010).

57. Durymanov, M., Kamaletdinova, T., Lehmann, S. E. & Reineke, J. Exploiting passive nanomedicine accumulation at sites of enhanced vascular permeability for non-cancerous applications. *J Control Release* **261**, 10–22 (2017).

58. Brusini, R., Varna, M. & Couvreur, P. Advanced nanomedicines for the treatment of inflammatory diseases. *Adv Drug Deliv Rev* **157**, 161–178 (2020).

59. Colombo, F. *et al.* Targeting CD34+ cells of the inflamed synovial endothelium by guided nanoparticles for the treatment of rheumatoid arthritis. *J Autoimmun* **103**, 102288 (2019).

60. Bregoli, L. *et al.* Nanomedicine applied to translational oncology: A future perspective on cancer treatment. *Nanomedicine* **12**, 81–103 (2016).

61. Fang, J., Nakamura, H. & Maeda, H. The EPR effect: Unique features of tumor blood vessels for drug delivery, factors involved, and limitations and augmentation of the effect. *Adv Drug Deliv Rev* **63**, 136–151 (2011).

62. Begines, B. *et al.* Polymeric Nanoparticles for Drug Delivery: Recent Developments and Future Prospects. *Nanomaterials (Basel)* **10**, 1403 (2020).

63. Sapra, P., Tyagi, P. & Allen, T. M. Ligand-targeted liposomes for cancer treatment. *Curr Drug Deliv* **2**, 369–381 (2005).

64. Alexis, F., Pridgen, E., Molnar, L. K. & Farokhzad, O. C. Factors affecting the clearance and biodistribution of polymeric nanoparticles. *Mol Pharm* **5**, 505–515 (2008).

65. Rosenblum, D., Joshi, N., Tao, W., Karp, J. M. & Peer, D. Progress and challenges towards targeted delivery of cancer therapeutics. *Nat Commun* **9**, 1410 (2018).

66. Dianzani, C. *et al.* Drug delivery nanoparticles in skin cancers. *Biomed Res Int* **2014**, 895986 (2014).

67. Biffi, S. *et al.* Targeted tumor imaging of anti-CD20-polymeric nanoparticles developed for the diagnosis of B-cell malignancies. *International Journal of Nanomedicine* 4099 (2015) doi:10.2147/IJN.S78995.

68. Sun, X. *et al.* The Blood Clearance Kinetics and Pathway of Polymeric Micelles in Cancer Drug Delivery. *ACS Nano* **12**, 6179–6192 (2018).

69. Longmire, M., Choyke, P. L. & Kobayashi, H. Clearance Properties of Nano-sized Particles and Molecules as Imaging Agents: Considerations and Caveats. *Nanomedicine (Lond)* **3**, 703–717 (2008).

70. Tsoi, K. M. *et al.* Mechanism of hard-nanomaterial clearance by the liver. *Nature Materials* **15**, 1212–1221 (2016).

71. Cheng, L., Yang, K., Chen, Q. & Liu, Z. Organic Stealth Nanoparticles for Highly Effective in Vivo Near-Infrared Photothermal Therapy of Cancer. *ACS Nano* **6**, 5605–5613 (2012).

72. Aggas, J. R. & Guiseppi-Elie, A. Responsive Polymers in the Fabrication of Enzyme-Based Biosensors. in *Biomaterials Science* 1267–1286 (Elsevier, 2020). doi:10.1016/B978-0-12-816137-1.00079-9.

73. Park, K. Controlled drug delivery systems: past forward and future back. *J Control Release* **190**, 3–8 (2014).

74. Yun, Y., Lee, B. K. & Park, K. Controlled Drug Delivery: Historical perspective for the next generation. *Journal of controlled release : official journal of the Controlled Release Society* (2015) doi:10.1016/j.jconrel.2015.10.005.

75. Zaffaroni, A. Overview and evolution of therapeutic systems. *Ann N Y Acad Sci* **618**, 405–421 (1991).

76. Immordino, M. L., Dosio, F. & Cattel, L. Stealth liposomes: review of the basic science, rationale, and clinical applications, existing and potential. *Int J Nanomedicine* **1**, 297–315 (2006).

77. Binauld, S. & Stenzel, M. H. Acid-degradable polymers for drug delivery: a decade of innovation. *Chem. Commun.* **49**, 2082–2102 (2013).

78. Brannon-Peppas, L. & Blanchette, J. O. Nanoparticle and targeted systems for cancer therapy. *Adv Drug Deliv Rev* **56**, 1649–1659 (2004).

79. Hoffman, A. S. The origins and evolution of 'controlled' drug delivery systems. *J Control Release* **132**, 153–163 (2008).

80. Anselmo, A. C. & Mitragotri, S. Nanoparticles in the clinic: An update. *Bioeng Transl Med* **4**, e10143 (2019).

81. Etheridge, M. L. *et al.* The big picture on nanomedicine: the state of investigational and approved nanomedicine products. *Nanomedicine* **9**, 1–14 (2013).

82. Farokhzad, O. C. *et al.* Targeted nanoparticle-aptamer bioconjugates for cancer chemotherapy in vivo. *Proc Natl Acad Sci U S A* **103**, 6315–6320 (2006).

83. Wang, S. *et al.* Novel Methods to Incorporate Photosensitizers Into Nanocarriers for Cancer Treatment by Photodynamic Therapy. *Lasers Surg Med* **43**, 686–695 (2011).

84. Tran, S., DeGiovanni, P.-J., Piel, B. & Rai, P. Cancer nanomedicine: a review of recent success in drug delivery. *Clin Transl Med* **6**, 44 (2017).

85. Elzoghby, A. O., Samy, W. M. & Elgindy, N. A. Albumin-based nanoparticles as potential controlled release drug delivery systems. *J Control Release* **157**, 168–182 (2012).

86. Jiang, Y. *et al.* Influencing Selectivity to Cancer Cells with Mixed Nanoparticles Prepared from Albumin-Polymer Conjugates and Block Copolymers. *Bioconjug Chem* **28**, 979–985 (2017).

87. Sharifi-Rad, J. *et al.* Chitosan nanoparticles as a promising tool in nanomedicine with particular emphasis on oncological treatment. *Cancer Cell International* **21**, 318 (2021).

88. Jhaveri, J., Raichura, Z., Khan, T., Momin, M. & Omri, A. Chitosan Nanoparticles-Insight into Properties, Functionalization and Applications in Drug Delivery and Theranostics. *Molecules* **26**, 272 (2021).

89. Agnihotri, S. A. & Aminabhavi, T. M. Controlled release of clozapine through chitosan microparticles prepared by a novel method. *Journal of Controlled Release* **96**, 245–259 (2004).

90. Lu, Z., Yeh, T.-K., Tsai, M., Au, J. L.-S. & Wientjes, M. G. Paclitaxel-Loaded Gelatin Nanoparticles for Intravesical Bladder Cancer Therapy. *Clin Cancer Res* **10**, 7677–7684 (2004).

91. Ke, W. *et al.* Gene delivery targeted to the brain using an Angiopep-conjugated polyethyleneglycol-modified polyamidoamine dendrimer. *Biomaterials* **30**, 6976–6985 (2009).

92. Merkel, O. M. *et al.* Triazine dendrimers as non-viral vectors for in vitro and in vivo RNAi: The effects of peripheral groups and core structure on biological activity. *Mol Pharm* **7**, 969–983 (2010).

93. Panyam, J. & Labhasetwar, V. Biodegradable nanoparticles for drug and gene delivery to cells and tissue. *Adv Drug Deliv Rev* **55**, 329–347 (2003).

94. Hu, Y. *et al.* Synthesis and characterization of chitosan–poly(acrylic acid) nanoparticles. *Biomaterials* **23**, 3193–3201 (2002).

95. Ramalho, M. J. *et al.* PLGA nanoparticles as a platform for vitamin D-based cancer therapy. *Beilstein J. Nanotechnol.* **6**, 1306–1318 (2015).

96. Cui, Y., Xu, Q., Chow, P. K.-H., Wang, D. & Wang, C.-H. Transferrin-conjugated magnetic silica PLGA nanoparticles loaded with doxorubicin and paclitaxel for brain glioma treatment. *Biomaterials* **34**, 8511–8520 (2013).

97. Hans, M. L. & Lowman, A. M. Biodegradable nanoparticles for drug delivery and targeting. *Current Opinion in Solid State and Materials Science* **6**, 319–327 (2002).

98. Rancan, F. *et al.* Investigation of Polylactic Acid (PLA) Nanoparticles as Drug Delivery Systems for Local Dermatotherapy. *Pharm Res* **26**, 2027–2036 (2009).

99. Soppimath, K. S., Aminabhavi, T. M., Kulkarni, A. R. & Rudzinski, W. E. Biodegradable polymeric nanoparticles as drug delivery devices. *J Control Release* **70**, 1–20 (2001).

100. Stéphanie Desgouilles, † *et al.* The Design of Nanoparticles Obtained by Solvent Evaporation: A Comprehensive Study. *ACS Publications* https://pubs.acs.org/doi/pdf/10.1021/la034999q (2003) doi:10.1021/la034999q.

101. Vauthier, C. & Bouchemal, K. Methods for the Preparation and Manufacture of Polymeric Nanoparticles. *Pharm Res* **26**, 1025–1058 (2009).

102. Gong, J. *et al.* Synthesis, characterization, drug-loading capacity and safety of novel octyl modified serum albumin micelles. *Int J Pharm* **376**, 161–168 (2009).

103. Kamaly, N., Xiao, Z., Valencia, P. M., Radovic-Moreno, A. F. & Farokhzad, O. C. Targeted polymeric therapeutic nanoparticles: design, development and clinical translation. *Chem Soc Rev* **41**, 2971–3010 (2012).

104. The extraordinary ligand binding properties of human serum albumin - Fasano - 2005 - IUBMB Life - Wiley Online Library. https://iubmb.onlinelibrary.wiley.com/doi/10.1080/15216540500404093.

105. Ulbrich, K., Hekmatara, T., Herbert, E. & Kreuter, J. Transferrin- and transferrin-receptor-antibody-modified nanoparticles enable drug delivery across the blood-brain barrier (BBB). *Eur J Pharm Biopharm* **71**, 251–256 (2009).

106. Kianfar, E. Protein nanoparticles in drug delivery: animal protein, plant proteins and protein cages, albumin nanoparticles. *Journal of Nanobiotechnology* **19**, 159 (2021).

107. An, F.-F. & Zhang, X.-H. Strategies for Preparing Albumin-based Nanoparticles for Multifunctional Bioimaging and Drug Delivery. *Theranostics* **7**, 3667–3689 (2017).

108. Davis, M. E., Chen, Z. (Georgia) & Shin, D. M. Nanoparticle therapeutics: an emerging treatment modality for cancer. in *Nanoscience and Technology* 239–250 (Co-Published with Macmillan Publishers Ltd, UK, 2009). doi:10.1142/9789814287005_0025.

109. Jain, A., Thakur, K., Kush, P. & Jain, U. K. Docetaxel loaded chitosan nanoparticles: formulation, characterization and cytotoxicity studies. *Int J Biol Macromol* **69**, 546–553 (2014).

110. Di Martino, A., Kucharczyk, P., Capakova, Z., Humpolicek, P. & Sedlarik, V. Enhancement of temozolomide stability by loading in chitosan-carboxylated polylactide-based nanoparticles. *Journal of Nanoparticle Research* **19**, (2017).

111. Pablo Játiva & Ceña, V. Use of nanoparticles for glioblastoma treatment: a new approach. *Nanomedicine* **12**, 2533–2554 (2017).

112. Chenthamara, D. *et al.* Therapeutic efficacy of nanoparticles and routes of administration. *Biomaterials Research* **23**, 20 (2019).

113. Kumari, A., Yadav, S. K. & Yadav, S. C. Biodegradable polymeric nanoparticles based drug delivery systems. *Colloids and Surfaces B: Biointerfaces* **75**, 1–18 (2010).

114. Argenziano, M. *et al.* Exploring Chitosan-Shelled Nanobubbles to Improve HER2+ Immunotherapy Through Dendritic Cells Targeting. (2021) doi:10.21203/rs.3.rs-787377/v1.

115. Lee, B. K., Yun, Y. & Park, K. PLA Micro- and Nano-Particles. *Adv Drug Deliv Rev* **107**, 176–191 (2016).

116. Essa, D., Kondiah, P. P. D., Choonara, Y. E. & Pillay, V. The Design of Poly(lactide-co-glycolide) Nanocarriers for Medical Applications. *Frontiers in Bioengineering and Biotechnology* **8**, 48 (2020).

117. Kumar, M. N. V. R. *et al.* Cationic Silica Nanoparticles as Gene Carriers: Synthesis, Characterization and Transfection Efficiency In vitro and In vivo. *Journal of nanoscience and nanotechnology* **4**, 876–81 (2004).

118. Zhou, J., Patel, T. R., Fu, M., Bertram, J. P. & Saltzman, W. M. Octa-functional PLGA nanoparticles for targeted and efficient siRNA delivery to tumors. *Biomaterials* **33**, 583–591 (2012).

119. Ganipineni, L. P. *et al.* Paclitaxel-loaded multifunctional nanoparticles for the targeted treatment of glioblastoma. *Journal of Drug Targeting* **27**, 614–623 (2019).

120. Kang, T. *et al.* Enhancing Glioblastoma-Specific Penetration by Functionalization of Nanoparticles with an Iron-Mimic Peptide Targeting Transferrin/Transferrin Receptor Complex. *Mol Pharm* **12**, 2947–2961 (2015).

121. Bertin, A. Emergence of Polymer Stereocomplexes for Biomedical Applications. *Macromolecular Chemistry and Physics* **213**, 2329–2352 (2012).

122. Hu, Y., Daoud, W. A., Cheuk, K. K. L. & Lin, C. S. K. Newly Developed Techniques on Polycondensation, Ring-Opening Polymerization and Polymer Modification: Focus on Poly(Lactic Acid). *Materials* **9**, 133 (2016).

123. Lopes, M. S., Jardini, A. & Filho, R. M. Synthesis and Characterizations of Poly (Lactic Acid) by Ring-Opening Polymerization for Biomedical Applications. *Chemical Engineering Transactions* **38**, 331–336 (2014).

124. Panyam, J. & Labhasetwar, V. Biodegradable nanoparticles for drug and gene delivery to cells and tissue. *Advanced Drug Delivery Reviews* **55**, 329–347 (2003).

125. Casalini, T., Rossi, F., Castrovinci, A. & Perale, G. A Perspective on Polylactic Acid-Based Polymers Use for Nanoparticles Synthesis and Applications. *Frontiers in Bioengineering and Biotechnology* **7**, 259 (2019).

126. Chen, J. *et al.* Preparation, characterization and transfection efficiency of cationic PEGylated PLA nanoparticles as gene delivery systems. *J Biotechnol* **130**, 107–113 (2007).

127. Bangham, A. D. & Horne, R. W. Negative staining of phospholipids and their structural modification by surface-active agents as observed in the electron microscope. *Journal of Molecular Biology* **8**, 660-IN10 (1964).

128. Zamboni, W. C. Liposomal, nanoparticle, and conjugated formulations of anticancer agents. *Clin Cancer Res* **11**, 8230–8234 (2005).

129. Barenholz, Y. Liposome application: problems and prospects. *Current Opinion in Colloid & Interface Science* **6**, 66–77 (2001).

130. Torchilin, V. P. Recent advances with liposomes as pharmaceutical carriers. *Nat Rev Drug Discov* **4**, 145–160 (2005).

131. Din, F. ud *et al.* Effective use of nanocarriers as drug delivery systems for the treatment of selected tumors. *Int J Nanomedicine* **12**, 7291–7309 (2017).

132. Leaf Huang, Y. L. In vivo delivery of RNAi with lipid-based nanoparticles - PubMed. *Annu Rev Biomed Eng* https://pubmed.ncbi.nlm.nih.gov/21639780/ (2011).

133. Çağdaş, M., Sezer, A. D. & Bucak, S. *Liposomes as Potential Drug Carrier Systems for Drug Delivery*. *Application of Nanotechnology in Drug Delivery* (IntechOpen, 2014). doi:10.5772/58459.

134. Irache, J. M., Esparza, I., Gamazo, C., Agüeros, M. & Espuelas, S. Nanomedicine: novel approaches in human and veterinary therapeutics. *Vet Parasitol* **180**, 47–71 (2011).

135. Jesorka, A. & Orwar, O. Liposomes: technologies and analytical applications. *Annu Rev Anal Chem (Palo Alto Calif)* **1**, 801–832 (2008).

136. Barenholz, Y. (Chezy). Doxil® — The first FDA-approved nano-drug: Lessons learned. *Journal of Controlled Release* **160**, 117–134 (2012).

137. Allen, T. M. & Martin, F. J. Advantages of liposomal delivery systems for anthracyclines. *Semin Oncol* **31**, 5–15 (2004).

138. Immordino, M. L., Dosio, F. & Cattel, L. Stealth liposomes: review of the basic science, rationale, and clinical applications, existing and potential. *Int J Nanomedicine* **1**, 297–315 (2006).

139. Hanafy, N. A. N., El-Kemary, M. & Leporatti, S. Micelles Structure Development as a Strategy to Improve Smart Cancer Therapy. *Cancers (Basel)* **10**, 238 (2018).

140. Ma, P., Benhabbour, S. R., Feng, L. & Mumper, R. J. 2'-Behenoyl-Paclitaxel Conjugate Containing Lipid Nanoparticles for the Treatment of Metastatic Breast Cancer. *Cancer Lett* **334**, 253–262 (2013).

141. Arleth, L. *et al.* Detailed structure of hairy mixed micelles formed by phosphatidylcholine and PEGylated phospholipids in aqueous media. *Langmuir* **21**, 3279–3290 (2005).

142. Patil, V. K., Gawali, I. T. & Usmani, G. A. Synthesis and Properties of Novel Cationic Triazolium Gemini Surfactants. *Journal of Dispersion Science and Technology* **37**, 1630–1637 (2016).

143. Giorgio, G., Colafemmina, G., Mavelli, F., Murgia, S. & Palazzo, G. The impact of alkanes on the structure of Triton X100 micelles. *RSC Adv.* **6**, 825–836 (2015).

144. Pottage, M. J., Greaves, T. L., Garvey, C. J. & Tabor, R. F. The effects of alkylammonium counterions on the aggregation of fluorinated surfactants and surfactant ionic liquids. *J Colloid Interface Sci* **475**, 72–81 (2016).

145. Feng, L. & Mumper, R. J. A critical review of lipid-based nanoparticles for taxane delivery. *Cancer Lett* **334**, 157–175 (2013).

146. Lalatsa, A., Schätzlein, A. G., Mazza, M., Le, T. B. H. & Uchegbu, I. F. Amphiphilic poly(L-amino acids) - new materials for drug delivery. *J Control Release* **161**, 523–536 (2012).

147. Veronese, F. M. *et al.* PEG-doxorubicin conjugates: influence of polymer structure on drug release, in vitro cytotoxicity, biodistribution, and antitumor activity. *Bioconjug Chem* **16**, 775–784 (2005).

148. Cavalli, R., Soster, M. & Argenziano, M. Nanobubbles: a promising efficient tool for therapeutic delivery. *Ther Deliv* **7**, 117–138 (2016).

149. Perera, R. H. *et al.* Nanobubble ultrasound contrast agents for enhanced delivery of thermal sensitizer to tumors undergoing radiofrequency ablation. *Pharm Res* **31**, 1407–1417 (2014).

150. Wang, J.-P., Zhou, X.-L., Yan, J.-P., Zheng, R.-Q. & Wang, W. Nanobubbles as ultrasound contrast agent for facilitating small cell lung cancer imaging. *Oncotarget* **8**, 78153–78162 (2017).

151. Cavalli, R. *et al.* New chitosan nanobubbles for ultrasound-mediated gene delivery: preparation and in vitro characterization. *IJN* 3309 (2012) doi:10.2147/IJN.S30912.

152. Cavalli, R., Bisazza, A. & Lembo, D. Micro- and nanobubbles: a versatile non-viral platform for gene delivery. *Int J Pharm* **456**, 437–445 (2013).

153. Cavalli, R. *et al.* Preparation and in vitro characterization of chitosan nanobubbles as theranostic agents. *Colloids Surf B Biointerfaces* **129**, 39–46 (2015).

154. Gao, Z., Kennedy, A. M., Christensen, D. A. & Rapoport, N. Y. Drug-Loaded Nano/Microbubbles for Combining Ultrasonography and Targeted Chemotherapy. *Ultrasonics* **48**, 260–270 (2008).

155. Sheeran, P. S., Matsunaga, T. O. & Dayton, P. A. Phase change events of volatile liquid perfluorocarbon contrast agents produce unique acoustic signatures. *Phys Med Biol* **59**, 379–401 (2014).

156. Chen, J., Pan, H., Lanza, G. M. & Wickline, S. A. Perfluorocarbon Nanoparticles for Physiological and Molecular Imaging and Therapy. *Adv Chronic Kidney Dis* **20**, 466–478 (2013).

157. Winter, P. M. Perfluorocarbon nanoparticles: evolution of a multimodality and multifunctional imaging agent. *Scientifica (Cairo)* **2014**, 746574 (2014).

158. Li, D. S. *et al.* Spatially Localized Sono-Photoacoustic Activation of Phase-Change Contrast Agents. *Photoacoustics* **20**, 100202 (2020).

159. Zullino, S., Argenziano, M., Stura, I., Guiot, C. & Cavalli, R. From Micro- to Nano-Multifunctional Theranostic Platform: Effective Ultrasound Imaging Is Not Just a Matter of Scale. *Mol Imaging* **17**, 1536012118778216 (2018).

160. Endo-Takahashi, Y. & Negishi, Y. Microbubbles and Nanobubbles with Ultrasound for Systemic Gene Delivery. *Pharmaceutics* **12**, 964 (2020).

161. Khan, M. S. *et al.* Oxygen-Carrying Micro/Nanobubbles: Composition, Synthesis Techniques and Potential Prospects in Photo-Triggered Theranostics. *Molecules* **23**, 2210 (2018).

162. Jiang, Q. *et al.* Production and characterization of a novel long-acting Herceptin-targeted nanobubble contrast agent specific for Her-2-positive breast cancers. *Breast Cancer* **23**, 445–455 (2016).

163. Su, C. *et al.* Current advances in ultrasound-combined nanobubbles for cancer-targeted therapy: a review of the current status and future perspectives. *RSC Adv.* **11**, 12915–12928 (2021).

164. Ma, R. *et al.* Co-delivery of CPP decorated doxorubicin and CPP decorated siRNA by NGR-modified nanobubbles for improving anticancer therapy. *Pharm Dev Technol* **26**, 634–646 (2021).

165. Marano, F. *et al.* Combining doxorubicin-nanobubbles and shockwaves for anaplastic thyroid cancer treatment: preclinical study in a xenograft mouse model. *Endocrine-Related Cancer* **24**, 275–286 (2017).

166. Zhou, X., Guo, L., Shi, D., Duan, S. & Li, J. Biocompatible Chitosan Nanobubbles for Ultrasound-Mediated Targeted Delivery of Doxorubicin. *Nanoscale Res Lett* **14**, 24 (2019).

167. Argenziano, M. *et al.* Comparative Evaluation of Different Chitosan Species and Derivatives as Candidate Biomaterials for Oxygen-Loaded Nanodroplet Formulations to Treat Chronic Wounds. *Marine Drugs* **19**, 112 (2021).

168. Argenziano, M. *et al.* Improvement in the Anti-Tumor Efficacy of Doxorubicin Nanosponges in In Vitro and in Mice Bearing Breast Tumor Models. *Cancers* **12**, 162 (2020).

169. Huang, H.-C., Barua, S., Sharma, G., Dey, S. K. & Rege, K. Inorganic nanoparticles for cancer imaging and therapy. *J Control Release* **155**, 344–357 (2011).

170. Samer, B. *et al.* Inorganic Nanoparticles for Cancer Therapy: A Transition from Lab to Clinic. *Current Medicinal Chemistry* **25**, 4269–4303 (2018).

171. Cherukula, K. *et al.* Multifunctional Inorganic Nanoparticles: Recent Progress in Thermal Therapy and Imaging. *Nanomaterials* **6**, 76 (2016).

172. Spirescu, V. A., Chircov, C., Grumezescu, A. M., Vasile, B. Ștefan & Andronescu, E. Inorganic Nanoparticles and Composite Films for Antimicrobial Therapies. *International Journal of Molecular Sciences* **22**, 4595 (2021).

173. Vassallo, A., Silletti, M. F., Faraone, I. & Milella, L. Nanoparticulate Antibiotic Systems as Antibacterial Agents and Antibiotic Delivery Platforms to Fight Infections. *Journal of Nanomaterials* **2020**, e6905631 (2020).

174. Núñez, C., Estévez, S. V. & del Pilar Chantada, M. Inorganic nanoparticles in diagnosis and treatment of breast cancer. *J Biol Inorg Chem* **23**, 331–345 (2018).

175. Ji, S. *et al.* Carbon nanotubes in cancer diagnosis and therapy. *Biochimica et Biophysica Acta (BBA) - Reviews on Cancer* **1806**, 29–35 (2010).

176. Chen, W., Fan, Z., Pan, X. & Bao, X. Effect of Confinement in Carbon Nanotubes on the Activity of Fischer−Tropsch Iron Catalyst. *J. Am. Chem. Soc.* **130**, 9414–9419 (2008).

177. Holmes, D. The next big things are tiny. *The Lancet Neurology* **12**, 31–32 (2013).

178. Boussiotis, V. A. & Charest, A. Immunotherapies for malignant glioma. *Oncogene* **37**, 1121–1141 (2018).

179. Haen, S. P., Löffler, M. W., Rammensee, H.-G. & Brossart, P. Towards new horizons: characterization, classification and implications of the tumour antigenic repertoire. *Nat Rev Clin Oncol* **17**, 595–610 (2020).

180. Zhu, G., Zhang, Q., Zhang, J. & Liu, F. Targeting Tumor-Associated Antigen: A Promising CAR-T Therapeutic Strategy for Glioblastoma Treatment. *Frontiers in Pharmacology* **12**, 1568 (2021).

181. Nance, E. *et al.* Brain-Penetrating Nanoparticles Improve Paclitaxel Efficacy in Malignant Glioma Following Local Administration. *ACS Nano* **8**, 10655–10664 (2014).

182. Lam, F. C. *et al.* Enhanced efficacy of combined temozolomide and bromodomain inhibitor therapy for gliomas using targeted nanoparticles. *Nature Communications* **9**, (2018).

183. Ramalho, M. J. *et al.* Receptor-mediated PLGA nanoparticles for glioblastoma multiforme treatment. *International Journal of Pharmaceutics* **545**, 84–92 (2018).

184. Chu, L. *et al.* Nose-to-brain delivery of temozolomide-loaded PLGA nanoparticles functionalized with anti-EPHA3 for glioblastoma targeting. *Drug Delivery* **25**, 1634–1641 (2018).

185. Hu, Q. *et al.* Glioma therapy using tumor homing and penetrating peptide-functionalized PEG–PLA nanoparticles loaded with paclitaxel. *Biomaterials* **34**, 5640–5650 (2013).

186. Heneweer, C., Holland, J. P., Divilov, V., Carlin, S. & Lewis, J. S. Magnitude of enhanced permeability and retention effect in tumors with different phenotypes: 89Zr-albumin as a model system. *J Nucl Med* **52**, 625–633 (2011).

187. Mahmoud, B. S., AlAmri, A. H. & McConville, C. Polymeric Nanoparticles for the Treatment of Malignant Gliomas. *Cancers (Basel)* **12**, 175 (2020).

188. Wang, S., Meng, Y., Li, C., Qian, M. & Huang, R. Receptor-Mediated Drug Delivery Systems Targeting to Glioma. *Nanomaterials* **6**, 3 (2016).

189. Golombek, S. K. *et al.* Tumor Targeting via EPR: Strategies to Enhance Patient Responses. *Adv Drug Deliv Rev* **130**, 17–38 (2018).

190. Blasi, P., Giovagnoli, S., Schoubben, A., Ricci, M. & Rossi, C. Solid lipid nanoparticles for targeted brain drug delivery☆. *Advanced Drug Delivery Reviews* **59**, 454–477 (2007).

191. Ohta, S. *et al.* Investigating the optimum size of nanoparticles for their delivery into the brain assisted by focused ultrasound-induced blood–brain barrier opening. *Sci Rep* **10**, 18220 (2020).

192. Cayero-Otero, M. D. *et al.* In vivo biodistribution of venlafaxine-PLGA nanoparticles for brain delivery: plain vs. functionalized nanoparticles. *Expert Opin Drug Deliv* **16**, 1413–1427 (2019).

193. Aso, E. *et al.* Poly(propylene imine) dendrimers with histidine-maltose shell as novel type of nanoparticles for synapse and memory protection. *Nanomedicine: Nanotechnology, Biology and Medicine* **17**, 198–209 (2019).

194. Tosi, G. *et al.* Exploiting Bacterial Pathways for BBB Crossing with PLGA Nanoparticles Modified with a Mutated Form of Diphtheria Toxin (CRM197): In Vivo Experiments. *Mol. Pharmaceutics* **12**, 3672–3684 (2015).

195. Filmus, J. & Selleck, S. B. Glypicans: proteoglycans with a surprise. *Journal of Clinical Investigation* **108**, 497–501 (2001).

196. Wang, S., Qiu, Y. & Bai, B. The Expression, Regulation, and Biomarker Potential of Glypican-1 in Cancer. *Front. Oncol.* **9**, 614 (2019).

197. Awad, W. *et al.* Structural Aspects of N-Glycosylations and the C-terminal Region in Human Glypican-1. *Journal of Biological Chemistry* **290**, 22991–23008 (2015).

198. Bernfield, M. *et al.* Functions of Cell Surface Heparan Sulfate Proteoglycans. *Annual Review of Biochemistry* **68**, 729–777 (1999).

199. Lin, X. & Perrimon, N. Role of heparan sulfate proteoglycans in cell–cell signaling in Drosophila. *Matrix Biology* **19**, 303–307 (2000).

200. Wael Awad, Derek T Logan, & Katrin Mani. GPC1 (glypican 1). **18**, 4 (2013).

201. Filmus, J., Capurro, M. & Rast, J. Glypicans. *Genome Biol* **9**, 224 (2008).

202. Svensson, G., Awad, W., Håkansson, M., Mani, K. & Logan, D. T. Crystal Structure of N-Glycosylated Human Glypican-1 Core Protein: STRUCTURE OF TWO LOOPS EVOLUTIONARILY CONSERVED IN VERTEBRATE GLYPICAN-1 *. *Journal of Biological Chemistry* **287**, 14040–14051 (2012).

203. Kaur, S. P. & Cummings, B. S. Role of glypicans in regulation of the tumor microenvironment and cancer progression. *Biochemical Pharmacology* **168**, 108–118 (2019).

204. Li, N., Gao, W., Zhang, Y.-F. & Ho, M. Glypicans as Cancer Therapeutic Targets. *Trends in Cancer* **4**, 741–754 (2018).

205. Shi, Z.-D., Wang, H. & Tarbell, J. M. Heparan Sulfate Proteoglycans Mediate Interstitial Flow Mechanotransduction Regulating MMP-13 Expression and Cell Motility via FAK-ERK in 3D Collagen. *PLoS One* **6**, e15956 (2011).

206. Lund, M. E., Campbell, D. H. & Walsh, B. J. The Role of Glypican-1 in the Tumour Microenvironment. *Adv Exp Med Biol* **1245**, 163–176 (2020).

207. Matsuda, K. *et al.* Glypican-1 Is Overexpressed in Human Breast Cancer and Modulates the Mitogenic Effects of Multiple Heparin-binding Growth Factors in Breast Cancer Cells. *Cancer Res* **61**, 5562–5569 (2001).

208. Harada, E. *et al.* Glypican-1 targeted antibody-based therapy induces preclinical antitumor activity against esophageal squamous cell carcinoma. *Oncotarget* **8**, 24741–24752 (2017).

209. Jen, Y.-H. L., Musacchio, M. & Lander, A. D. Glypican-1 controls brain size through regulation of fibroblast growth factor signaling in early neurogenesis. *Neural Dev* **4**, 33 (2009).

210. Su, G. *et al.* Glypican-1 Is Frequently Overexpressed in Human Gliomas and Enhances FGF-2 Signaling in Glioma Cells. *The American Journal of Pathology* **168**, 2014–2026 (2006).

211. Saito, T. *et al.* High Expression of Glypican-1 Predicts Dissemination and Poor Prognosis in Glioblastomas. *World Neurosurgery* **105**, 282–288 (2017).

212. Melo, S. A. *et al.* Glypican-1 identifies cancer exosomes and detects early pancreatic cancer. *Nature* **523**, 177–182 (2015).

213. Truong, Q. *et al.* Glypican-1 as a Biomarker for Prostate Cancer: Isolation and Characterization. *J. Cancer* **7**, 1002–1009 (2016).

214. Hara, H. *et al.* Overexpression of glypican-1 implicates poor prognosis and their chemoresistance in oesophageal squamous cell carcinoma. *Br J Cancer* **115**, 66–75 (2016).

215. Matsuzaki, S. *et al.* Anti-glypican-1 antibody-drug conjugate exhibits potent preclinical antitumor activity against glypican-1 positive uterine cervical cancer. *Int. J. Cancer* **142**, 1056–1066 (2018).

216. Shiau, C. E., Hu, N. & Bronner-Fraser, M. Altering Glypican-1 levels modulates canonical Wnt signaling during trigeminal placode development. *Dev Biol* **348**, 107–118 (2010).

217. Zhang, Z., Coomans, C. & David, G. Membrane Heparan Sulfate Proteoglycan-supported FGF2-FGFR1 Signaling: EVIDENCE IN SUPPORT OF THE "COOPERATIVE END STRUCTURES" MODEL *. *Journal of Biological Chemistry* **276**, 41921–41929 (2001).

218. Qiao, D., Meyer, K., Mundhenke, C., Drew, S. A. & Friedl, A. Heparan Sulfate Proteoglycans as Regulators of Fibroblast Growth Factor-2 Signaling in Brain Endothelial Cells. *Journal of Biological Chemistry* **278**, 16045–16053 (2003).

219. Li, X. *et al.* Overexpression of Annexin A2 promotes proliferation by forming a Glypican 1/c-Myc positive feedback loop: prognostic significance in human glioma. *Cell Death Dis* **12**, 261 (2021).

220. Listik, E. & Toma, L. Glypican-1 in human glioblastoma: implications in tumorigenesis and chemotherapy. *Oncotarget* **11**, 828–845 (2020).

221. Armento, A., Ehlers, J., Schötterl, S. & Naumann, U. Molecular Mechanisms of Glioma Cell Motility. in *Glioblastoma* (ed. De Vleeschouwer, S.) (Codon Publications, 2017).

222. Daniel, P. *et al.* Temozolomide Induced Hypermutation in Glioma: Evolutionary Mechanisms and Therapeutic Opportunities. *Front Oncol* **9**, 41 (2019).

223. Köhler, G. & Milstein, C. Continuous cultures of fused cells secreting antibody of predefined specificity. *Nature* **256**, 495–497 (1975).

224. Parray, H. A. *et al.* Hybridoma technology a versatile method for isolation of monoclonal antibodies, its applicability across species, limitations, advancement and future perspectives. *Int Immunopharmacol* **85**, 106639 (2020).

225. Ashrafizadeh, M. *et al.* Chitosan-based advanced materials for docetaxel and paclitaxel delivery: Recent advances and future directions in cancer theranostics. *Int J Biol Macromol* **145**, 282–300 (2020).

226. Hartshorn, C. M. *et al.* Nanotechnology Strategies to Advance Outcomes in Clinical Cancer Care. *ACS Nano* **12**, 24–43 (2018).

227. Arslan, F. B., Ozturk Atar, K. & Calis, S. Antibody-mediated drug delivery. *International Journal of Pharmaceutics* **596**, 120268 (2021).

228. Canoll, P. & Goldman, J. E. The interface between glial progenitors and gliomas. *Acta Neuropathol* **116**, 465–77 (2008).

229. Levine, J. H. *et al.* Data-Driven Phenotypic Dissection of AML Reveals Progenitor-like Cells that Correlate with Prognosis. *Cell* **162**, 184–97 (2015).

230. Chen, Y. & Liu, L. Modern methods for delivery of drugs across the blood-brain barrier. *Adv Drug Deliv Rev* **64**, 640–65 (2012).

231. Miura, Y. *et al.* Cyclic RGD-linked polymeric micelles for targeted delivery of platinum anticancer drugs to glioblastoma through the blood-brain tumor barrier. *ACS Nano* **7**, 8583–92 (2013).

232. Novak, U. & Kaye, A. H. Extracellular matrix and the brain: components and function. *J Clin Neurosci* **7**, 280–90 (2000).

233. Mahesparan, R. *et al.* Expression of extracellular matrix components in a highly infiltrative in vivo glioma model. *Acta Neuropathol* **105**, 49–57 (2003).

234. Kim Y *et al.* Role of extracellular matrix and microenvironment in regulation of tumor growth and LAR-mediated invasion in glioblastoma. *PLoS One.* **4**, 13 (2018).

235. Giese, A. & Westphal, M. Glioma invasion in the central nervous system. *Neurosurgery* **39**, 235–50; discussion 250-2 (1996).

236. Nimsky, C. *et al.* Preoperative and intraoperative diffusion tensor imaging-based fiber tracking in glioma surgery. *Neurosurgery* **56**, 130–7; discussion 138 (2005).

237. Gritsenko, P. G., Ilina, O. & Friedl, P. Interstitial guidance of cancer invasion. *J Pathol* **226**, 185–99 (2012).

238. Batchelor, D. V. B. *et al.* Nested Nanobubbles for Ultrasound-Triggered Drug Release. *ACS Appl Mater Interfaces* **12**, 29085–29093 (2020).

239. Alameh, M. *et al.* siRNA Delivery with Chitosan: Influence of Chitosan Molecular Weight, Degree of Deacetylation, and Amine to Phosphate Ratio on in Vitro Silencing Efficiency, Hemocompatibility, Biodistribution, and in Vivo Efficacy. *Biomacromolecules* **19**, 112–131 (2018).

240. Cao, Y., Tan, Y. F., Wong, Y. S., Liew, M. W. J. & Venkatraman, S. Recent Advances in Chitosan-Based Carriers for Gene Delivery. *Mar Drugs* **17**, 381 (2019).

241. Jhaveri, J., Raichura, Z., Khan, T., Momin, M. & Omri, A. Chitosan Nanoparticles-Insight into Properties, Functionalization and Applications in Drug Delivery and Theranostics. *Molecules* **26**, 272 (2021).

242. Mohammed, M. A., Syeda, J. T. M., Wasan, K. M. & Wasan, E. K. An Overview of Chitosan Nanoparticles and Its Application in Non-Parenteral Drug Delivery. *Pharmaceutics* **9**, 53 (2017).

243. Hwang, H.-Y., Kim, I.-S., Kwon, I. C. & Kim, Y.-H. Tumor targetability and antitumor effect of docetaxel-loaded hydrophobically modified glycol chitosan nanoparticles. *Journal of Controlled Release* **128**, 23–31 (2008).

244. Kripfgans, O. D., Fabiilli, M. L., Carson, P. L. & Fowlkes, J. B. On the acoustic vaporization of micrometer-sized droplets. *The Journal of the Acoustical Society of America* **116**, 272–281 (2004).

Acknowledgments

I want to thank all the staff of the National Cancer Institute (IRCCS CRO-Aviano). First, Dr. Giuseppe Toffoli, the director of the Clinical and Experimental Pharmacology division that has given me the opportunity to become a member of this research unit. I especially thank my PhD tutor Dr. Michele Dal Bo, Principal Investigator of the Nanomedicine Lab for his supervision during my PhD period.

I want to dedicate a special acknowledgement to Prof. Alberto Morgante, director of the Doctoral School for Nanotechnology in the University of Trieste, and the former one Prof. Lucia Pasquato for their supervision during the PhD period.

Then, I would like to thank all the people involved in the project: Prof. Roberta Cavalli and Dr. Monica Argenziano for NBs production, Prof. Paolo Macor and Dr. Sara Capolla for the antibody production.

I thank my mentor and friend Dr. Lorena Baboçi, for her guidance, patience, openness, persistence in my regards and also for the support provided during these three years.

I want to thank all the colleagues and friends in the FSC unit and especially in the Nanomedicine Lab (Nicole, Aharon, Idris, Monica, Davide), with whom I shared lots during these 3 years of intense research and experimental work. I believe they can understand my satisfaction more than anyone else.

Eventually, I thank my lovely family, for the continuous and unconditional support during these years and also for believing in my efforts.